

# We are IntechOpen, the world's leading publisher of Open Access books Built by scientists, for scientists

6,300

Open access books available

171,000

International authors and editors

190M

Downloads

Our authors are among the

154

Countries delivered to

TOP 1%

most cited scientists

12.2%

Contributors from top 500 universities



WEB OF SCIENCE™

Selection of our books indexed in the Book Citation Index  
in Web of Science™ Core Collection (BKCI)

Interested in publishing with us?  
Contact [book.department@intechopen.com](mailto:book.department@intechopen.com)

Numbers displayed above are based on latest data collected.  
For more information visit [www.intechopen.com](http://www.intechopen.com)



# Introductory Chapter: Dyes and Pigments - Past, Present, and Future

Raffaello Papadakis

## 1. Introduction

Dyes and pigments have been playing an undoubtedly important role in human life since the ancient years. Today their mass production is well established, and a vast number of dyes and pigments are globally produced. Currently, the industrial interest for new dyes and pigments with special properties is constantly growing. This has triggered significant research attempts all over the world and new multifunctional dyes and pigments suitable for novel, hi-tech applications have been proposed/created. The steady growth of the global dyes and pigments market signifies a vibrant future for research in the corresponding, wide research field.

## 2. Historical background

Dyes and pigments are narrowly connected to human culture and different types of them have been used from people since the ancient years in order to decorate various types of materials including textiles, ceramics, wood etc. [1] It is well documented that more than 2000 years ago, in ancient China, Egypt, Rome and Greece natural dyes and pigments obtained from plant roots, animals or mineral sources were used. [1, 2] They were mostly used for decorative applications but also as protective layers against wear and corrosion of various objects. [2]

The big revolution in the field occurred in the beginning of 19th century when Sir William Henry Perkin produced the first synthetic organic dye, the so-called *mauveine*, using aniline as a starting compound. [1, 3] *Mauveine* proved to be a suitable dyestuff for various types of textiles predominantly silk, and mass production of the *aniline purple* (the original industrial name of *Mauveine*) commenced. Industrial revolution made the production of many more synthetic dyes feasible, and the expansion of synthetic dyes industry became enormous in later years. In fact, the majority of the currently known classes of dyes and pigments were invented during 19th century. [4]

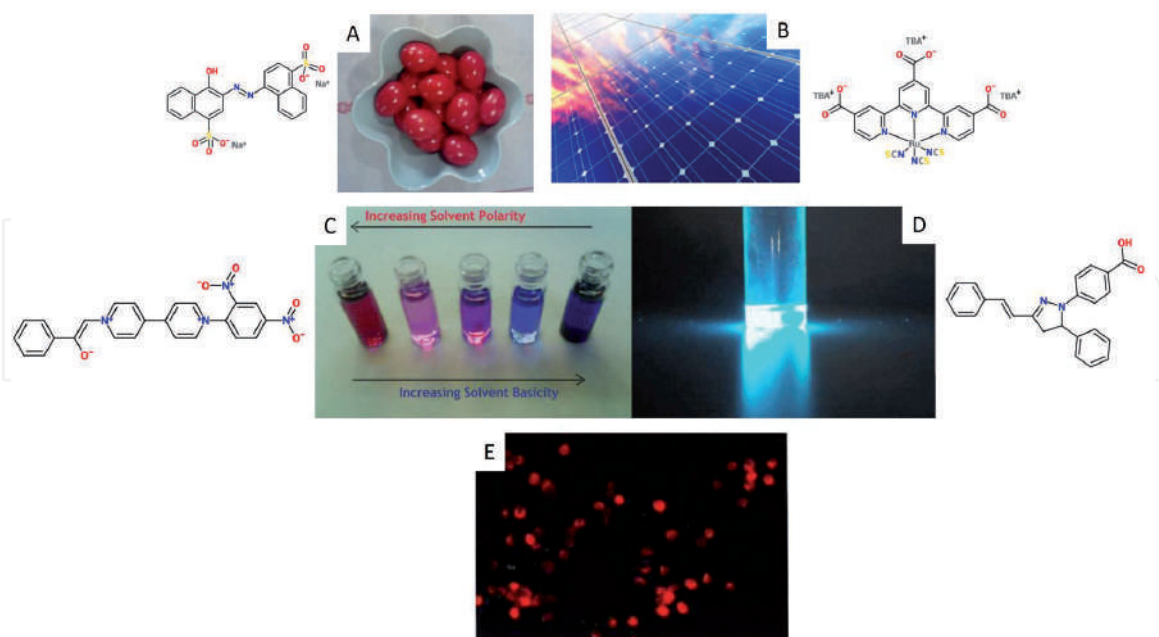
## 3. Contemporary trends and the future of dyes and pigments

Today, the classes of dyes and pigments have been enriched with numerous entries. The scope of this field extends to and aims at novel high-tech applications such as laser dyes, [5] dyes and pigments for bio-labelling, [6] intravital microscopy applications, [7] and smart sensing devices responding to various external stimuli [8].

It comes as no surprise that the global dyes and pigments market for the year 2020 was determined to be as large as \$ 32.9 billion with an estimated growing rate of about 5% for the next few years. [9] The largest shares of the global production of dyes and pigments are the ones pertaining to textile-dyes and leather-dyes covering together nearly 75% of the global production. Furthermore, printing inks and paper dyes industry hold important shares.

All the above information indicates that the use of dyes and pigments is well-established in everyday life. They appear in our lives dyeing objects made out of various materials e.g. plastic, wood, metals, ceramics, leather, textiles etc. (see **Figure 1**) and are either applied by the manufacturers of the products or can be used by the end-user in order to protect, modify or decorate variety of objects and materials. The variety of paints depending on use and target-surface is enormous and most of the dyes and pigments are readily available to the user. This indicates a vitally tight connection between production and everyday life. Some examples of dyes and pigments used in everyday life are depicted in **Figure 1**. Their versatility is huge, and their applications are massive.

Yet, science is constantly pushing the limits of the corresponding research field and attempts to obtain novel dyes with special functions are unceasingly being made. (Multi)functional dyes and pigments fall in a wider group of materials which can provide certain types of functionality parallel to their main operational scope. In this sense, a functional dye may for instance not only act as protective and/or decorative layer on a material (main scope), but it could act as an environment-responsive component which could in turn render a new material or device responsive and sensitive to various external stimuli (including light, pressure, heat, environment pH changes, solvent polarity etc.). In the large family of functional dyes (and pigments) fall the so-called chromic compounds/materials. These are compounds or materials which are capable of undergoing (ideally) reversible changes in a way that the user can



**Figure 1.**

Examples of dyes used in everyday life as well as in specific applications. (A) Structure of azorubine (also known as E122) a water soluble food-colorant. Photo depicts red-dyed eggs colored with azorubine. (B) Structure of "black-dye" a prominent candidate for dyes-sensitized solar cells. Photograph depicts a solar cell. (C) Structure of a viologen enolate, highly responsive in solvent polarity changes (solvatochromic dye). Photo indicates the drastic color change when moving from water (red) to solvents of lower polarity (adapted with permission by Papadakis et al. [10]) (D) a pyrazoline fluorescent dye of high emission intensity. [11] (photo source: author's property). (E) Antonia Red™ Dextran: a novel polysaccharide with fluorescent labelling and its application in cell-imaging (source: TdB Labs) [12].

grasp information regarding the environment of the material/compound. [8] Novel research attempts intent to render sensing systems applicable in microenvironments e.g. living cells and they have led to a sizable family of dyes suitable for microscopy with numerous applications in biology and medicine (see **Figure 1E**).

#### 4. Conclusion

The variety of commercial dyes and pigments with novel properties and applications is increasing as the needs of the end-users expand. This fact is clearly reflected in the size of the corresponding market and it accounts for the extended global contemporary research endeavors towards new dyes and pigments. Based on these facts, a colorful future is envisioned.

#### Author details

Raffaello Papadakis  
TdB Labs, Uppsala, Sweden

\*Address all correspondence to: [rafpapadakis@gmail.com](mailto:rafpapadakis@gmail.com)

#### IntechOpen

© 2021 The Author(s). Licensee IntechOpen. This chapter is distributed under the terms of the Creative Commons Attribution License (<http://creativecommons.org/licenses/by/3.0>), which permits unrestricted use, distribution, and reproduction in any medium, provided the original work is properly cited. 

## References

- [1] Klaus Hunger (Editor) Industrial Dyes Chemistry, Properties, Applications ISBN 3-527-30426-6. WILEY-VCH Verlag GmbH & Co. KGaA, Weinheim, 2003.
- [2] Maria J. Melo. History of Natural Dyes in the Ancient Mediterranean World in Handbook of Natural Colorants Edited by Bechtold T. and Mussak R., John Wiley & Sons, Ltd, 2009.
- [3] Garfield, S. Mauve: How One Man Invented a Color That Changed the World. W. W. Norton & Company; 2002. ISBN: 978-0393323139.
- [4] Gordon P. F., Gregory, P. Organic Chemistry in Colour, Springer-Verlag, Berlin, 1983
- [5] Kuehne A. J. C. and Gather M.C. Organic Lasers: Recent Developments on Materials, Device Geometries, and Fabrication Techniques Chem. Rev. 2016, 116 (21), 12823-12864. DOI: 10.1021/acs.chemrev.6b00172
- [6] Zhang K. Y., Yu Q., Wei H., Liu S., Zhao Q., and Huang, W. Long-Lived Emissive Probes for Time-Resolved Photoluminescence Bioimaging and Biosensing. Chem. Rev. 2018, 118 (4) 1770-1839 DOI: 10.1021/acs.chemrev.7b00425
- [7] Weigert R. (ed.) Advances in Intravital Microscopy. From Basic to Clinical Research. Springer Dordrecht 2014. ISBN 978-94-017-9360-5. DOI 10.1007/978-94-017-9361-2.
- [8] Bamfield, P. Chromic Phenomena: Technological Applications of Colour Chemistry: Edn 2nd RSC, Cambridge, 2010. ISBN 978-1-84755-868-8. DOI: 10.1039/9781849731034
- [9] Global Dyes & Pigments Market Size Report, 2021-2028 (grandviewresearch.com)
- [10] Papadakis R., Deligkiozi I., Tsolomitis A. Spectroscopic investigation of the solvatochromic behavior of a new synthesized non symmetric viologen dye: Study of the solvent–solute interactions. Anal. Bioanal. Chem. 2010, 397, (6), 2253-2259. DOI: 10.1007/s00216-010-3792-7.
- [11] Matiadis D., Nowak K., Alexandratou E., Hatzidimitriou A., Sagnou M., Papadakis R. Synthesis and (fluoro)solvatochromism of two 3-styryl-2-pyrazoline derivatives bearing benzoic acid moiety: A spectral, crystallographic and computational study. J. Mol. Liq. 2021, 331, 1, 115737. DOI: 10.1016/j.molliq.2021.115737.
- [12] <https://tdblabs.se/products/fluorescent-derivatives/antonia-red-products/antonia-red-dextran/>



# Probing Solvation Effects in Binary Solvent Mixtures with the Use of Solvatochromic Dyes

*Ioanna Deligkiozi and Raffaello Papadakis*

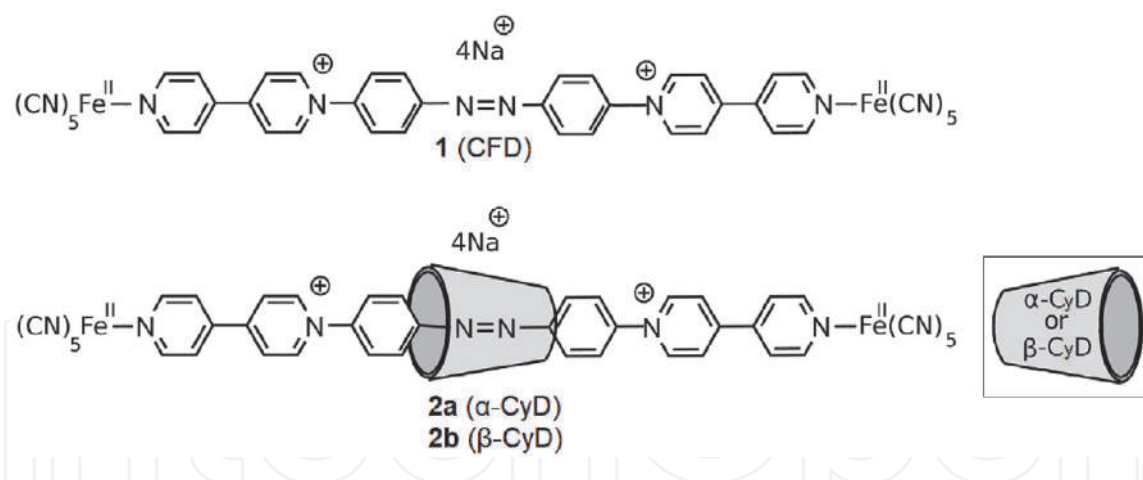
## Abstract

In this work three molecules exhibiting dual sensing solvatochromic behaviors are examined in the context of solvation in binary solvent mixtures (BSMs). The compounds studied involve two functional groups with high responsiveness to solvent polarity namely pentacyanoferrate(II) (PC) and azo groups. Two of these compounds are [2]rotaxanes involving *alpha*- or *beta*- cyclodextrin (CyD) and the third is their CyD-free precursor. The dual solvatochromic behavior of these compounds is investigated in water/ethylene glycol (EG) mixtures and their dual solvatochromic responses are assessed in terms of the intensity of solvatochromism and the extent of preferential solvation. To achieve this the linear solvation model by Kamlet, Abboud and Taft [*J. Organomet. Chem.* 1983, 48, 2877–2887] and the two-phase model of solvation by Bagchi and coworkers [*J. Phys. Chem.* 1991, 95, 3311–3314] are employed. The influence of the presence or lack of CyD (*alpha*- or *beta*-) on these dual solvatochromic sensors is analyzed.

**Keywords:** solvatochromic dyes, rotaxanes, preferential solvation, (non) specific solute-solvent effects, azo dyes

## 1. Introduction

Nowadays, solvatochromic probes (SPs) are regularly utilized in various types of applications which require sensing of environmental/medium effects in either a qualitative or a quantitative manner [1–9]. Today there is a large variety of published solvatochromic dyes corresponding to different media, e.g. organic solvents [8, 10], ionic liquids [10, 11], solvent mixtures [10, 12–15] or solvent comprising polarity modifiers [16]. What often appears to be challenging is the choice of a suitable solvatochromic probe for the description of a physicochemical problem encompassing solvent polarity effects. It has been observed that for the same solvent/cosolvent mixture, different solvatochromic dyes may provide different quantitative results [17, 18]. Indeed in many cases, different spectroscopic techniques applied on the same ternary system solvent/cosolvent/probe(solute) may provide different results. Therefore, probing solvent polarity effects and preferential solvation (PS) phenomena occurring in solvent mixtures of two or more



**Figure 1.**  
The three solvatochromic compounds involved in this study.

solvents are considered as highly difficult tasks [17]. The complexity of those physicochemical problems is high and the interpretation of the solvent-solute or solute-solvent effects sensed by SPs needs to be carefully undertaken. In this work, the authors examine the solvatochromic responses of two probing groups: the azo-group and the pentacyanoferrate(II) group of three molecules dissolved in binary solvent mixtures (BSMs) involving water and ethylene glycol (EG). From the three molecules employed two are [2]rotaxanes involving *alpha*- or *beta*- cyclodextrin (CyD) (compounds **2a** and **2b** respectively, **Figure 1**) and the third is their precursor lacking a CyD wheel (compound **1**, **Figure 1**; in the text will be called cyclodextrin-free dumbbell-like compound or CFD). All three are recently developed solvatochromic compounds [19] and they involve the same  $\pi$ -conjugated viologen-based linear skeletons bearing an azobenzene bridge and pentacyanoferrate(II) end-groups (**Figure 1**). The aforementioned compounds fall under the umbrella of an important family of multifunctional dyes primarily because of the high technological and industrial importance of azobenzene dyes [20–22] as well as the pronounced chromic and redox behavior [23], photochromism [24], photoconductivity [25] and strong electron withdrawing aptitude of viologens (also known as paraquats) [23, 26]. This strong electron accepting capacity of para- and mono-quats is vital for the development of push-pull systems [27–30]. Towards the latter milestone the use of suitable electron donating substituents is vital. Papadakis et al. has shown that pentacyanoferrate(II) units can trigger an intense solvatochromic behavior in such systems in various types of media [14, 16, 30, 31] and more recently Deligkiozi et al. hinted that the  $n \rightarrow \pi^*$  transitions of the azo group in **1** and **2a,b** are sensitive to solvent polarity [19]. In this work the dual solvatochromic sensing of these compounds is thoroughly examined in terms of solvent-solute, solvent-solvent and preferential solvation effects. In this work water/ethylene glycol mixtures were chosen as perfect BSM candidate-models of dipolar media with substantial contributions in the development of specific effects (mainly H-bonding).

## 2. Materials and methods

### 2.1 General information

All correlations (single or multi- parameter linear, polynomial regressions and contribution analyses were carried out using statistical software *R* (ver.:3.5.3). Integrations as well as the graphical determination of isosolvation points were all performed using QtiPlot (ver.: 0.9.9).

All compounds involved in this work (**1** and **2a,b**; **Figure 1**) have been reported in earlier publication by the author and coworkers and their synthesis, isolation and spectral analysis have been also thoroughly described [19]. All solvatochromic UV–Vis shifts have been recorded on a Perkin–Elmer Lambda 25 UV/Vis spectrophotometer. The deconvolutions of all UV–Vis spectra were implemented according to previous work [19].

## 2.2 Examining the stability of compounds 1,2a,b in solution

All solvatochromic compounds used in this work are isolated as stable solid compounds of green-blue color. The measurements presented were conducted in fresh solutions of each compound in the desired H<sub>2</sub>O/EG mixtures (typically prepared 15 min prior to measurement). That time corresponds to the equilibration time (each sample was vigorously stirred after mixing). Directly after this period of time their electronic absorption spectra were recorded. It was observed that in all cases the solutions remained unmodified as concluded through check of the absorbances of the bands maxima which were found to be stable for at least 30 minutes after equilibration. This observation clearly indicates that all three compounds are stable in solution and therefore suitable for the current investigation.

## 2.3 Preferential solvation model

In this work a renowned PS model is employed in order to describe PS phenomena occurring in BSMs comprising solvatochromic solutes. The model was introduced by Bagchi and coworkers about thirty years ago and is also known as “the two-phase model of solvation” (TPMS) [32–34]. TPMS considers that solvent molecules in a BSM are distributed between a local phase and a bulk phase according to Eq. 1. The local phase lies in the vicinity of the solvation area.

$$\overline{S_2} + S_1 \rightleftharpoons \overline{S_1} + S_2 \quad (1)$$

In Eq. 1  $S_1$  and  $S_2$  symbolize the two mixed solvents in the bulk phase while  $\overline{S_1}$  and  $\overline{S_2}$  symbolize the two solvents in the solvation (local) phase. Throughout this work water will be considered as  $S_1$  whereas EG as  $S_2$ . At the equilibrium described by Eq. 1, PS constant ( $K_{ps}$ ) will be related to an expression comprising both solvent-solute interaction energies (Eq. 2).

$$kT \ln K_{PS} = [\epsilon_{S2} - \epsilon_{S1}] + \left[ (N_1 - N_2)\epsilon_{12} - (N_1^0 - N_2^0)\epsilon_{12}^0 - N_1\epsilon_{11} + N_1^0\epsilon_{11}^0 + N_2\epsilon_{22} - N_2^0\epsilon_{22}^0 + \frac{(\epsilon_{11} - \epsilon_{22})}{2} - \frac{(\epsilon_{11}^0 - \epsilon_{22}^0)}{2} \right] \quad (2)$$

In Eq. 2  $\epsilon_{Si}$  are the interaction energies among the solute and  $i$ -solvent while  $\epsilon_{ij}$  corresponds to the interaction energies between solvents  $i$  and  $j$ .  $N_i$  corresponds to the number of  $i$ -solvent molecules. The bulk phase in solvent molecule numbers is designated with the superscript 0. It is noteworthy that Eq. 2 involves two terms. The first bracketed term in the right-hand side of the equation corresponds to the contribution of solute-solvent interactions, while the terms in the second bracket describe the solvent non-ideality effects.

Finally, Eq. 3, provides  $K_{ps}$  (the preferential solvation constant) related to both bulk ( $x$ ) and local ( $y$ ) solvent mole fractions along with the measured transition



energies of the indicator solute ( $E_T$ ) observed in neat solvent  $S_1$  ( $E_{T,1}$ ), neat solvent  $S_2$  ( $E_{T,2}$ ) and the mixture of  $S_1$  and  $S_2$  ( $E_{T,m}$ ).

$$K_{PS} = \frac{y_1 x_2}{y_2 x_1} = \frac{E_{T,m} - E_{T,2}}{E_{T,1} - E_{T,2}} \cdot \frac{x_2}{x_1} \quad (3)$$

## 2.4 Applying the CNIBS/R-K equation

In order to determine isosolvation points (see below) pertaining to PS occurring in solutions of **1** and **2a,b** in aqueous EG, Redlich–Kister (CNIBS/R–K) equation [35], was employed so as to algebraically describe the dependence of experimental transition energy  $E_T$  ( $n \rightarrow \pi^*$  (azo) and Metal to Ligand Charge Transfer (MLCT)) on solvent/cosolvent bulk mole fractions ( $x_1, x_2$ ) (Eq. (4)). In this work water is considered as solvent  $S_1$  (i.e. water mole fraction is  $x_1$ ). Noteworthy, Eq. 4 yields  $E_T$  values corresponding to neat solvents  $S_1$  and  $S_2$  ( $E_{T,1}^0$  and  $E_{T,2}^0$ ) when any of  $x_2$  and  $x_1$  is set to 0 respectively.

$$E_{T,m} = x_1 E_{T,1}^0 + x_2 E_{T,2}^0 + x_1 x_2 \sum_{j=0}^k A_j (x_1 - x_2)^j \quad (4)$$

## 2.5 Determining isosolvation points

For a BSM involving solvents  $S_1$  and  $S_2$  and a solvatochromic solute, when  $x_{iso}^T(S_2) < 0.5$  then PS of the solute by solvent  $S_2$  is observed and vice versa when  $x_{iso}^T(S_1) > 0.5$  [18] (where  $T$  corresponds to the transition of interest i.e. MLCT (PCF) or  $n \rightarrow \pi^*$  (azo) for this study).

$$x_{iso}^T = x^T \text{ at which } E_{T,m} = \frac{E_{T,1}^0 + E_{T,2}^0}{2}.$$

For the determination of  $x_{iso}^T$  the polynomial expressions obtained through Eq. 5 were utilized.  $E_{T,m} = f(x_1)$  were first plotted and then  $x_{iso}^T$  were determined graphically using the data reader tool of Qtiplot 0.9.9.

## 2.6 Quantifying the difference in the extent of PS

In order to quantify the difference of the extent of PS in aqueous EG through the two different types of transitions (MLCT(PCF) or  $n \rightarrow \pi^*$  (azo)) of **1,2a,b** the following integrals difference ( $\Delta \int$ ) was employed.

$$\Delta \int = \left( \int_0^1 y_{EG}^{n \rightarrow \pi^*}(x_{EG}) dx_{EG} \right) - \left( \int_0^1 y_{EG}^{mlct}(x_{EG}) dx_{EG} \right) \quad (5)$$

In Eq. 5  $y_{EG}^{n \rightarrow \pi^*}$  and  $y_{EG}^{MLCT}$  are the local EG molar fractions determined through the TPMS methodology pertaining to the  $n \rightarrow \pi^*$  (azo) and MLCT (PCF) transitions respectively.

## 2.7 Single parameter regression analyses

To understand the role of various solvatochromic parameters expressing solvent polarity, single regression analyses were implemented (general Eq. (6)). SSP-LSERs

$$E_{T,m} = E_{T,m}^0 + p_i \cdot SP_i, r^2 \tag{6}$$

Where  $T = MLCT$  or  $n \rightarrow \pi^*$  and  $SP$  a solvent polarity parameter (in this work:  $E_T^N$ ,  $\pi^*$ ,  $\alpha$ , or  $\beta$ ).  $r^2$ : correlation coefficient.

### 2.8 KAT equation and contribution analysis

Moreover a multiparametric model was employed in order to assess the relative contribution of various solvatochromic parameters expressing solvent polarity, simultaneously. That model is the LSER introduced by Kamlet Abboud and Taft (KAT equation). This renowned LSER (Eq. 7) can provide information on the importance of dipolarity/polarizability, Hydrogen bond donor (HBD) acidity and Hydrogen bond acceptor (HBA) basicity of neat solvents or solvent mixtures.

$$E_{T,m} = E_{T,m}^0 + s\pi^* + a\alpha + b\beta \tag{7}$$

Where

$$T = MLCT \text{ or } n \rightarrow \pi^*$$

Through Eqs. 8–9 it is possible to determine the relative contribution ( $r_{s_i}$ ) of each of the involved parameters. The procedure has thoroughly been described in previous works [28, 31, 36].

$$r_{s_i} = \frac{\sigma_i'}{\sum_{i=1}^n \sigma_i'} \tag{8}$$

and

$x_{EG}$	$E_{n \rightarrow \pi^*} \text{ (kcal.mol}^{-1}\text{)}^a$			$E_{MLCT} \text{ (kcal.mol}^{-1}\text{)}^a$		
	<b>1</b>	<b>2a</b>	<b>2b</b>	<b>1</b>	<b>2a</b>	<b>2b</b>
0	73.12	74.26	74.26	51.46	49.02	50.71
0.051	71.48	73.88	73.50	49.06	48.67	48.85
0.097	72.38	73.50	73.88	48.44	47.16	47.18
0.139	70.77	72.38	72.57	47.26	46.15	47.18
0.178	69.91	71.48	71.48	46.23	45.36	46.67
0.212	69.73	71.48	71.48	46.34	44.50	46.50
0.245	69.73	71.48	71.84	45.29	44.10	46.50
0.392	69.73	70.95	71.66	45.78	43.74	44.85
0.492	69.73	70.77	71.12	45.06	42.94	43.66
0.659	69.73	70.77	70.77	43.95	41.85	42.83
0.854	69.73	70.77	70.77	42.94	41.08	41.94
1	69.73	70.42	70.42	41.60	40.35	40.94

<sup>a</sup>Data from reference: [19].

**Table 1.**  
 Solvatochromic shifts of **1** and **2a,b** in aqueous EG and solvent polarity parameters.

$$\sigma'_i = |\sigma_i| \sqrt{\frac{\sum_{j=1}^m (S_{ij} - \bar{S}_i)^2}{\sum_{j=1}^m (E_{Tj} - \bar{E}_T)^2}} \quad (9)$$

where  $S_i$  corresponds to the correlation to each of any of the three parameter involved in Eq. 8 for the various solvent/cosolvent molar ratios examined (number of different mole ratios examined in this work:  $m = 12$ ; see **Table 1**).

### 3. Results and discussion

#### 3.1 The bisensing solvatochromic compounds **1** and **2a,b**

Recently Deligkiozi et al. [19] and subsequently Papadakis et al. [37] reported on the solvatochromic behavior of compounds **1**, **2a-b** (**Figure 1**). It has been pointed out that the energy of the MLCT transition in these compounds is intensely dependent on the polarity of the environment and its nature and characteristics have been thoroughly described in a series of research works [14–16, 19, 30, 31]. These compounds have been studied in a rather narrow solvent polarity range and specifically in aqueous EG mixtures as well as in neat water and EG. All three compounds are very soluble in both those solvents and their mixtures. Despite the small solvent polarity difference observed when moving from water to EG, the recorded difference in MLCT energy of **1** and **2a,b** was reported to be significantly high, following the sequence:

$$\begin{aligned} |\Delta_{\text{H}_2\text{O}}^{\text{EG}}(\tilde{\nu}_{\text{MLCT}}\mathbf{1})| &= 3451 \text{ cm}^{-1} > |\Delta_{\text{H}_2\text{O}}^{\text{EG}}(\tilde{\nu}_{\text{MLCT}}\mathbf{2a})| = 3419 \text{ cm}^{-1} > \\ &> |\Delta_{\text{H}_2\text{O}}^{\text{EG}}(\tilde{\nu}_{\text{MLCT}}\mathbf{2b})| = 3033 \text{ cm}^{-1}. \end{aligned}$$

Interestingly, all three compounds also exhibit another transition which is significantly influenced by solvent polarity. The latter is attributed to the azobenzene group and corresponds to the forbidden  $n \rightarrow \pi^*$  transition of the lone pairs of electrons of the azo nitrogen atoms and is located at  $\lambda$  ranging within 385–410 nm strongly depending on the polarity of the solvent. The solvatochromism of azobenzene-based compounds has been thoroughly investigated in the past and there is clear evidence of the solvent dependent nature of the  $n \rightarrow \pi^*$  and  $\pi \rightarrow \pi^*$  azo transitions [38–41]. This comes as no surprise as the nitrogen atoms of the azo group can readily interact with solvent molecules (in case of compound **1**) or the interior groups of CyDs (*alpha*- for **2a** and *beta*- for **2b**). Typically, the energy of the  $n \rightarrow \pi^*$  transition shifts about 6 nm hypsochromically just upon insertion of the CyD wheel. For instance while in neat water  $\lambda_{(n \rightarrow \pi^*)} \cong 391$  nm for the CFD compound (**1**) while  $\lambda_{(n \rightarrow \pi^*)} \cong 385$  nm when the CyD wheel is threaded and stationed around the azobenzene group (same value for both **2a** and **2b**). Comparable shifts are observed at various mole fractions of water in aqueous EG (see **Table 1**). Yet, the effect of solvents is much more important as shifts of even 25 nm are observed when simply moving from water to EG i.e. two solvents with many similarities when it comes to solvent polarity and structuredness [18]. The observed shifts recorded followed the trend:

$$|\Delta_{\text{H}_2\text{O}}^{\text{EG}}(\tilde{\nu}_{n \rightarrow \pi^*}\mathbf{1})| = 1186 \text{ cm}^{-1} < |\Delta_{\text{H}_2\text{O}}^{\text{EG}}(\tilde{\nu}_{n \rightarrow \pi^*}\mathbf{2a})| = |\Delta_{\text{H}_2\text{O}}^{\text{EG}}(\tilde{\nu}_{n \rightarrow \pi^*}\mathbf{2b})| = 1345 \text{ cm}^{-1}.$$

It is important to note here that the  $n \rightarrow \pi^*$  transition is convoluted with the MLCT and  $\pi \rightarrow \pi^*$  transitions and a thorough deconvolution analysis has been already published recently [19]. In this work the used values of the energies for  $n \rightarrow \pi^*$  and MLCT transitions for **1** and **2a,b** correspond to the aforementioned published deconvolution values (see **Figure 2** and **Table 1**).

Taken together, there is clear evidence that all three compounds are considered to be bisensing as they involve two functional groups (FC and azo groups) both responding to solvent polarity changes however at different extents (**Table 1**) as it will be thoroughly analyzed.

### 3.2 Resonance structures of compounds **1** and **2a,b**

For a better understanding of the dual solvatochromic behavior of all compounds the analysis of their resonance structures is vital. While resonance structure **I** (**Figure 3**) is more important in the electronic ground state and comprises Fe(II) and the all-aromatic structure of the ligand (L), Resonance structure **II** (**Figure 3**) becomes more important in the MLCT excited state of molecules **1** and **2a,b**. The latter resonance structure comprises the oxidized metal center (Fe(III)) and the quinoidal structured ligand as a result of the acceptance of an electron transferred by Fe(II) upon oxidation occurring via absorption of light (MLCT). (Structure **II** is one of the corresponding resonance structures of the type:  $[(\text{Fe}^{\text{III}} - \text{L}^{\bullet+})]$ ).

Finally, structure **III** (**Figure 3**) retains the oxidized  $\text{Fe}^{\text{III}}$  center however displays the possibility of stabilization of the  $>\text{N}^{\bullet+}$  by the azo group. (It is noteworthy that the azo group is known to stabilize carbocations in a similar fashion [42]). The interplay between Resonance structures **II** and **III** can be alternatively written as:  $[(\text{Fe}^{\text{III}} - (\text{py}^{\bullet+}) - \text{azo}) \leftrightarrow (\text{Fe}^{\text{III}} - (\text{py}^+) - \text{azo}^{\bullet})]$ .

The latter interaction of the azo group with its partly reduced neighboring viologen pyridin heterocycle obviously influences the  $n \rightarrow \pi^*$  transition of the azo group which is in turn largely influenced by its interactions in solution with solvent molecules (this applies only to the case of compound **1**) or the interactions with the CyD interior environment (this is obviously valid only for rotaxanes **2a** and **b**). In any case, through Structures **II** and **III** it becomes obvious that the  $n \rightarrow \pi^*$  transitions and the solvatochromism of the azo group is largely influenced by the  $(\text{Fe}^{\text{II}} - \text{L})$  system attached to it in  $\pi$ -conjugation.

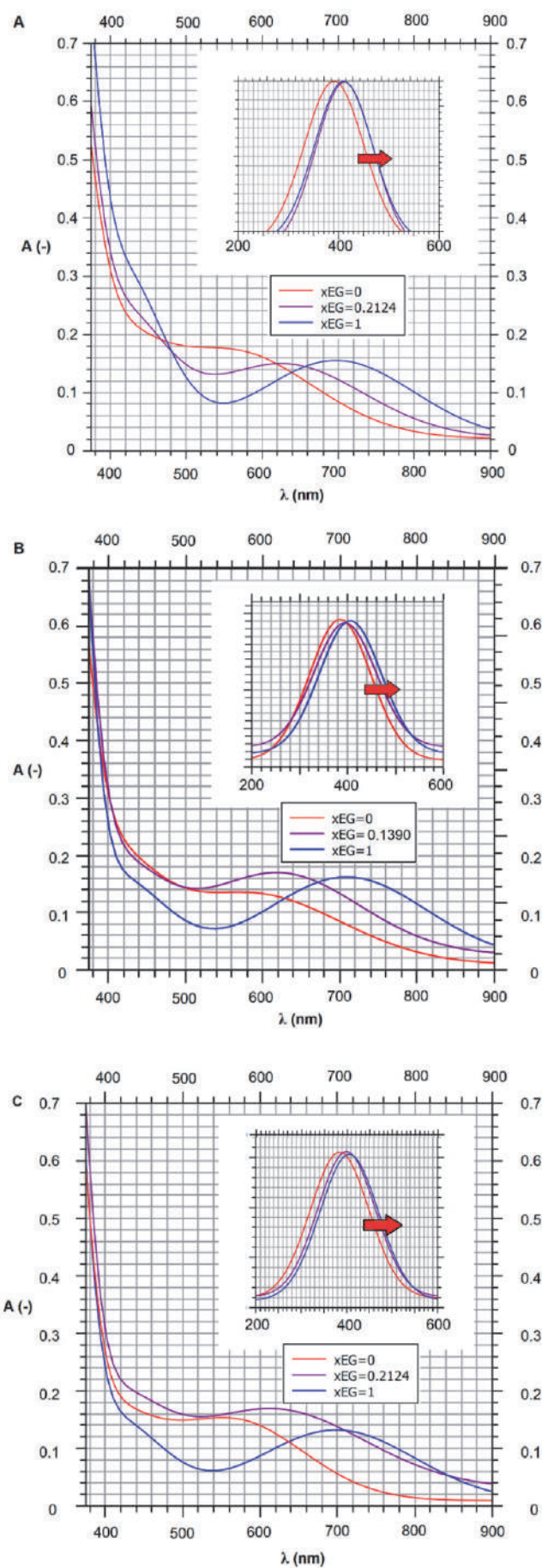
Frontier orbital representations of the tetraanion of dye **1** ( $1^{4-}$ ) (for more details see ref.: [19]) also support the fact that the FC groups and azo groups are behaving as electron donating since the HOMO are mostly localized in the regions of the FC and azobenzene moieties (**Figure 4**). On the other hand, LUMO are mostly localized around the quaternized electron deficient viologen parts of the solvatochromic compounds (**Figure 4**). This is an additional hint to the dominating resonance structures presented in **Figure 3**.

### 3.3 Solute-solvent interactions

It is also noteworthy that in cases **2a,b** the  $n \rightarrow \pi^*$  transition of the azo group is even more affected by the behavior of the 4,4'-bipyridine-Fe(II) system (which is in  $\pi$ -conjugation with the azobenzene moiety) than happens in case **1**. This is associated with the fact that CyD (either *alpha*- or *beta*-) does not allow any direct interaction of the azo group with any of the solvents (water or EG; see **Figure 5**).

It is known that solvents with  $\log P_{oc/w} < -0.3$  cannot penetrate the highly lipophilic cavity of cyclodextrins (for EG it is  $\log P_{oc/w} = -1.3 < -0.3$  rendering it very hydrophilic to enter the CyD cavity ( $P_{oc/w}$  is the 1-octanol/water partition coefficient) [43]. This is clearly manifested by the linear correlation between the

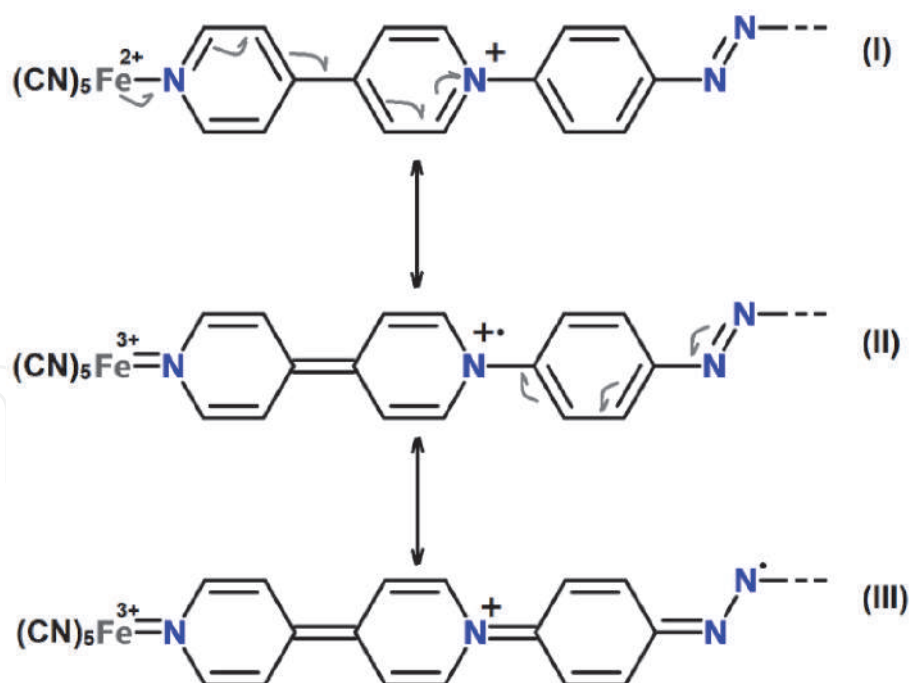




**Figure 2.**

The electronic spectra of compounds A) **1**, B) **2a**, and C) **2b** recorded in water, EG and selected water/EG mixtures. Displayed wavelength range 380–900 nm. Insets indicate the  $n \rightarrow \pi^*$  bands after deconvolution.





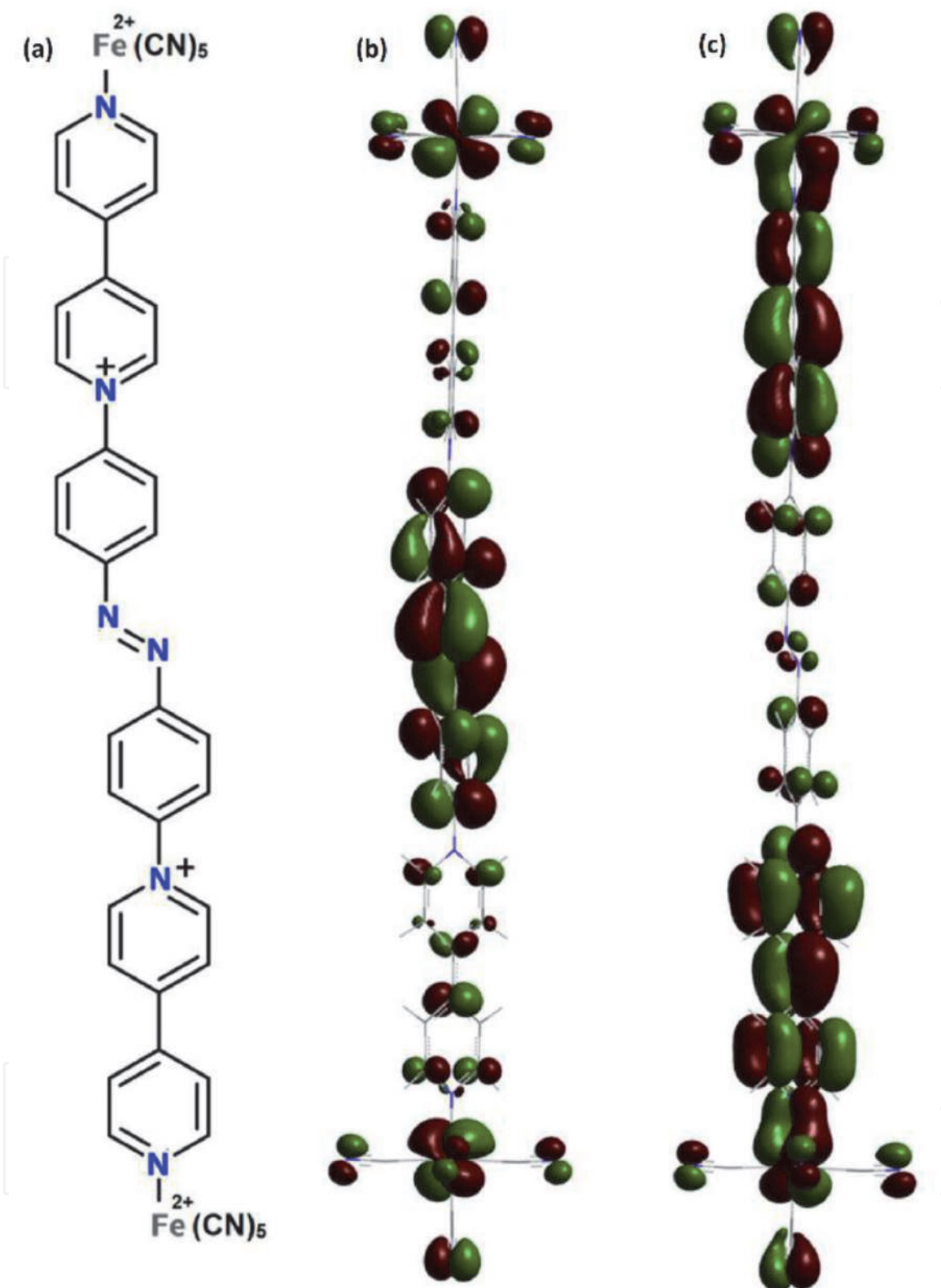
**Figure 3.**  
 Characteristic resonance structures of compound 1.

MLCT and  $n \rightarrow \pi^*$  transitions energies of **2a,b** at various mole fractions of EG (see **Figure 6**). In case of compound **1** such a linear behavior is not observed (**Figure 6**).

### 3.4 Quantification of the solvatochromism of the FC and azo groups

A pertinent way to quantify, predict and rationalize solvent effects is the use of linear solvation energy relationships (LSERs). This approach has been employed in numerous research works focusing on solvent effect on a large variety of physico-chemical properties [8, 10, 44–46]. The solvatochromism of PC complexes has been thoroughly investigated in this fashion as well [15, 16, 19, 31]. Particularly in case of PC complexes bearing pyridinic ligands (such as **1** and **2a,b**) it has been shown that the MLCT transition energies are largely affected by the dipolarity/polarizability of the medium as well as hydrogen bond donor (HBD) and Lewis acidity [15, 16, 19, 31]. Deligkiozi et al. recently reported the corresponding correlations and furthermore hinted that the energy of the  $n \rightarrow \pi^*$  of the azo group in **1** and **2a,b** is also sensitive to solvent polarity changes, thus revealing a dual sensing aptitude of solvent polarity for these compounds [19]. Nevertheless, that work mainly focused on the MLCT transitions of these three compounds. Herein, the author focuses further on the solvents effects on the solvatochromic behavior of the azo group of **1** and **2a,b** and examines this dual solvatochromic behavior.

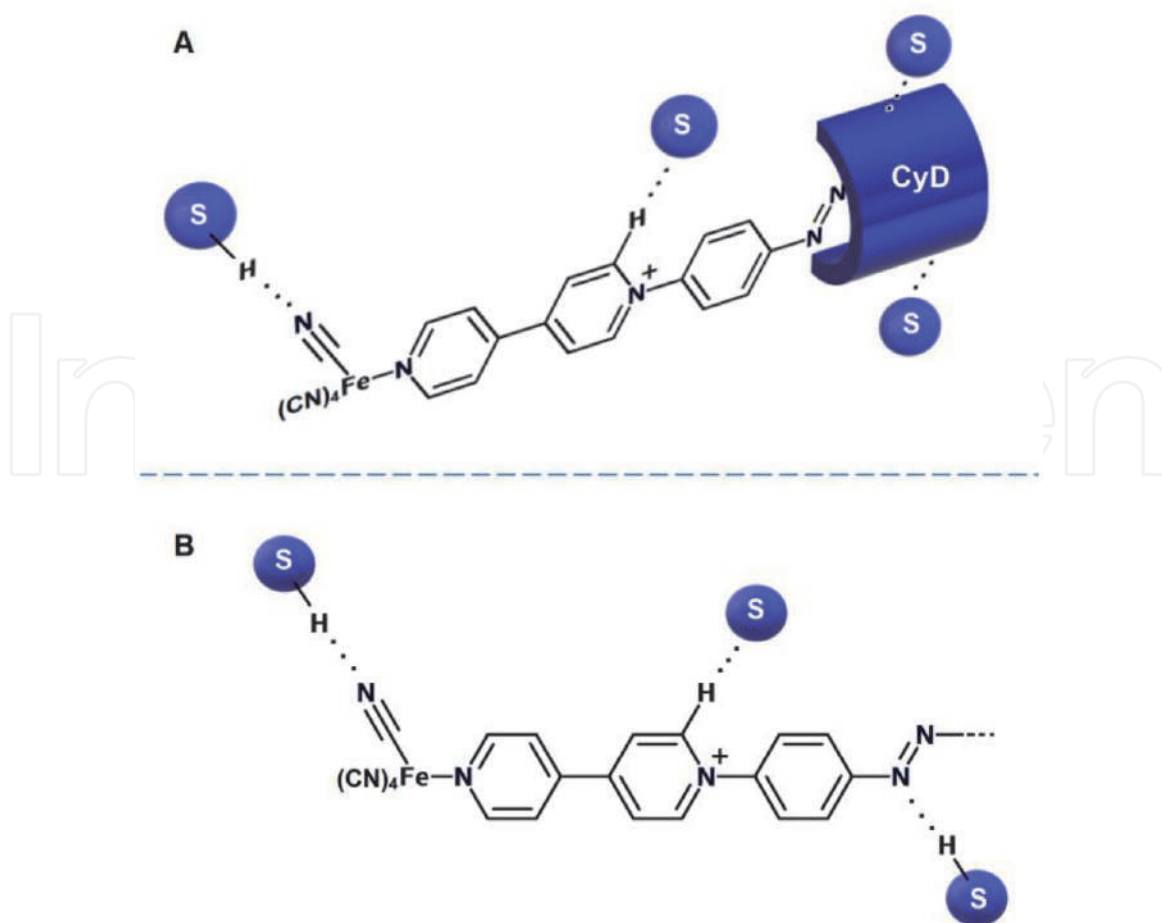
Plots  $E_{n \rightarrow \pi^*}$  vs  $E_{MLCT}$  (**Figure 6**) indicate fairly good linear correlations for the two rotaxanes (**2a,b**) however a severe deviation from linearity in case of the CFD compound (**1**). This is a stimulating finding pertaining to the structural diversity between the two rotaxanes and their CFD precursor. What this finding implies is that for compounds **2a,b** the medium responsive behavior of the azo group (expressed through  $n \rightarrow \pi^*$  transitions) is expected to be analogous to that of the FC groups, at least qualitatively. Furthermore, the duality of solvent polarity sensing aptitude of **1** is anticipated as more pronounced. In order to shed light on these two hypotheses a series of correlations utilizing monoparametric LSERs was accomplished for all three compounds.



**Figure 4.** Structure of the anion of dye **1** (a) and illustrations of the frontier molecular orbitals (MOs) of the anion of the dye **1**<sup>4-</sup>: HOMO (b) and LUMO (c) calculated on the B3P86/6-311++G(d,p) basis/vacuum (0.02 contour plots).

### 3.5 Single solvent polarity parameter involving LSERs

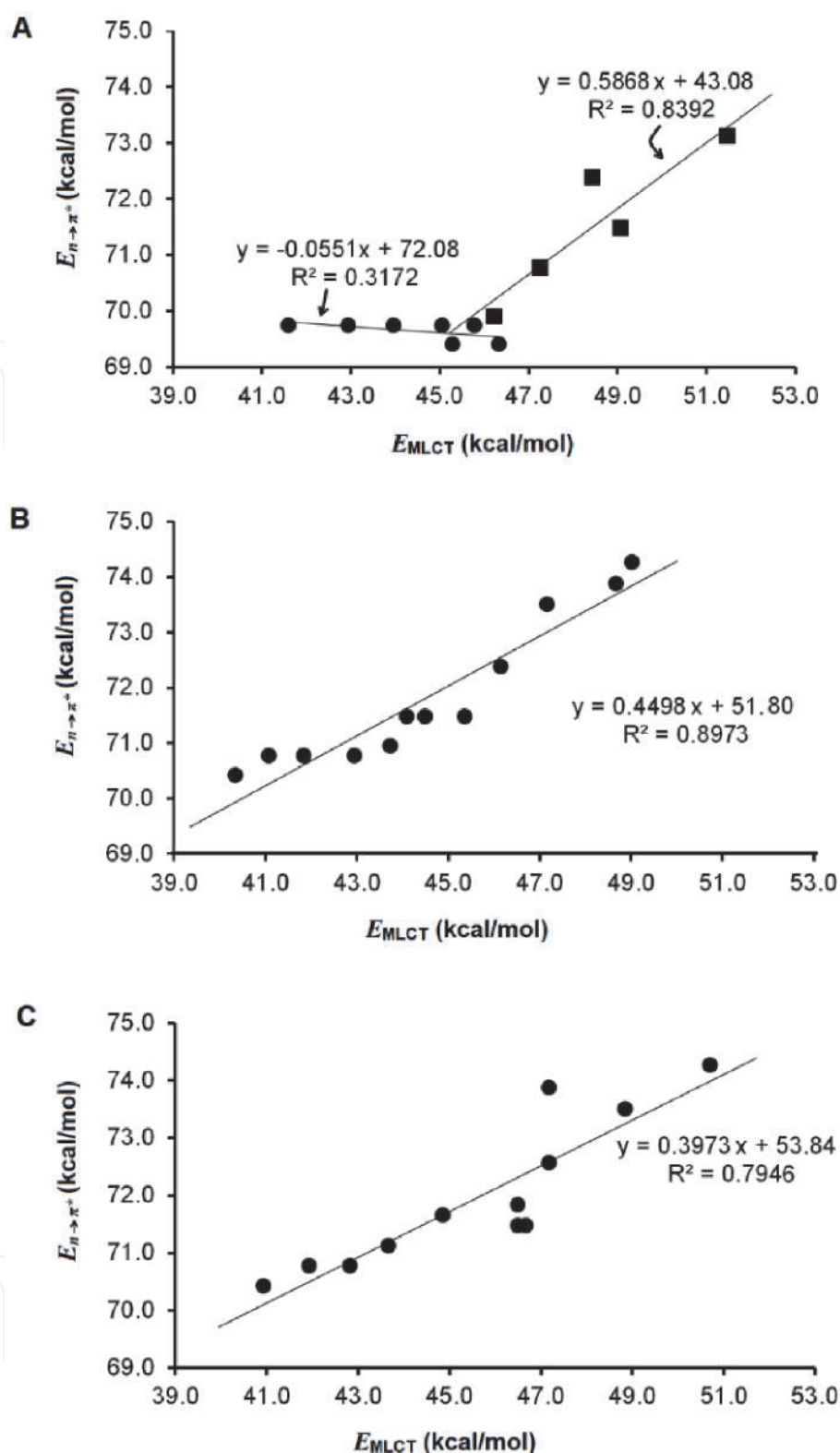
Single solvent polarity parameter involving LSERs (SSP-LSERs) were employed in order to investigate the importance of various solvent polarity parameters on  $n \rightarrow \pi^*$  and MLCT transitions of **1** and **2a,b**. The SPPs utilized were the following:



**Figure 5.**  
 Illustration of the possible solute-solvent interactions in A) the rotaxanes **2a,b** and B) their CFD precursor **1** (S represents a solvent molecule or a solvent-cosolvent complex).

Reichardt's solvent polarity scale:  $E_T^N$ ,  $\pi^*$ ,  $\alpha$ , and  $\beta$ . The latter three are parameters involved in KAT equation expressing dipolarity/polarizability, HBD-acidity, and HBA-basicity respectively [47]. It is obvious that rotaxanes **2a** and **2b** exhibit  $n \rightarrow \pi^*$  transition energies which correlate linearly with Reichardt's polarity scale  $E_T^N$  varying within 1.000 for water and 0.790 for EG (**Figure 7**). In contrast, the fitted curve between  $n \rightarrow \pi^*$  transition energies of **1** and  $E_T^N$  is not a straight line (**Figure 7**). This finding for the solvatochromism of the azo group of compound **1** implies a different behavior compared to either of the rotaxanes **2a,b** or even the MLCT transitions of the same compound. Moreover, as  $E_T^N$  is a measure of dipolarity and Lewis acidity of the medium, the aforementioned results indicate a significantly lower dependence of the  $n \rightarrow \pi^*$  energies on these solvent polarity features for compound **1**. Similar results were obtained for the correlations between  $n \rightarrow \pi^*$  transitions for all three compounds and parameters  $\pi^*$  and  $\alpha$ , expressing solvent dipolarity/polarizability and HBD-acidity respectively (**Figures 7 and 8**). In those cases compound **1** continued to differ from compounds **2a-b**. This comes as no surprise as the connection between  $E_T^N$  scale and KAT parameters  $\pi^*$  and  $\alpha$  is known (as already mentioned  $E_T^N$  is a measure of solvent dipolarity and Lewis acidity) [10]. Very interestingly, the  $n \rightarrow \pi^*$  energies of compound **1** correlate better with parameter  $\beta$  (involved in KAT equation and expressing HBA-basicity) than happens in case of the two rotaxanes **2a,b** (**Figure 8**).

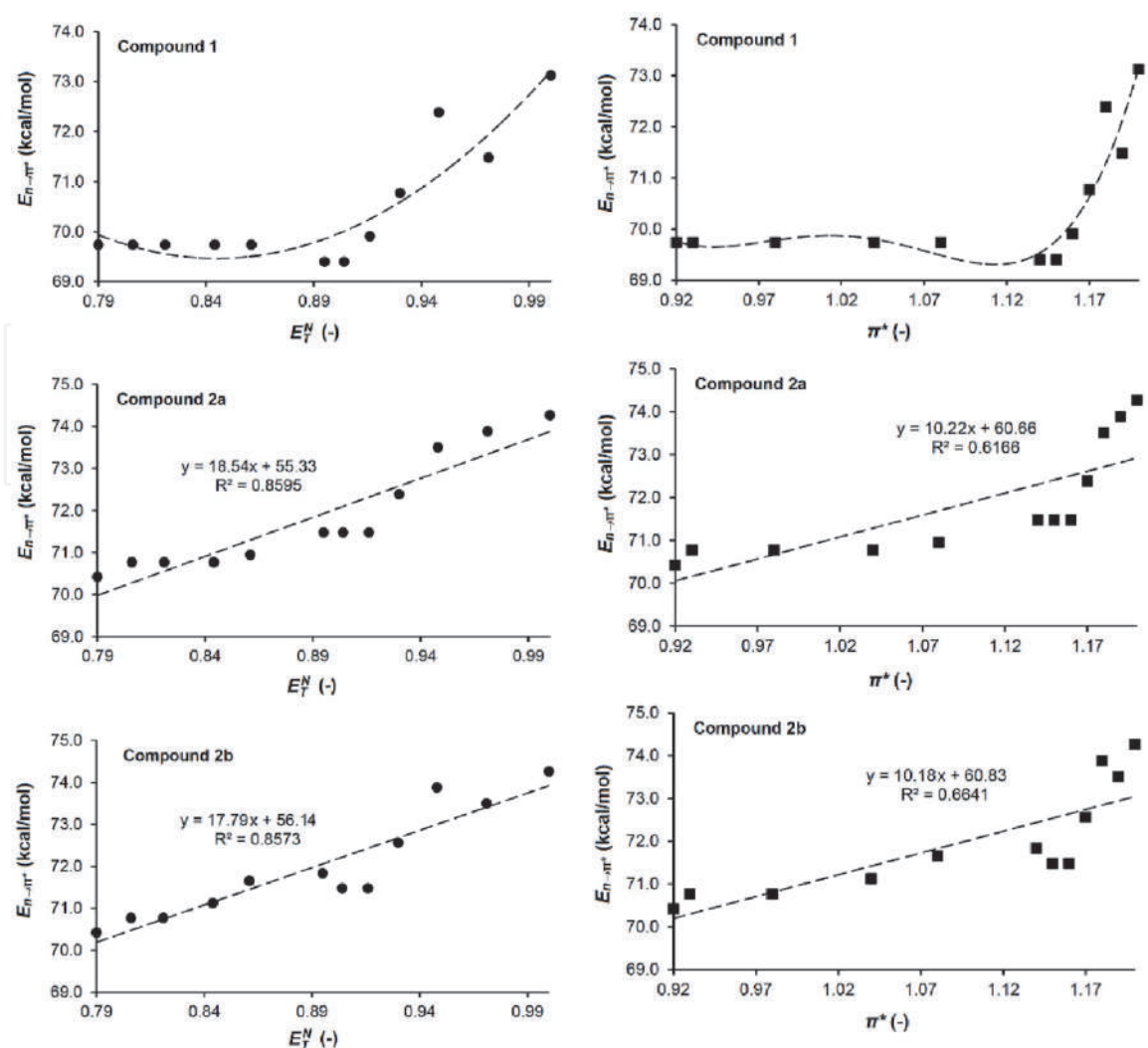
For all three compounds the two main solvatochromic functional groups are the PCF and azo groups which both behave as fairly good HBA-bases being prone to formation of hydrogen bonds between the  $-\text{CN}$  and  $-\text{N}=\text{N}-$  groups respectively and

**Figure 6.**

Plots of the type  $E_{n \rightarrow \pi^*}$  vs  $E_{MLCT}$  for (A) compound **1**, (B) compound **2a**, and (C) compound **2b**.

hydrogen atoms of protic solvents (like water and EG). Therefore, the nearly linear correlation observed between  $E_{n \rightarrow \pi^*}$  and parameter  $\beta$  for compound **1**, indicates another type of solute-solvent interaction less pronounced in rotaxanes **2a,b** (Figure 5). The *ortho*-hydrogen atoms of pyridinium salts lying very close to the quaternized nitrogen are known to undergo deuterium-exchange [49–51]. The *ortho*-protons are significantly deshielded with chemical shifts around 9 ppm and sometimes close to 10 ppm (9.30 for **1**, 9.28 for **2b** and 9.27 ppm for **2a**) [19]. It is therefore anticipated that these hydrogen atoms are prone to interactions with polar





**Figure 7.** *Left column:* Plots of  $n \rightarrow \pi^*$  energies determined in aqueous EG mixtures vs Reichardt's solvent polarity scale for compounds **1**, **2a** and **2b**. *Right column:* Plots of  $n \rightarrow \pi^*$  energies determined in aqueous EG mixtures vs solvent polarity parameter  $\pi^*$  for compounds **1**, **2a** and **2b** [48].

solvent molecules. Nevertheless, due to the presence of *alpha*- or *beta*- CyD in compounds **2a** and **2b** this interaction is somewhat hindered when compared to the CFD precursor **1**. In the latter case the *ortho*-hydrogen atoms can freely interact with the solvent molecules which in this particular case of interaction behave as HBA-bases. This interaction can clearly influence the  $n \rightarrow \pi^*$  energy of **1**, as this region lies very close to the azobenzene group but also due to  $\pi$ -conjugation between the azobenzene group and the viologen.

Taken together, compound **1**, behaves differently than compounds **2a,b** and constitutes an interesting case where the two solvatochromic functional groups provide significantly different “information” about the polarity effects in their vicinity. In other words, based on SSP-LSERs compound **1** clearly behaves as a solvatochromic compound with dual sensitivity. The overall situation for all three compounds is schematically illustrated in **Figure 9** where the degree of success of each SSP-LSER is marked with colors (**Table 2**).

### 3.6 Multiparametric LSERs

An alternative way to compare and quantify the solvatochromism of the two solvatochromic chromophores for **1** and **2a,b** is by employing the multiparametric LSERs. Such LSERs may involve various solvent polarity parameters, each of them



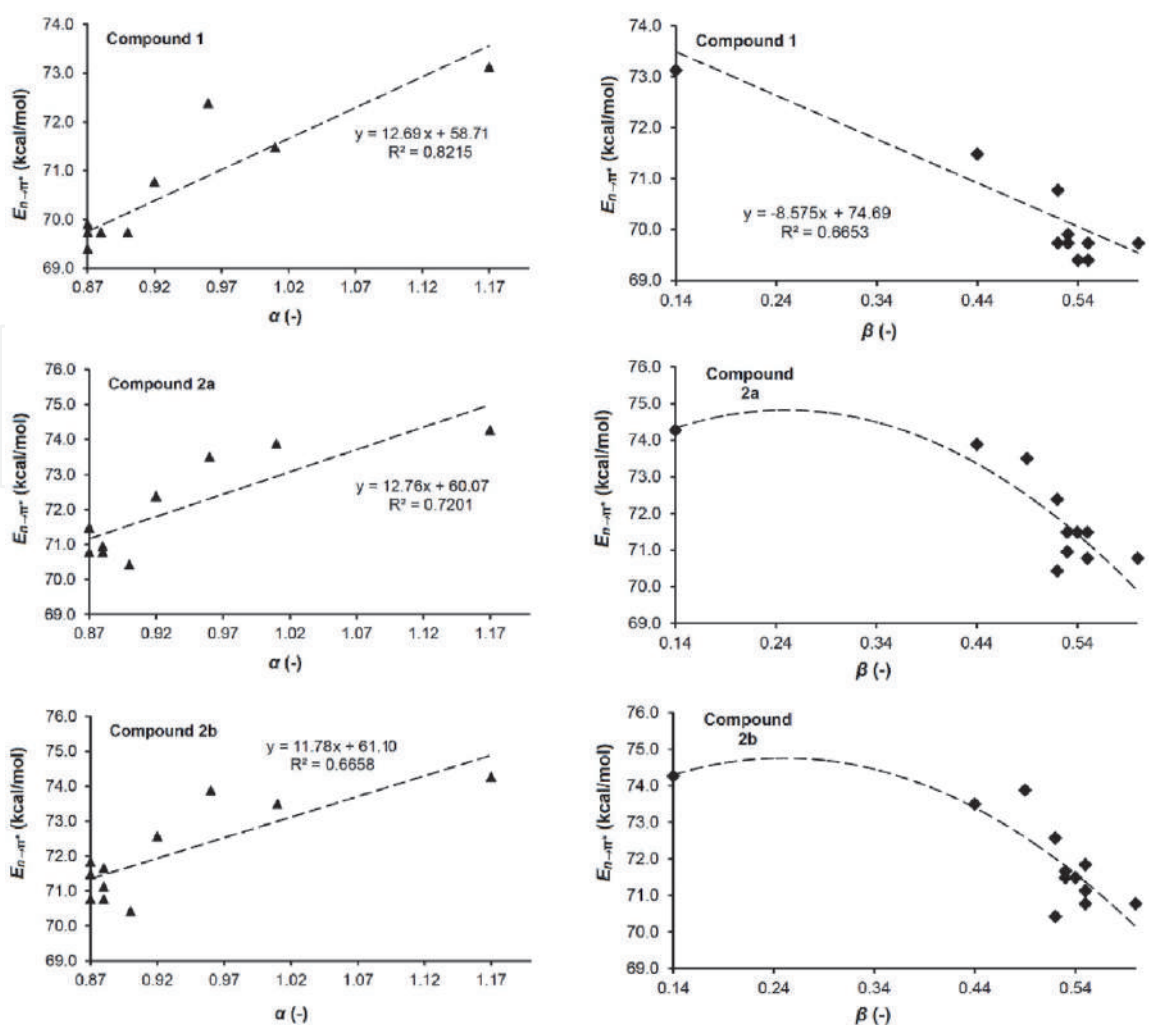


Figure 8.

Left column: Plots of  $n \rightarrow \pi^*$  energies determined in aqueous EG mixtures vs solvent polarity parameter  $\alpha$  for compounds **1**, **2a** and **2b**. Right column: Plots of  $n \rightarrow \pi^*$  energies determined in aqueous EG mixtures vs solvent polarity parameter  $\beta$  for compounds **1**, **2a** and **2b** [48].

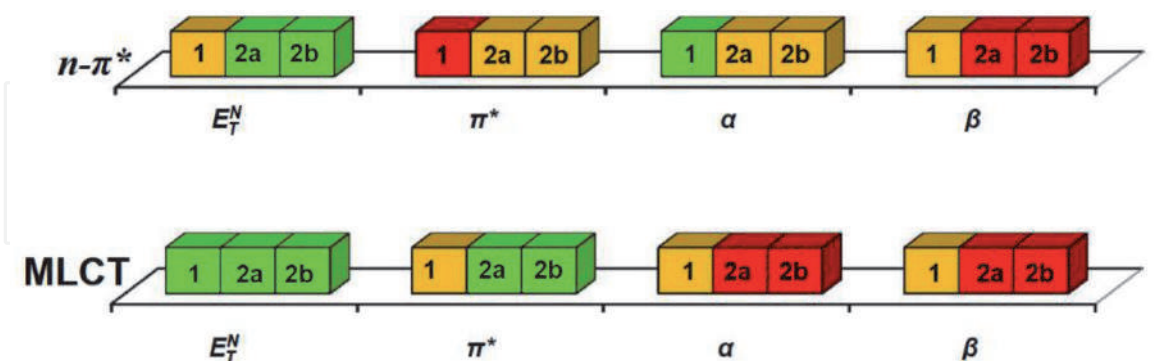


Figure 9.

Illustration depicting the goodness of linear fit between  $E_{n \rightarrow \pi^*}$  or  $E_{MLCT}$  and a SPP ( $E_T^N$ ,  $\pi^*$ ,  $\alpha$ , or  $\beta$ ). Colors are based on correlation coefficients of the fits ( $r^2$ ). Color code: Red:  $r^2 < 0.55$ ; orange  $0.55 \leq r^2 \leq 0.79$ ; green:  $r^2 > 0.79$ .

describing a property of a solvent (or a solvent mixture). A prominent member of the family of such relationships is Kamlet-Abboud-Taft (KAT) equation which can provide information on the solvent polarity effect on various physicochemical properties in terms of specific and non-specific solute-solvent interactions [47]. Deligkiozi et al. employed the triparametric KAT equation (see Eq. 7) and found that for the solvatochromism of the PCF groups (MLCT transitions) in **1** and **2a,b**

Dimesionless BSM polarity parameters <sup>a</sup>				
$x_{EG}$	$E_T^N(-)$	$\pi^*(-)$	$\alpha(-)$	$\beta(-)$
0	1.000	1.20	1.17	0.14
0.051	0.971	1.19	1.01	0.44
0.097	0.948	1.18	0.96	0.49
0.139	0.930	1.17	0.92	0.52
0.178	0.916	1.16	0.87	0.53
0.212	0.904	1.15	0.87	0.54
0.245	0.895	1.14	0.87	0.55
0.392	0.861	1.08	0.88	0.53
0.492	0.844	1.04	0.88	0.55
0.659	0.821	0.98	0.87	0.60
0.854	0.806	0.93	0.88	0.55
1	0.790	0.92	0.90	0.52

<sup>a</sup>The values of the BSM polarity parameters are based on published data [52, 53] and they were determined through polynomial interpolation.

**Table 2.**  
Solvent polarity parameters employed in this work for the quantification of solvent plarity effects in aqueous EG mixtures.

Compound	$E_0^\dagger$	$s^\dagger$	$a^\dagger$	$b^\dagger$	% $P_{\pi^*}$	% $P_\alpha$	% $P_\beta$	rse	$r^2$
<b><math>n(azo) \rightarrow \pi^*(azo)</math> Transitions</b>									
<b>1</b>	41.70	2.106	23.58	9.370	14.07	51.05	34.88	0.4687	0.8973
<b>2a</b>	36.73	6.425	24.15	11.64	34.70	39.18	26.12	0.2422	0.9762
<b>2b</b>	41.37	6.902	19.94	9.330	40.71	35.11	24.18	0.3461	0.9473
<b><math>dp(Fe^{II}) \rightarrow \pi^*(bpy)</math> Transitions (MLCT)</b>									
<b>1</b>	5.724	17.50	20.44	4.753	51.27	26.63	22.10	0.6124	0.9630
<b>2a</b>	-11.10	20.42	28.96	13.26	58.56	23.77	17.67	0.3999	0.9854
<b>2b</b>	16.34	22.53	6.521	-2.764	64.66	18.21	17.13	0.4214	0.9845

<sup>†</sup>Units: kcal/mol.  
rse: residual standard error is the square root of the residual sum of squares divided by the residual degrees of freedom (here 8 for all cases).

**Table 3.**  
Results of the correlation of experimental  $n \rightarrow \pi^*$  and MLCT energies of **1** and **2a-b** with KAT equation parameters.

both specific and non-specific interactions are important at various extents depending on the compound (results are summarized in **Table 3**) [19]. Herein, the author reports the corresponding results pertaining to the solvatochromism of the azo group ( $n \rightarrow \pi^*$  transitions). By use of Eqs. 8 and 9 (contribution analysis) the relative contribution of each of the parameters  $\pi^*$ ,  $\alpha$ , and  $\beta$  was quantified (detailed results in **Table 3**). Through this analysis it can easily be made clear that for all three compounds the relative importance of the parameters  $\pi^*$ ,  $\alpha$ , and  $\beta$ , on the energy of the  $n \rightarrow \pi^*$  is different when compared to the MLCT transitions. In case of MLCT transitions, parameter  $\pi^*$  appears to contribute the most for all three

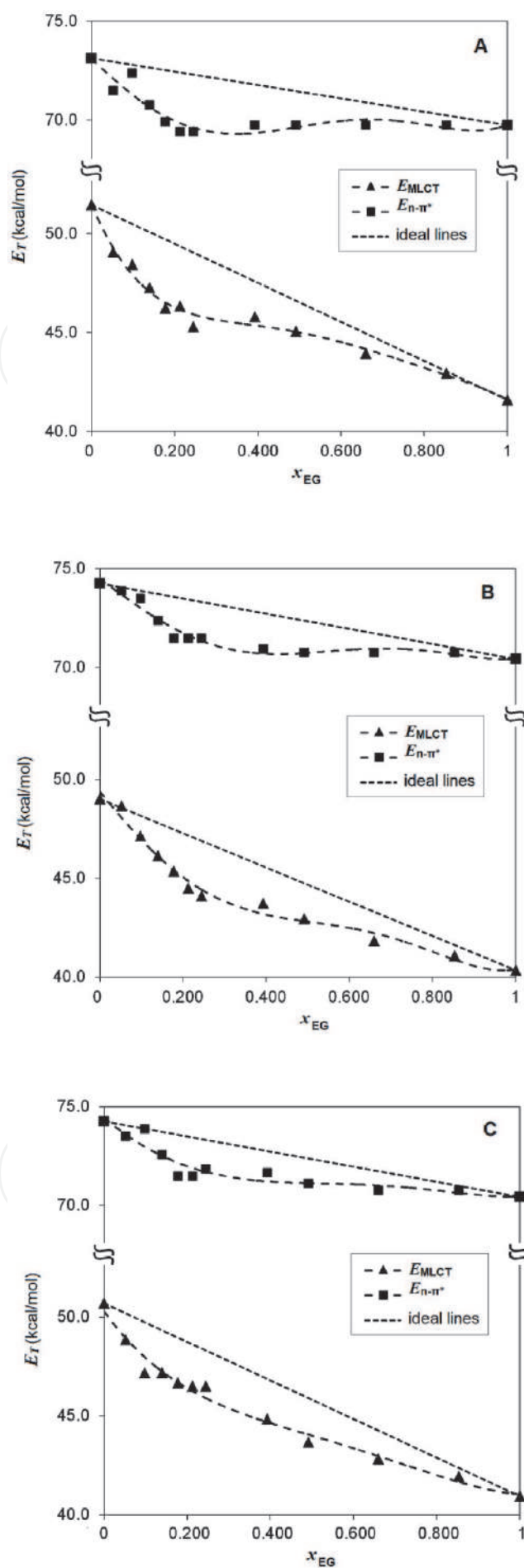
compounds ( $\%P_{\pi^*}$  ranging from 51.27 to 64.66%). Specific solute-solvent interactions described by HBA-basicity (parameter  $\beta$ ) and HBD-acidity (parameter  $\alpha$ ) appear to demonstrate almost equal contribution. In other words, specific and non-specific interactions are almost evenly weighted when it comes to MLCT transitions and that is true for all three compounds. The situation gets way different when interpreting  $n \rightarrow \pi^*$  transitions in the same fashion.

The behavior of compound **1** becomes different than those of compound **2a** and **2b**, and the uniformity of the contribution pattern that the MLCT transitions exhibit is lost. While for compound **1** HBD-acidity is the most contributing property (expressed through parameter  $\alpha$ ) compounds **2a** and **2b** exhibit almost equal contributions of all parameters  $\pi^*$ ,  $\alpha$ , and  $\beta$ . This is easily explained if the role of CyD (*alpha*- or *beta*-) is taken into account. As analyzed, in these [2]rotaxanes the CyD wheel preferably resides in the region of the azobenzene moiety so as to reduce the interaction with the ionic viologen parts of the axial molecule [54]. This effect hinders solvent molecules from interacting directly and specifically with the azo group (note that the azo group is highly prone to act as HBA-basic group; see **Figure 5B**). In case of **1** i.e. the CFD-precursor of these [2]rotaxanes, the lack of the CyD wheel renders the azo group-solvent interactions highly probable (**Figure 5B**). Therefore, **1** exhibits polarity responsive  $n \rightarrow \pi^*$  transitions mainly influenced by parameter  $\alpha$ . This constitutes a major differentiation among the studied compound and of course also between the two types of transitions. Obviously, the two transitions discussed herein convey spectrally different polarity information and that holds true for all three compounds but mostly for compound **1**.

### 3.7 PS effects as sensed by the FC and azo groups

It is well established that when a polar compound is dissolved in a BSM consisted of two solvents of different polarity, the compound/solute gets solvated selectively by one of the two solvents [17, 18]. This effect is obviously associated with preferential solute-solvent interactions developed in the vicinity of the solute molecules. Due to this effect the region around the solute (the so-called cybotactic region) is characterized by a different solvent/cosolvent molar ratio when compared to the bulk part of the solution i.e. the regions away from the cybotactic region. This interesting phenomenon, is attenuated when the two solvents consisting the BSM are similar in terms of structure and polarity [18]. There are numerous published models allowing for the quantification of selective solvation phenomena applicable to various types of solutes and BSMs. These models are generally categorized in thermodynamic and spectroscopy-based models [18]. In the latter case a solvatochromic solute is often employed in order to probe preferential solvation phenomena in BSMs and using spectrally measured shifts as inputs one can obtain various types of information pertaining to preferential solvation as output e.g. the solvent and cosolvent molar ratios in the cybotactic region. Through various spectroscopy-based models thermodynamic properties can also be determined for instance the molar free energy of transfer of the solute from one solvent to its cosolvent [18]. In this work preferential solvation of compounds **1** and **2a,b** in BSMs shall be used as a tool to rationalize the responsiveness of the two types of probing chromophores encompassed in these solvatochromic compounds i.e. the FC and azo groups.

By plotting the experimentally determined MLCT and  $n \rightarrow \pi^*$  transition energies of **1** and **2a,b** at various water/EG mole fractions against the mole fraction of water or EG one can easily realize that for both types of transitions a significant deviation from linearity exists (see **Figure 10**). For all compounds the measured energies for either of the transitions MLCT or  $n \rightarrow \pi^*$  were lower than the ideal/linear situations



**Figure 10.**  
 Plots of experimental transition (MLCT or  $n \rightarrow \pi^*$ ) energies measured in aqueous EG, against the bulk mole fraction of EG for A) compound 1, B) [2] rotaxane 2a, and C) [2] rotaxane 2b.

(dashed lines in **Figure 10**). Given the fact that both probing chromophores FC and azo, exhibit negative solvatochromism (i.e. increase of transition energy, or hypsochromism, when solvent polarity increases) the plots of **Figure 10** all describe preferential solvation of compounds **1,2a** and **2b** by EG (as will be thoroughly analyzed below). Indeed this effect has been thoroughly discussed in a recent paper by Papadakis et al. pertaining solely to the MLCT transitions. However, the new finding here is that the same effect is beautifully probed also by the azo group at least qualitatively. As can be easily seen, the shape of the non-linear  $E_T = f(x_{EG})$  curves of **Figure 10** have very similar shapes for the both types of transitions. It is for instance apparent that the maximization of the linear deviation occurs in all six plots depicted at bulk molar ratio of EG  $0.15 \leq x_{EG} \leq 0.25$  i.e. in the water-rich bulk solvent composition region. Yet, important differences are revealed when the results are treated quantitatively through the TPMS model by Bagchi and coworkers [32] (details in the Materials and Methods section).

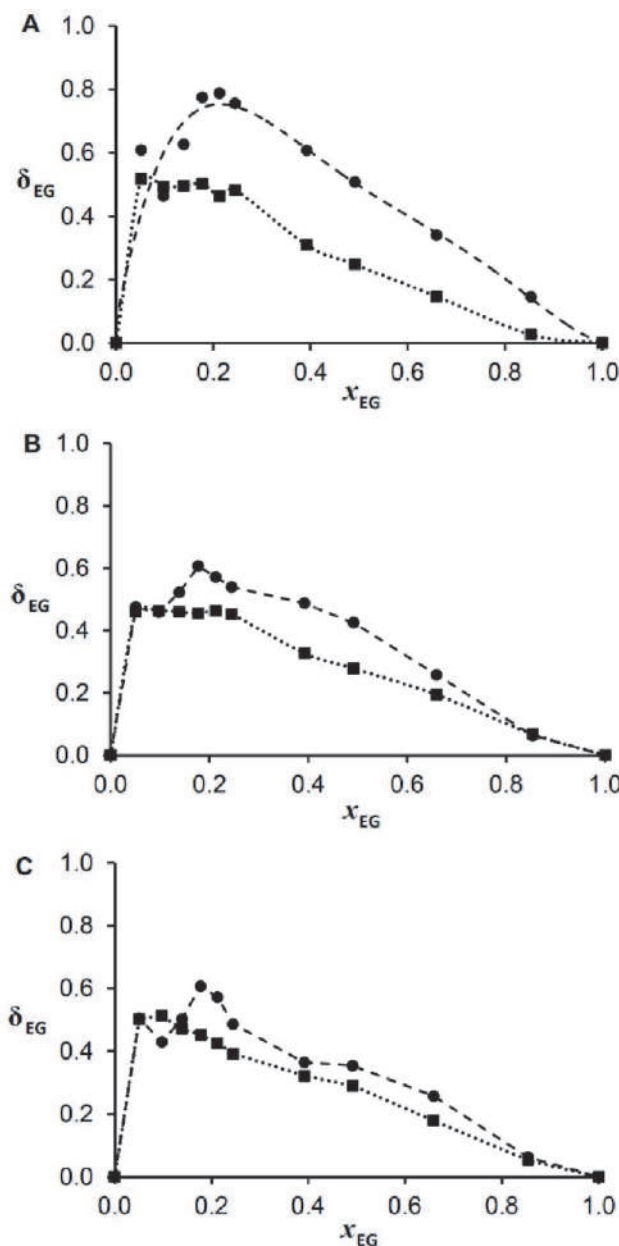
First of all, through the TPMS quantitative treatment the composition of the cybotactic region of solutions of **1** and **2a,b** were determined (see **Table 4**). Compound **1** appears to behave differently than the [2]rotaxanes (**2a,b**). The local EG mole fractions predicted by the same model for the MLCT and azo transition ( $y_{EG}^{mlct}$  and  $y_{EG}^{n \rightarrow \pi^*}$  respectively) of **1** differ a lot. Interestingly,  $y_{EG}^{n \rightarrow \pi^*}$  exhibits a propensity to maximize to the value of 1 (which denotes total solvation by EG) at a very low  $x_{EG}$  ( $x_{EG} = 0.212$ ) whereas  $y_{EG}^{mlct}$  follows a much more “legitimate” increase and maximizes only in neat EG. For compounds **2a** and **2b**,  $y_{EG}^{mlct}$  and  $y_{EG}^{n \rightarrow \pi^*}$  exhibit a very similar increase rate when going from neat water to neat EG (**Table 4**).

This becomes more obvious when plotting the  $\delta_{EG}$  values obtained through the TPMS model against the bulk EG mole fractions (note:  $\delta_{EG} = y_{EG} - x_{EG}$ ) as predicted through the experimentally observed MLCT and  $n \rightarrow \pi^*$  energies. Apparently, compound **1** a different behavior compared to the [2]rotaxanes. The  $\delta_{EG}$  predicted using the MLCT energies are significantly smaller than those predicted using  $n \rightarrow \pi^*$  energies (**Figure 11A**). The difference in  $\delta_{EG}$  drops when *alpha*-CyD is on (compound **2a**, **Figure 11B**) and drops even more when *beta*-CyD is threaded around the azobenzene group (compound **2b**, **Figure 11C**). In fact only  $\delta_{EG}$  predicted using

$x_{EG}$	Compound 1		Compound 2a		Compound 2b	
	$y_{EG}^{mlct}$	$y_{EG}^{n \rightarrow \pi^*}$	$y_{EG}^{mlct}$	$y_{EG}^{n \rightarrow \pi^*}$	$y_{EG}^{mlct}$	$y_{EG}^{n \rightarrow \pi^*}$
0	0	0	0	0	0	0
0.051	0.569	0.660	0.510	0.526	0.553	0.555
0.097	0.590	0.561	0.560	0.555	0.610	0.526
0.139	0.635	0.766	0.599	0.662	0.610	0.642
0.178	0.681	0.952	0.634	0.784	0.630	0.784
0.212	0.675	1.000	0.676	0.784	0.637	0.784
0.245	0.728	1.000	0.698	0.784	0.637	0.731
0.392	0.702	1.000	0.719	0.880	0.714	0.757
0.492	0.740	1.000	0.770	0.917	0.782	0.846
0.659	0.807	1.000	0.853	0.917	0.838	0.917
0.854	0.880	1.000	0.922	0.917	0.907	0.917
1	1	1	1	1	1	1

**Table 4.**  
Preferential solvation results obtained through the PS model.





**Figure 11.** Plots of TPMS- predicted  $\delta_{EG} = y_{EG} - x_{EG}$  versus the bulk EG mole fraction for A) **1**, B) **2a** and C) **2c**. Circles and dashed lines correspond to the prediction based on the azo-group whereas squares and dotted lines correspond to the prediction based on the FC group.

	Compound 1	Compound 2a	Compound 2b
$x_{iso}^{mlct}(EG)$	0.18	0.20	0.30
$x_{iso}^{n \rightarrow \pi}(EG)$	0.055	0.15	0.13
$\Delta \int$	0.18	0.070	0.047
$^* \Delta_{mlct}^{n \rightarrow \pi}(x_{iso})$	0.12	0.053	0.17

**Table 5.** Isosolvation points and  $\Delta \int$  results for compounds **1** and **2a,b** in aqueous EG.

$n \rightarrow \pi^*$  energies of compound **1** obtain values as high as 0.8. In other words, the azo group of compound **1** “feels” an excess of EG mole fraction of roughly 0.6 when the bulk EG mole fraction is only 0.2. Such large a preferential effect is not probed by the rest of the compounds. By integrating the differences in  $\delta_{EG}$  for the three compounds one can easily see a decrease in  $\Delta \int$  following the sequence:

$\Delta \int(1) = 0.19 > \Delta \int(2a) = 0.071 > \Delta \int(2b) = 0.046$ ). Similar conclusions can be drawn when comparing the isosolvation points for the different probes of all compounds (**Table 5**). The results clearly illustrate a different probing aptitude of preferential solvation by the azo group of compound **1**. Of course all results indicate qualitatively the same PS effect i.e. EG is the preferred solvent in the cybotactic region at all measured mole fractions.

#### 4. Conclusions

A general conclusion of the present study is that two distinct functional groups acting as chromophores (specifically the FC and azo groups) can probe solvation effects in different ways however this is true only on a quantitative basis. Qualitatively, both functional groups probed a strong negative solvatochromic effect in all cases of molecules studied. It became apparent though that FC is more sensitive to the dipolarity/polarizability of the medium whereas the azo group is slightly more responsive to polarity changes associated to the Lewis acidity and HBD-acidity of the medium. This holds true for compound **1** and **2a** but not for compound **2b** where the bulkiness of *beta*-CyD hinders any azobenzene-solvent direct interaction. In that case (**2b**) the azo group appears to have very similar sensitivity to solvent polarity to that that the FC group exhibits. On the other hand, both functional groups probed an intense PS effect by EG molecules however for each compound different extents in PS were probed. Compound **1**, again appeared to behave differently on a quantitative basis. The difference in probed extent PS between the azo and the FC group was the largest for **1** and dropped significantly in case of the *alpha*- or *beta*-CyD comprising [2]rotaxanes (compounds **2a**, and **2b**). Overall, compound **1**, exhibits a distinct dual sensing aptitude in terms of solute-solvent specific and non-specific effects as well as PS effects. The [2]rotaxanes have a rather attenuated dual sensing capacity presumably due to the presence of CyD which hinders the direct interaction of the azo-group (and its surrounding regions) with solvent molecules. As a result of the extended  $\pi$ -conjugation and the “shielding” effect of CyD the azo groups of compounds **2a** and **2b** tend to probe the same solvent polarity information as the FC group. It is important to mention that compound **1** clearly exhibits a dual solvatochromic behavior, however in water/EG BSMs the response of the azo group gets saturated to the value corresponding to neat EG very fast as one moves from neat water to neat EG (see **Table 4**). Nonetheless, as analyzed this corresponds to a special PS effect and taken together compound **1**, appears to be a very good polarity sensor candidate for future application mainly pertaining to polar media such as water solutions and mixtures with polar organic solvents.

#### Acknowledgements

The author would like to thank Dr. D. Matiadis (NCSR Demokritos, Athens, Greece) for fruitful discussions revolving around the solvatochromism of heterocyclic compounds. IKY (Greek State Scholarship Foundation) is gratefully acknowledged for financial support to R.P. during his PhD; a part of this work is connected to the work carried out then.

#### Notes

The authors declare no competing financial interest.

IntechOpen

### Author details

Ioanna Deligkiozi<sup>1</sup> and Raffaello Papadakis<sup>1,2\*</sup>

<sup>1</sup> Laboratory of Organic Chemistry, School of Chemical Engineering, National Technical University of Athens (NTUA), Athens, Greece

<sup>2</sup> TdB Labs, Uppsala, Sweden

\*Address all correspondence to: [rafpapadakis@gmail.com](mailto:rafpapadakis@gmail.com)

### IntechOpen

© 2021 The Author(s). Licensee IntechOpen. This chapter is distributed under the terms of the Creative Commons Attribution License (<http://creativecommons.org/licenses/by/3.0>), which permits unrestricted use, distribution, and reproduction in any medium, provided the original work is properly cited. 

## References

- [1] Liu, H.; Xu, X.; Peng, H.; Chang, X.; Fu, X.; Li, Q.; Yin, S.; Blanchard G. J.; Fang, Y. New solvatochromic probes: Performance enhancement via regulation of excited state structures. **Phys. Chem. Chem. Phys.**, **2016**, *18*, 25210-25220. DOI: 10.1039/C6CP04293G.
- [2] Ali, R.; Lang, T.; Saleh, S. M.; Meier, R. J. Wolfbeis O. S. Optical sensing scheme for carbon dioxide using a Solvatochromic probe. *Anal. Chem.*, **2011**, *83*, 2846-2851. DOI: 10.1021/ac200298j.
- [3] Landis, R. F.; Yazdani, M.; Creran, B.; Yu, X.; Nandwana, V.; Cooke, G.; Rotello. V. M. Solvatochromic probes for detecting hydrogen-bond-donating solvents. *Chem. Commun.*, **2014**, *50*, 4579-4581. DOI: 10.1039/C4CC00805G.
- [4] Florindo, C.; McIntosh, A. J. S.; Welton, T. ; Brancod, L. C.; Marrucho. I. M. A closer look into deep eutectic solvents: exploring intermolecular interactions using solvatochromic probes. *Phys. Chem. Chem. Phys.*, **2018**, *20*, 206-213. DOI: 10.1039/C7CP06471C.
- [5] Liu, H.; Xu, X.; Shi, Z.; Liu, K.; Yu, L.; Fang Y. Solvatochromic probes displaying unprecedented organic liquids discriminating characteristics. *Anal. Chem.*, **2016**, *88*, 10167-10175. DOI: 10.1021/acs.analchem.6b02721.
- [6] Li, Z.; Askim, J. R.; Suslick, K. S. The optoelectronic nose: Colorimetric and Fluorometric sensor arrays. *Chem. Rev.* **2019**, *119*, 231-292. DOI: 10.1021/acs.chemrev.8b00226.
- [7] Machado, V. G.; Stock, R. I.; Reichardt, C. Pyridinium N-Phenolate Betaine Dyes. *Chem. Rev.* **2014**, *114*, 10429-10475. DOI: 10.1021/cr5001157.
- [8] Reichardt, C. Solvatochromic dyes as solvent polarity indicators. *Chem. Rev.* **1994**, *94*, 2319-2358. DOI: 10.1021/cr00032a005.
- [9] Cabota, R.; Hunter, C. A. Molecular probes of solvation phenomena. *Chem. Soc. Rev.*, **2012**, *41*, 3485-3492. DOI: 10.1039/C2CS15287H.
- [10] Reichardt, C.; Welton. T. Solvents and solvent effects in organic chemistry. 4<sup>th</sup> Edn. Wiley-VCH, 2011, Weinheim.
- [11] Eilmes, A. Kubisiak, P. Explicit solvent modeling of Solvatochromic probes in ionic liquids: Implications of solvation Shell structure. *J. Phys. Chem. B*, **2015**, *119*, 113185-113197. DOI: 10.1021/acs.jpcc.5b07767.
- [12] Khajehpour, M.; Welch, C. M. Kleiner, K. A. Kauffman J. F. Separation of dielectric nonideality from preferential solvation in binary solvent systems: An experimental examination of the relationship between Solvatochromism and local solvent composition around a dipolar solute. *J. Phys. Chem. A*, **2001**, *105*, 5372-5379. DOI: 10.1021/jp010825a.
- [13] Duereh, A.; Sato, Y.; Smith, R. L.; Inomata, H. Spectroscopic analysis of binary mixed-solvent-polyimide precursor systems with the preferential solvation model for determining solute-centric Kamlet–Taft Solvatochromic parameters. *J. Phys. Chem. B*, **2015**, *119*, 14738-14749. DOI: 10.1021/acs.jpcc.5b07751.
- [14] Papadakis, R. Preferential solvation of a highly medium responsive Pentacyanoferrate(II) complex in binary solvent mixtures: Understanding the role of dielectric enrichment and the specificity of solute–solvent interactions. *J. Phys. Chem. B*, **2016**, *120*, 9422-9433. DOI: 10.1021/acs.jpcc.6b05868
- [15] Papadakis, R. Solute-centric versus indicator-centric solvent polarity

parameters in binary solvent mixtures. Determining the contribution of local solvent basicity to the solvatochromism of a pentacyanoferrate(II) dye. *J. Mol. Liq.* **2017**, *241*, 211–221. DOI: 10.1016/j.molliq.2017.05.147

[16] Papadakis, R. The solvatochromic behavior and degree of ionicity of a synthesized pentacyano (N-substituted-4,40-bipyridinium) ferrate(II) complex in different media. Tuning the solvatochromic intensity in aqueous glucose solutions. *Chem. Phys.*, **2014**, *430*, 29-39. DOI: 10.1016/j.chemphys.2013.12.008.

[17] Ben-Naim, A. Theory of preferential solvation of nonelectrolytes. *Cell Biophys.* **1988**, *12*, 255-269. DOI: 10.1007/BF02918361.

[18] Marcus, Y. Solvent mixtures: Properties and selective solvation, Marcel Dekker, Inc., 2002, New York.

[19] Deligkiozi, I; Voyiatzis, E.; Tsolomitis, A.; Papadakis, R. Synthesis and characterization of new azobenzene-containing bis pentacyanoferrate(II) stoppered push-pull [2]rotaxanes, with  $\alpha$ - and  $\beta$ -cyclodextrin. Towards highly medium responsive dyes. *Dyes Pigment.*, **2015**, *113*, 709-722. DOI: 10.1016/j.dyepig.2014.10.005.

[20] Qu, D-H.; Ji, F-Y.; Wang, Q-C.; Tian H. A double INHIBIT logic gate employing configuration and fluorescence changes. *Adv. Mater.* **2006**, *18*, 2035-2038. DOI: 10.1002/adma.200600235.

[21] Baroncini, M.; Gao, C.; Carboni, V.; Credi, A.; Previtera, E.; Semeraro, M.; Venturi, M.; Silvi, S. Light control of stoichiometry and motion in pseudorotaxanes comprising a cucurbit [7]uril wheel and an azobenzene-bipyridinium axle. *Chem. Eur. J.* **2014**, *20*, 10737-10744. DOI: 10.1002/chem.201402821.

[22] Qu, D-H.; Wang, Q-C.; Tian, H. A half adder based on a photochemically driven [2] rotaxane. *Angew. Chem. Int. Ed.*, **2005**, *44*, 5296-5299. DOI: 10.1002/anie.200501215.

[23] Monk, P.M.S. The viologens: Physicochemical properties, synthesis and applications of the salts of 4,40-Bipyridine. John Wiley & Sons Ltd; 1998, Chichester.

[24] Crano, J.C.; Guglielmetti, R.J. (Eds). Organic photochromic and thermochromic compounds. Main photochromic families, vol. 1. Kluwer Academic Publishers; 2002. New York. p. 341-67.

[25] Deligkiozi, I.; Tsolomitis, A.; Papadakis, R. Photoconductive properties of a  $\pi$ -conjugated  $\alpha$ -cyclodextrin containing [2]rotaxane and its corresponding molecular dumbbell. *Phys. Chem. Chem. Phys.*, **2013**, *15*, 3497-3503. DOI: 10.1039/C3CP43794A

[26] Papadakis, R.; Deligkiozi, I.; Giorgi, M.; Faure, B.; Tsolomitis, A. Supramolecular complexes involving non-symmetric viologen cations and hexacyanoferrate (II) anions. A spectroscopic, crystallographic and computational study. *RSC Adv.*, **2016**, *6*, 575-585. DOI: 10.1039/C5RA16732A.

[27] Papadakis, R; Deligkiozi, I; Tsolomitis A. Synthesis and characterization of a group of new medium responsive non-symmetric viologens. Chromotropism and structural effects. *Dyes Pigment.*, **2012**, *95*, 478-484. DOI: 10.1016/j.dyepig.2012.06.013.

[28] Papadakis, R; Deligkiozi, I; Tsolomitis A. Spectroscopic investigation of the solvatochromic behavior of a new synthesized non symmetric viologen dye: Study of the solvent-solute interactions. *Anal. Bioanal. Chem.* **2010**, *397*, 2253-2259. DOI: 10.1007/s00216-010-3792-7.



- [29] Zhu, Y.; Zhou, Y.; Wang, X. Photoresponsive behavior of two well-defined azo polymers with different electron-withdrawing groups on pushpull azo chromophores. *Dyes Pigment.*, **2013**, *99*, 209-219. DOI: 10.1016/j.dyepig.2013.05.006.
- [30] Papadakis, R.; Tzolomitis, A. Study of the correlations of the MLCT Vis absorption maxima of 4-pentacyanoferrate- 4-arylsubstituted bipyridinium complexes with the Hammett substituent parameters and the solvent polarity parameters ETN and AN. *J. Phys. Org. Chem.* **2009**, *22*, 515-521. DOI: 10.1002/poc.1514.
- [31] Papadakis, R.; Tzolomitis, A. Solvatochromism and preferential solvation of 4-pentacyanoferrate 4-aryl substituted bipyridinium complexes in binary mixtures of hydroxylic and non-hydroxylic solvents. *J. Solut. Chem.*, **2011**, *40*, 1108-1125. DOI: 10.1007/s10953-011-9697-z.
- [32] Chatterjee, P.; Bagchi, S. Preferential solvation of a dipolar solute in mixed binary solvent: A study of UV-visible spectroscopy. *J. Phys. Chem.* **1991**, *95*, 3311-3314. DOI: 10.1021/j100161a064.
- [33] Banerjee, D.; Laha, A.K.; Bagchi, S. Preferential solvation in mixed binary solvent. *J. Chem. Soc. Faraday Trans.*, **1995**, *91*, 631-636. DOI: 10.1039/FT9959100631.
- [34] Laha, A.K.; Das, P.K.; Bagchi, S. Study of preferential solvation in mixed binary solvent as a function of solvent composition and temperature by UV-vis spectroscopic method. *J. Phys. Chem. A*, **2002**, *106*, 3230-3234. DOI: 10.1021/jp0121116.
- [35] Redlich, O.; Kister, A.T.. Algebraic representation of thermodynamic properties and the classification of solutions. *Ind. Eng. Chem.* **1948**, *40*, 345-348. DOI: 10.1021/ie50458a036.
- [36] Krygowski, T.M.; Fawcett, W. R. Complementary Lewis acid-base description of solvent effects. I. Ion-ion and ion-dipole interactions. *J. Am. Chem. Soc.*, **1975**, *97*, 2143-2148. DOI: 10.1021/ja00841a026.
- [37] Papadakis, R.; Deligkiozi, I.; Nowak, E. K. Study of the preferential solvation effects in binary solvent mixtures with the use of intensely solvatochromic azobenzene involving [2] rotaxane solutes. *J. Mol. Liq.*, **2019**, *274*, 715-723. DOI: 10.1016/j.molliq.2018.10.164.
- [38] Hofmann, K.; Brumm, S.; Mende, C.; Nagel, K.; Seifert, A.; Roth, I.; Schaarschmidt, D.; Lang, H.; Spange, S. Solvatochromism and acidochromism of azobenzene-functionalized poly(vinyl amines). *New J. Chem.*, **2012**, *36*, 1655-1664. DOI: 10.1039/c2nj40313g.
- [39] Sıdır, Y. G.; Sıdır, I.; Taşal, E., E. Ermiş. Studies on the electronic absorption spectra of some monoazo derivatives. *Spectrochim. Acta A* **2011**, *78*, 640-647. DOI: 10.1016/j.saa.2010.11.0.
- [40] Gasbarri, C.; Angelini, G. Polarizability over dipolarity for the spectroscopic behavior of azobenzenes in room-temperature ionic liquids and organic solvents. *J. Mol. Liq.*, **2017**, *229*, 185-188. DOI: 10.1016/j.molliq.2016.12.033.
- [41] Qian, H-F.; Tao, T.; Feng, Y-N.; Wang, Y-G.; Huang, W. Crystal structures, solvatochromisms and DFT computations of three disperse azo dyes having the same azobenzene skeleton. *J. Mol. Struct.* **2016**, *1123*, 305-310. DOI: 10.1016/j.molstruc.2016.06.04.
- [42] Christoforou, D. Electronic effects of the azo group. PhD Thesis, University of Canterbury, New Zealand, 1981.
- [43] Mulski, M. J.; Connors, K.A. Solvent effects on chemical processes. 9. Energetic contributions to the

complexation of 4-nitroaniline with  $\alpha$ -cyclodextrin in water and in binary aqueous-organic solvents. **1995**, 4, 271-278. DOI: 10.1080/10610279508028936.

[44] Hickey, J.P.; Passlno-Reader D.R. Linear solvation energy relationships: "Rules of thumb" for estimation of variable values. *Environ. Sci. Technol.*, **1991**, 25, 1753-1760. DOI: 10.1021/es00022a012.

[45] Endo, S; Goss, K-U. Applications of Polyparameter linear free energy relationships in environmental chemistry. *Environ. Sci. Technol.*, **2014**, 48, 12477–12491. DOI: 10.1021/es503369t.

[46] Williams, A. Free Energy Relationships in Organic and Bio-Organic Chemistry. Royal Society of Chemistry, Cambridge UK, 2003.

[47] Kamlet, M.J.; Abboud, J.L.M.; Abraham, M.H.; Taft, R.W. Linear solvation energy relationships. 23. A comprehensive collection of the solvatochromic parameters,  $\pi^*$ ,  $\alpha$ , and  $\beta$ , and some methods for simplifying the generalized solvatochromic equation, *J. Organomet. Chem.* **1983**, 48, 2877–2887. DOI: [doi.org/10.1021/jo00165a018](http://dx.doi.org/10.1021/jo00165a018).

[48] The non-linear fit(s) in this figure correspond to polynomial fitting(s) and convey no physical meaning. They are simply used in order to visualize the sizable deviations from linearity.

[49] Ratts, K. W.; Howe, R. K.; Phillips, W. G. Formation of pyridinium ylides and condensation with aldehydes. *J. Amer. Chem.Soc.* **1969**, 91, 6115-6121. DOI: 10.1021/ja01050a032.

[50] Zoltewicz, J. A.; Smith, C. L.; Kauffman, G. M. Buffer catalysis and hydrogen-deuterium exchange of heteroaromatic carbon acids. *Heterocycl. Chem.* **1971**, 8, 337-338. DOI: 10.1002/jhet.5570080236.

[51] Elvidge, J.A.; Jones, J.R.; O'Brien, C.; Evans, E.A.; Sheppard, H.C. Base-Catalyzed Hydrogen Exchange. *Adv. Heterocycl. Chem.* **1974**, 16, 1-31. DOI: 10.1016/S0065-2725(08)60458-4.

[52] Marcus, Y. The use of chemical probes for the characterization of solvent mixtures. Part 2. Aqueous mixtures. *J. Chem. Soc. Perkin Trans.* **1994**, 2, 1751–1758. DOI: 10.1039/P2994000175

[53] Sindreu, R. J.; Moyá, M. L.; Sánchez Burgos, F.; González, A. G. Kamlet-Taft solvatochromic parameters of aqueous binary mixtures of tert-butyl alcohol and ethyleneglycol. *J. Solut. Chem.* **1996**, 25, 289-293. DOI: 10.1007/BF00972526.

[54] Deligkiozi, I.; Papadakis, R.; Tsolomitis, A. Synthesis, characterisation and photoswitchability of a new [2]rotaxane of  $\alpha$ -cyclodextrin with a diazobenzene containing  $\pi$ -conjugated molecular dumbbell. *Supramol. Chem.* **2012**, 24, 333-343. DOI: 10.1080/10610278.2012.660529.

# Dyes as Labels in Biosensing

*Hu Li, Yuanyuan Han, Haiyan Zhao, Hassan Jafri  
and Bo Tian*

## Abstract

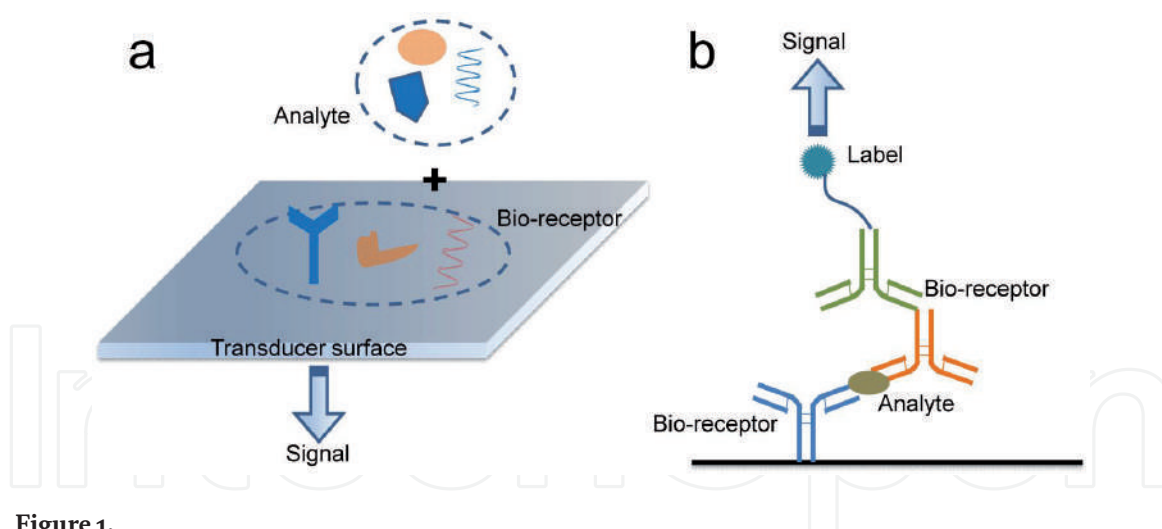
Investigation and evaluation of dyes play a vital role in the process of introduction novel labels and their corresponding sensing methods, which signify opportunities for the development of biosensors. This chapter introduces applications of various dyes as labels in biosensing. Bio-recognition molecules with dyes transduce biological information into measurable optical, electrochemical, magnetic or other kinds of signals for quantification. The dyes used in this field were summarized and reviewed according to their signal types, namely colorimetric, fluorescent and electrochemical. Some dyes can transduce signals between multiple physical signals. For some most important dyes, detailed descriptions were given focused on their unique properties, labeling methods and sensing mechanisms.

**Keywords:** biosensors, labels, micro- and nano-particles, optical dyes, charge-transfer complexes

## 1. Introduction

Applications of, e.g., clinical diagnosis, drug development, environmental research, security and defense, require self-contained rapid analytical platforms to get rid of tedious operation processes and long turn-around times. In 1960s, applications of enzymes explored a new way in analytical chemistry to obtain specific, sensitive and ease-of-use assays. At the same time, ion selective electrodes have been developed for rapid non-reagental analysis of inorganic ions. In 1962, the concept of enzyme transducer was proposed and sooner the device was developed [1]. Following this idea of enzyme electrode, the first enzyme electrode-based glucose meter was commercialized in 1975. After that, self-contained analytical platforms based on different principles were developed including thermistor, [2] optical fiber, [3] piezoelectric crystal detector, [4] surface plasmon resonance, [5] etc. Today, such analytical platforms are regarded as biosensors. A biosensor is a self-contained integrated device that is capable of providing specific quantitative or semi-quantitative analytical information using a biological recognition element (biochemical receptor) which is in direct spatial contact with a transducer element [6]. Today, biosensors have been applied to a wide variety of analytical problems, e.g., medicine, environmental research, food control, and process industry [7].

Biosensors can be divided into two groups based on involving a labeling process during the detection or not. A label is a foreign molecule that is chemically or temporarily attached to the target (i.e., the molecule of interest) through a labeling process to detect molecular presence or activity. In the above-mentioned early



**Figure 1.**  
Scheme of typical (a) label-free and (b) label-based biosensors.

period of the biosensor history, typical biosensing processes were usually realized by measuring the transduced mechanical, electrical, or optical signals without any labels, as illustrated in **Figure 1a**. Such label-free biosensors can provide direct information without complicated sample preparation steps. In contrast, label-based biosensors utilizing additional operation processes for higher signal-to-noise ratios and for a broader range of sensing/transducer systems. Conventional biosensing labels are optical molecules or radioactive elements borrowed from bio-analytical systems such as gel electrophoresis and enzyme linked immunosorbent assays. A typical strategy of sandwich assay for antibody-based detection is shown in **Figure 1b**.

Due to the fast development of nanotechnology and material science, nanomaterials are widely adopted as biosensing labels, many of which are dyes in senses of optics or electrochemistry. The special size of these nanomaterial dyes provides unique properties that greatly improve the performances of relevant biosensors. In this chapter, we focus on dyes used as biosensing labels and discuss their properties, applications and how they improve the biosensing properties.

## 2. Dyes in colorimetric biosensors

Colorimetry technique is a practical and direct analytical method to determine the concentration of colored analyte depending on the color change in solution. The colorimetric biosensing strategy based on this principle has become one of the most popular and important strategies due to its simplicity, visualization, low cost and non-destruction. Based on the strategies of signal generation, colorimetric assays can mainly be divided into two groups, i.e., assays based on enzymes for chromogenic reactions, and assays based on colored labels. Herein, we focus on the later group in which dyes play a crucial role.

### 2.1 Gold nanoparticles

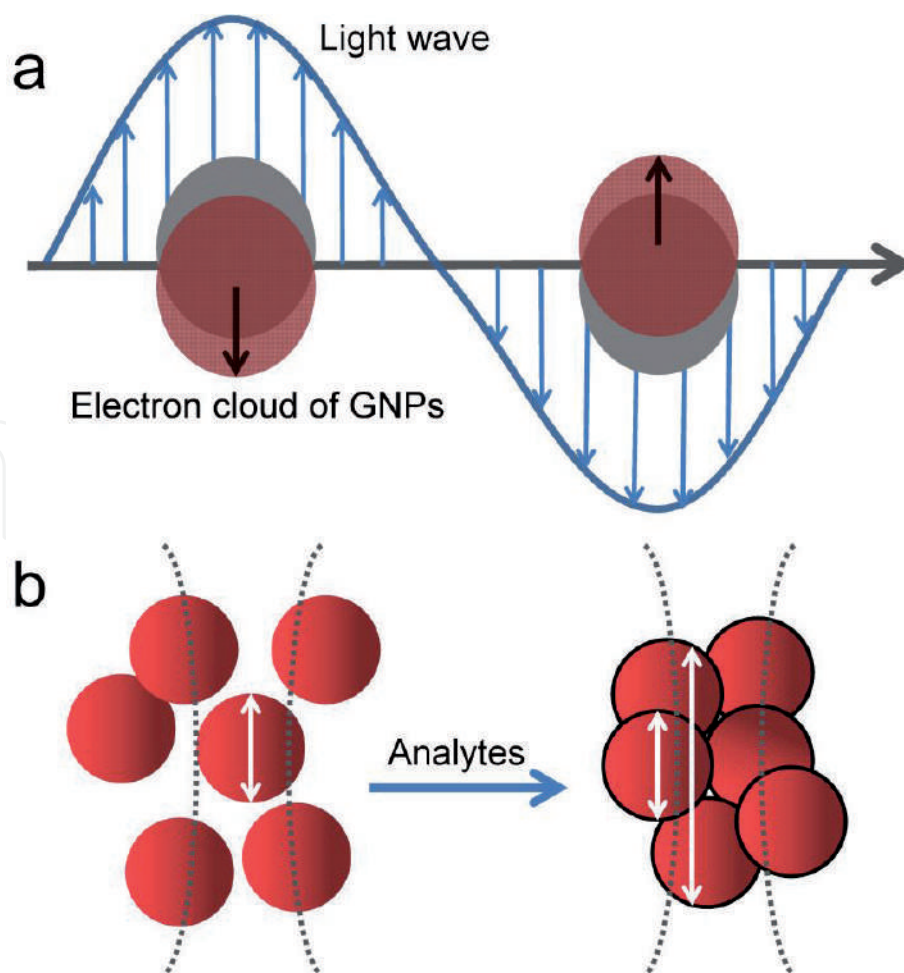
As a successful example to employ nanomaterial and nanotechnology to solve the biological problems, colloidal gold has been introduced in the biosensing fields more than 20 years with lots of amazing works being reported. Colorimetric biosensors based on gold nanoparticles (GNPs) have greatly developed in both scientific study and commercial applications.



### 2.1.1 Sensing mechanism

**Surface plasmon resonance.** Various GNP-based colorimetric biosensors were built depending on the same principle, i.e., surface plasmon resonance (SPR). SPR is a prominent spectroscopic feature that results in an intense and sharp absorption band in the visible range of noble metal nanoparticles that have an adequate density of free electrons. Localized SPR is an effect that the electron cloud of the nanoparticle sense and start to oscillate at the same frequency as the electromagnetic field of the incident light (**Figure 2a**). During this process the incident light is scattered and converted into heat, both leading to the intensity attenuation of the incident light. Meanwhile, localized SPR produce an electric field on the nanomaterial surface, which can be utilized for labeling several kinds of biosensors. The SPR-induced color is determined by several factors including the size, shape, modified ligands and aggregation state. In colorimetric biosensors, the aggregation state of GNPs is interested. As shown in **Figure 2b**, in bioanalytical assays, the combination of bio-receptors (or targets) labeled with GNPs can induce the isolated GNP assembly as well as the interparticle coupling of the surface plasmon, resulting in the color of solution transferring from red to blue.

**Surface-enhanced Raman spectroscopy.** Based on the SPR effect, GNPs have also been used in other types of biosensors, e.g., surface-enhanced Raman spectroscopy (SERS) based sensing. SERS as a versatile finger-print vibrational technology has been widely utilized in analytical chemistry, [8] electrochemistry, [9] and media diagnostics. [10] However, the mechanism of SERS is still



**Figure 2.**  
 (a) Localized SPR band formation. Red and gray circles represent negative and positive electron clouds, respectively. (b) GNP agglomeration leads to the shift of SPR absorption band.

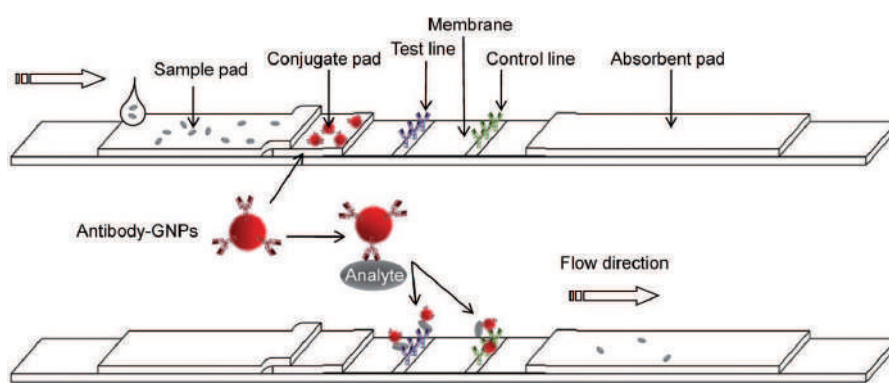
under debating [11]. Regarding to the mechanism of SERS, there are two broadly accepted opinions: electromagnetic (EM) theory and chemical enhancement (CE) mechanism [12]. The EM enhancement considers the molecules as point dipoles, which react with the local enhanced electric field on or near the surface [13]. The CE mechanism attributes the SERS intensity to molecular resonance through the interaction with the metal surface, thereby changing the molecular polarizability, resulting in enhancement such as resonance Raman scattering [14]. SERS does not occur on any metal surfaces, among which GNPs are currently the most widely used SERS substrate. SERS-based biosensors involving GNPs have been widely used in the sensitive and selective detection of antigens, [15] aptamers, [16] tumor biomarkers, [17] as well as *Staphylococcus aureus* [18].

**Lateral flow system.** The most well known biosensing application of GNPs must be the pregnancy test sticks, which belong to the most commercialized type of biosensor, i.e., the lateral flow (LF) system. LF biosensors are paper-based devices permit low-cost and rapid diagnostics with moderate robustness, specificity and sensitivity. The ease-of-synthesize, stability, biocompatibility and tunable size make GNPs suitable label for LF systems. Moreover, the SPR effect endows GNPs an intense red color that can be either detected qualitatively by naked eye or measured quantitatively using spectrometers for lower detection limits. Because of these properties, GNPs are the most widely used optical label in LF systems [19]. A standard and conventional LF strip consists of four main sections made of membranes, papers or glass fibers, including a sample pad for sample loading, a conjugate pad impregnated with bioreceptor-modified labels (usually GNPs), a detection pad/membrane where test line (to show whether the target is exist in the sample) and control line (to show whether the LF assay works well) are printed, and an absorption pad at the end of the strip, as illustrated in **Figure 3**. Except for GNPs, other colored materials are also used in LF biosensors, including carbon dots and latex particles.

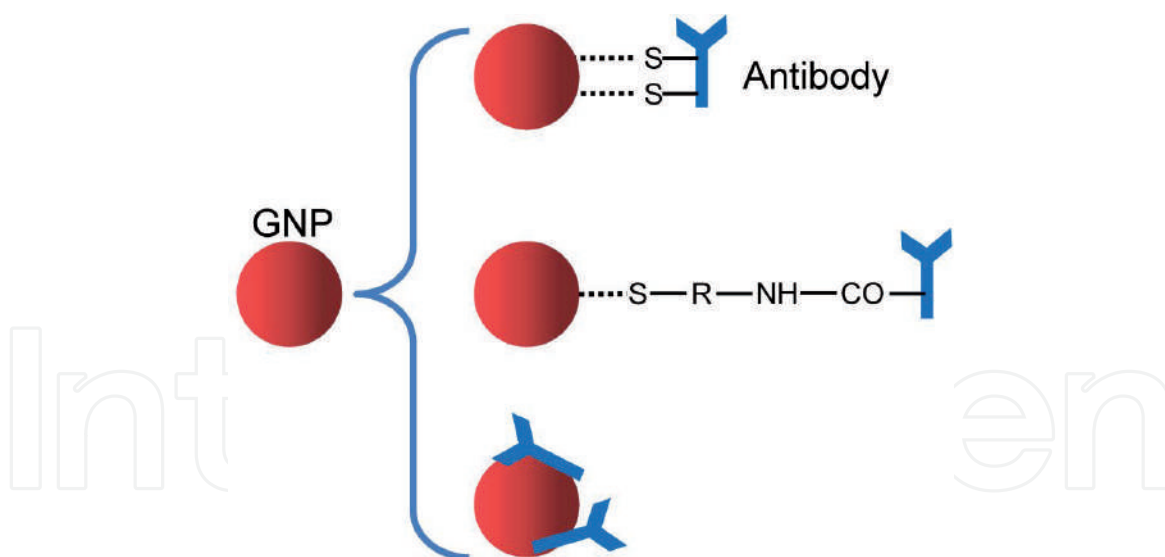
### 2.1.2 Labeling type

Three principle methods for modifying GNPs are briefly illustrated in **Figure 4**: (1) A simple and common way to immobilize the biomolecules on the GNPs is labeling through the sulfur-gold interactions; [20] (2) Ligands can be capped on the GNPs in the process of particle growth or though ligands replace after the synthesis; (3) Ligands can be absorbed on the GNPs surface directly via non-covalent interactions.

In 1997, the first GNP-based colorimetric biosensor was reported [21]. In this work, the hybridization of DNA probes capped on GNP surface and target DNA



**Figure 3.**  
Schematic of a typical lateral-flow immunological detection system.



**Figure 4.**  
 Illustration of different GNP conjugation methods.

resulted in the formation of GNP agglomeration, accompanying a visually red-to-purple color change. This is the most typical biosensor that uses biochemical reactions to induce the cross-linked aggregation of GNPs. Since then, a new generation of medical diagnostic technology based on the nanomaterials has begun. Oligonucleotides, peptides, antibodies and aptamers have been labeled with GNPs for the colorimetric detection of different targets based on the similar principle. Such strategy designs usually achieve naomolar detection limits, which is limited by the signal-to-noise ratio related to the intrinsic properties of labels and sensors [22]. To amplify the signals and optimize the performance of biosensor, the biochemical and molecular amplification methods are introduced in the biosensing process. Via duplex-specific nuclease-assisted amplification method, a colorimetric method was developed for microRNA dection based on GNPs aggregation [23]. DNAzyme-assisted target recycling was utilized, combined with surface plasmons of GNPs coupling in the colorimetric biosensor, obtaining a fast and simple detection of genetic targets with 50 pM sensitivity [24]. Using imaging-based analysis instead of spectrographic analysis has higher signal-to-noise ratio and thus potentially lower detection limit. A dark-field microscope based methodology was applied for the sensing of GNP aggregation, obtaining a detection limit of 43 aM of DNA, which was 5–9 orders of magnitude lower than conventional colorimetric sensor based strategies [25].

## 2.2 Carbon nanoparticles

Carbon nanoparticles, also named colloidal carbon, can be visually detected in a qualitative or semi-quantitative manner and thus being used as colored labels. Compared to GNPs, carbon nanoparticles have several excellent properties, e.g., high stability, nontoxicity, ease-of-preparation, and ease-of-modification [26]. The dark black color of carbon dots endows a high signal-to-noise ratio, allowing sensitivities below the low picomolar range even by visual inspection [27].

## 2.3 Latex particles

Colored latex particles are also often used as labels in the colorimetric biosensor. Latex particles are natural or synthetic polymer nano- and micro-particles that suspend stably in water, and the polystyrene particles are used mostly.

There are three ways to prepare colored latex particles by dyeing latex particles with different types of dyes molecules: (1) co-polymerization of polymer monomer with dyes; (2) cross-linking the dyes on particles surface by covalent bonds; (3) physical embedding or absorption dyes in particles. After the dyeing, usually dyes on the surface are removed in order to functionalize the active groups (sulfhydryl groups, amino groups and carboxyl groups) on the latex particles for further labeling the biomolecules [28].

Benefit its wide variety of sources, low cost and easy to be functionalized, the latex particles are applied as probes in immunochromatographic analysis quite early [29]. The good properties enable them are still used now. A lateral flow immunoassay was developed by covalent functionalizing the antigens on colored latex particles for the visual diagnosis of canine visceral leishmaniasis [30]. A latex particles-GNPs composites labeled with antibodies were synthesized as probed for the immunochromatographic test. The nanocomposites amplified the binding capacity of GNPs with target antigens and improved the sensitivity 2 orders of magnitude compared with GNPs-antibodies probes [31].

### **3. Dyes in fluorescent biosensors**

In the field of biotechnology, diagnosis and drug discovery, fluorescent assay is by far the most popular methodology because of not only its sensitivity and versatility but also the high commercialization of fluorescent labels [32]. In addition to the new fluorescent nanomaterials (e.g., upconversion fluorescent materials and aggregation-induced emission (AIE) materials that are described further below), new spectroscopic sensors have also been developed based on rising technologies such as fiber optics, LEDs and fast imaging devices, all of which contributed to the fast development as well as high interdisciplinarity of fluorescent biosensors.

#### **3.1 Organic dyes**

Organic fluorescent dyes are a class of organic molecules that contain a fluorescent core skeleton with a large conjugate system and some auxochrome or active group (such as carboxyl, amino, amide, etc). The fluorescent core skeleton enables them absorb a certain excitation light and emitting it as fluorescence. The auxochrome or active group is capable of altering wavelengths and enhance fluorescence or labeling them to bio-receptors for recognizing various biomolecules in biosensing [33]. Briefly, the fluorescent dyes labeled bio-receptors, also called fluorescent probes, can recognize various biomolecules and then convert the recognition events into fluorescent signal output to achieve biosensing or imaging.

Currently, there are many kinds of organic fluorescent dyes, most of which can be used to label bio-receptors for biosensing and imaging. Here, some major organic fluorescent dyes labels are introduced, including fluorescein derivatives, rhodamine derivatives, cyanine derivatives and other commonly used organic fluorescent dyes.

##### *3.1.1 Sensing mechanism*

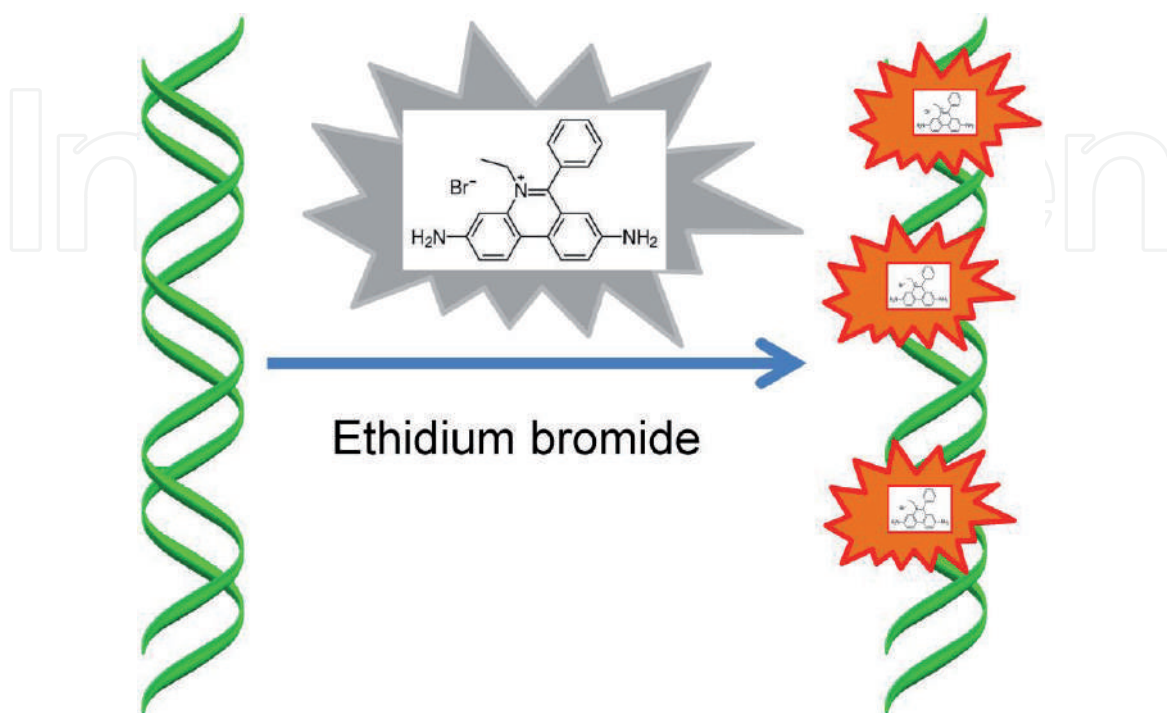
The signal conversion mechanism in sensing process are various, such as electron transfer quenching or fluorescence recovery, fluorescence resonance energy transfer (FRET), or monomer-excimer emission conversion with pyrene fluorophores. The following will introduce the major signal conversion mechanism involved in the fluorescence biosensing process.



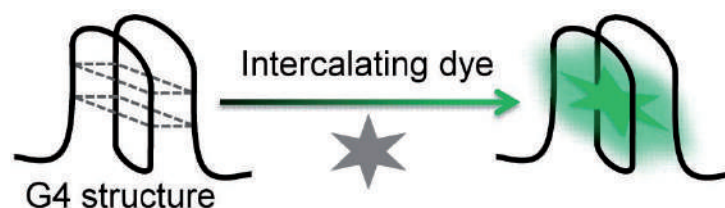
**Nucleic acid intercalating dyes.** Nucleic acid intercalating dyes [34–36] is a special kind of organic fluorescent dyes that have no fluoresce or the fluorescence is weak in solution, which may be caused by the quenching of solvent. However, when they are embedded in specific DNA structures, the fluorescence intensity will increase significantly, due to the protection of the hydrophobic groups of the oligonucleotide (**Figure 5**). Commercially available nucleic acid intercalating dyes for labels in biosensing mainly include ethidium bromide (EB), thioflavin T (ThT), N-methylporphyrin dipropionic acid IX (NMM) and triphenylmethane dyes. The most classical biosensing application is EB staining-mediated gel electrophoresis for nucleic acids detection [37]. Nucleic acid fragments can be separated in gel under the action of electric field, then EB contains a tricyclic planar group can insert between nucleic acid stacking bases, resulting in increased fluorescence intensity of EB for detection.

An emerging biosensing strategy is designed based on the G-quadruplex (G4) DNA structure and corresponding intercalating dyes such as ThT, NMM, etc. (**Figure 6**) [38]. G4 DNA structure is formed from DNA guanine-rich sequences, which has been confirmed to be stably present in human live cell [39]. Therefore, endogenous G4 DNA can be easily detected by using intercalating dyes targeting G4 DNA. Additionally, G4 DNA structures can be formed by the amplicons of any kinds of DNA amplification methods that produce single-stranded DNA, making G4 structure a convenient cascade amplification tool (a molecular amplification followed by a signal amplification) that can be applied in homogeneous and isothermal bioanalytical assays. Moreover, the formation or consume of the G4 structure after binding to the target molecules will change the interaction between G4 and intercalating dyes, resulting in increased or decreased fluorescence intensity for detection.

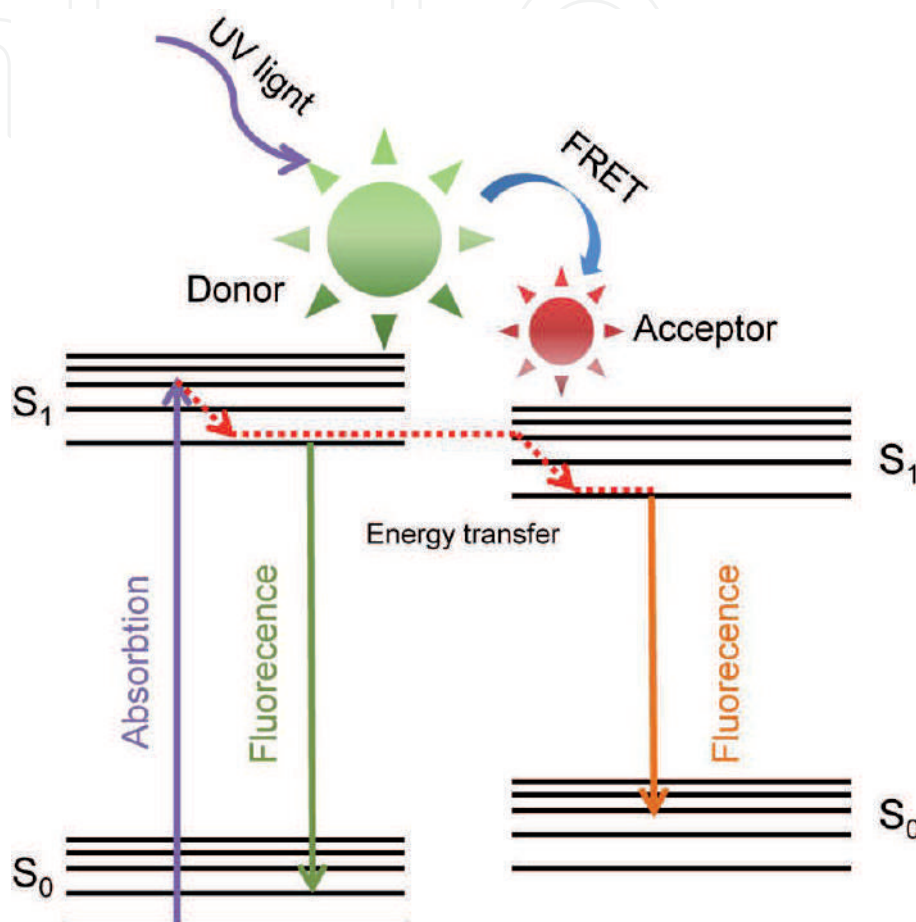
**Fluorescence resonance energy transfer.** Measuring the presence of labels always means employing tedious operation steps for separation and washing. Today, homogeneous reaction processes are highly preferred due to its potential for point-of-care applications. FRET assays are frequently used in biosensors due to achieve homogeneous reaction processes with high sensitivity.



**Figure 5.**  
 EB staining for nucleic acids detection.

**Figure 6.**

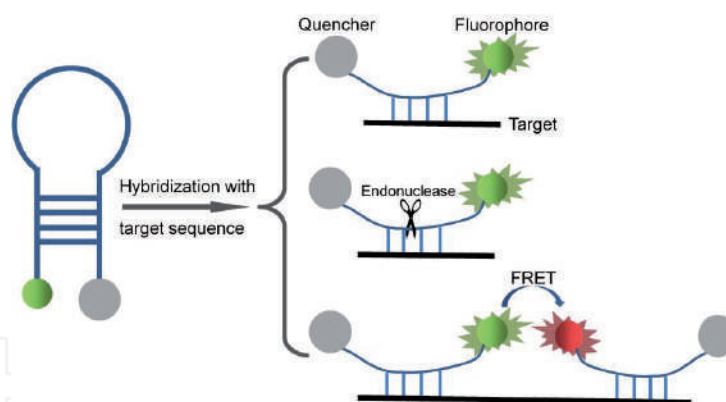
Fluorescence enhancement based on the intercalating dyes and G4 structure.

**Figure 7.**

Schematic illustration of fluorescence resonance energy transfer.

A FRET technique includes an energy transfer between two fluorophores, i.e., from high energy donor to a lower energy acceptor (**Figure 7**). The FRET occurs when the donor and acceptor are close to each other, approximately between 1–10 nm, and this distance meets the dimensions of biological molecules. Since the FRET is sensitive to the relative distance between donors and acceptors, when biological acceptor labeled with donors (or acceptors) comes close to the biological target labeled with acceptors (or donors), FRET signals can be detected.

Rather than labels the donor and the acceptor on different biomolecules, a molecular beacon (MB) utilized a donor linked with an acceptor through a biore sponsive probe, further simply the design of FRET biosensors [40]. Typically, a MB is a single-stranded oligonucleotide probe labeled with a fluorophore at its one end and a quencher at the other. Due to the length and/or the secondary structure of the oligonucleotide, the probe holds the fluorophore and quencher close to each other, thus inducing a quenching. Upon the hybridization between the probe and the target, the distance between the fluorophore and the quencher changes, restoring the fluorescence [41] (**Figure 8**).



**Figure 8.**  
 Illustration of a molecular beacon and examples of its applications.

**Monomer-Excimer.** Generally, when the distance and position between fluorescent dyes with the same or different structures are appropriate, the excited state fluorescent dye and the other ground state fluorescent dye would form an excimer. Therefore, the fluorescence emission intensity of the original monomer weakens or disappears, and the fluorescence emission of the formed excimer appears [42, 43]. For monomer-excimer based biosensing process, the reaction between the fluorescent dyes-labeled probe and the target biomolecules will trigger or hinder the monomer-excimer process, causing the variation of fluorescence emission spectra.

### 3.1.2 Labeling type

The labeling type between organic fluorescent dyes and bio-receptors can generally be divided into two types: covalent and non-covalent (such as intercalation, groove binding or electrostatic interaction). Different labeling method has different fluorescent sensing mechanisms.

Covalently binding labeled fluorescent probes including single-labeled fluorescent probe and dual-labeled fluorescent probe. Single-labeled fluorescent probes are obtained by covalently binding single fluorescent dye molecules to bio-receptors. The single-labeled probe sensing mechanism may be summarized as follows: when the bio-receptor of the fluorescent probe recognizes the target molecules, the fluorescence properties of dyes would be changed, such as changes in fluorescence intensity and fluorescence anisotropy, thus converting the recognition process into a measurable fluorescence signal [44–46]. Dual-labeled fluorescent probes are obtained by covalently binding dual fluorescent dye molecules (or a dye and a quencher) to bio-receptors. The dual-labeled probes are all distance dependent, the rearrangement of the probe structure after binding to the target molecules will change the distance between the two labels, resulting in changes in the fluorescence properties of the system.

Non-covalently binding fluorescent probes mainly refer to nucleic acid fluorescent probes that obtained by the binding of intercalating dyes and DNA. As mentioned above, when the nucleic acid intercalating dye binds to a specific DNA structure, the fluorescent signal changes. Based on this principle, a series of biosensors have been developed. Compared with covalently binding fluorescent probes, the non-covalently binding fluorescent probes will not affect the binding affinity of the probe to the target, and also have the advantages of easy operation and low cost [47].

### 3.1.3 Fluorescein derivatives

Fluorescein and its derivatives are one class of xanthene dyes. Fluorescein was first produced by Von Bayer in 1871, which has a good rigid coplanar structure

and can produce strong green fluorescence under the action of laser. Due to its easy synthesis, low cost, low biological and cytotoxicity, high molar absorption coefficient, and high fluorescence quantum yield, fluorescein can be widely used in biological imaging and analysis [48]. However, fluorescein also has some defects, such as high pH sensitivity [49], small Stokes [50] and poor light stability [51]. In order to improve the fluorescence performance of fluorescein, many important fluorescein derivatives have been developed by introducing functional group modification to fluorescein [52]. Additionally, fluorescein derivatives contain some active groups, which can bind with bio-receptors to obtain fluorescent dyes labeled probes with high selectivity, good stability and high sensitivity for biosensing [53]. Currently, commercially available fluorescein derivatives dye mainly includes 6-carboxy-fluorescein (FAM), 5-tetrachloro-fluorescein (TET), 5-hexachloro-fluorescein (HEX).

#### *3.1.4 Rhodamine derivatives*

It was discovered in the late 1980s that rhodamine and its derivatives are important fluorescent dyes and also belong to xanthene dyes. The molecular structure of rhodamine dyes is very stable, coplanar, and can produce strong red fluorescence under the excitation. They also can bind with bio-receptors to obtain fluorescent dyes labeled probes with high selectivity, good stability and high sensitivity for biosensing. Compared with fluorescein derivatives, rhodamine derivatives have stronger photostability, higher fluorescence quantum yield and lower pH sensitivity. Commercially available rhodamine derivatives dyes for labels in biosensing mainly include 6-carboxyl-x-rhodamine (ROX), tetramethyl-6-carboxyrhodamine (TAMRA) and Texas red.

It was discovered in the late 1880s that rhodamine and its derivatives are important fluorescent dyes and also belong to xanthene dyes [54]. The molecular structure of rhodamine dyes is very stable, coplanar, and can produce strong red fluorescence under the excitation [55]. They also can bind with bio-receptors to obtain fluorescent dyes labeled probes with high selectivity, good stability and high sensitivity for biosensing. Compared with fluorescein derivatives, rhodamine derivatives have stronger photostability, higher fluorescence quantum yield and lower pH sensitivity [56]. Commercially available rhodamine derivatives dyes for labels in biosensing mainly includes 6-carboxyl-x-rhodamine (ROX), tetramethyl-6-carboxyrhodamine (TAMRA) and Texas red.

#### *3.1.5 Cyanine derivatives*

Cyanine dyes were first discovered by Williams in 1856, subsequently, Vogel discovered that these dyes have very good photosensitivity, which promote the development of cyanine dyes [57]. Cyanine dyes and derivatives have excellent spectral characteristics, such as high molar extinction coefficient, high fluorescence quantum yield, and long fluorescence emission wavelength. More importantly, the maximum emission and absorption of these dyes are located in the near-infrared region. In this region, the self-absorption and background fluorescence of biomolecules are relatively small [58]. Thus, cyanine dye derivatives have become the most commonly used fluorescent signal groups in protein, nucleic acid and other biological analysis [59]. Commercially available cyanine derivatives dyes for labels in biosensing mainly refers to N-carboxypentyl-5-sulfonate-3H-indocyanine dyes, including Cy3, Cy5, Cy5.5 and Cy7.



## 3.2 Quantum dots

Quantum dots (QDs) are spherical or quasiballistic semiconductor nanoparticles that bind excitons in the three dimensions, with a diameter no larger than twice the Bohr radius of the excitons of their corresponding semiconductor material, thus confining the motion of electrons, holes, or excitons in three dimensions. Due to the quantum confinement effects, the quantum dots display unique optical and electronic properties compared to the bulk materials.

QDs were firstly synthesized in glass matrix in 1970s and with their fluorescent properties reported [60]. Later some groups studied the novel properties of quantum dots and tried to investigate influences of quantum effects on the optical properties of QDs [61]. In 1980s, CdS nanospheres were synthesized in colloidal solution and the basic theory of QDs were studied [62]. In 1993, the high quality colloidal QDs were prepared first time with uniform size in the solution [63], which provided favorable materials for both theoretical study and practical applications. Since then, various types of QDs with different compositions and properties have been synthesized by the solution growth method.

According to the chemical compositions, QDs can be mainly divided to two groups. Single component QDs, such as metal chalcogenides, [64] attracted much attentions at the early stage of the QDs development. Due to the uniformity, optical and electronic properties of such QDs can be tuned by simply controlling their sizes. Multiple component QDs are either core-shell structural or alloyed. Core-shell structural QDs have a core with one component embedded in another material as a shell, such as CdSe/ZnS [65]. Usually, to reduce the nonradioactive recombination of electron-hole pairs, the material used as the shell has a larger band gap than that in the core, thus improving the fluorescence quantum yield. Coating the same core with different shells adjust the properties of the QDs. Alloyed QDs that have homogeneous or heterogeneous alloyed internal composition, for example, CdS<sub>x</sub>Se<sub>1-x</sub>/ZnS [66]. This type of QDs allows tuning the properties by changing the proportion of the component without changing the size. Interestingly, alloyed QDs not only exhibit the original properties of each component, but also display newly additional and adjustable properties because of the merge of the different composites. Now despite classical nanocrystals, there are various new species of QDs that have been prepared, such as perovskite QDs [67] and graphene QDs [68].

Generally, the size of QDs, i.e., in the range of 2–10 nm, endows these nanoparticles high surface-to-volume ratios. The large surface provides rich sites for further functionalization and immobilization of molecules, including nucleic acids and proteins. [69] Importantly, after functionalized with hydrophilic ligands, QDs are soluble and stable in aqueous solution, which is the common environment for biological reactions.

### 3.2.1 Sensing mechanism

The most obvious and widely utilized properties of QDs are the optical properties. Compared with organic dyes, QDs display higher fluorescence quantum yield and extinction coefficient, broader excitation spectra, longer lifetimes and tunable fluorescent emissions [70]. As the size of QDs decreases, the band gap between valence band (VB) and conduction band (CB) increases, which means more energy needed for electrons excitations (from ground state in VB to CB) as well as more energy released from the electrons de-excitation (from CB to ground state in VB), leading to the fluorescent emission shift to the high frequency range. In addition, the fluorescence wavelength can also be tuned flexibly by adjusting the structure



and chemical compositions of QDs as mentioned above. These stand out properties make QDs appealing for bio-medical applications including imaging and biosensing [71]. In biosensing systems, QDs, used with or without nano-sized quenchers, are transducers and functionalized with bio-recognition molecules (bio-receptors). Because of the tunable size and broad spectral width, QDs can play as either energy donors or acceptors in the FRET biosensor [72]. Furthermore, due to their high fluorescence intensity, photostability and long lifetimes than conventional organic fluorophores, QDs were also involved in the design of molecular beacons.

**Bioanalytical systems using QDs as labels.** QDs were first applied as bioanalytical labels in 1998, [73] an ultrasensitive bioanalytical system involving QDs was demonstrated for protein imaging. Since then, QDs have been widely applied in various bioanalytical methodologies, e.g., the enzyme-linked immunosorbent assay (ELISA), fluorescence resonance energy transfer (FRET) assay and cell tracking.

QDs can be simply used as fluorescent labels in immunosensors to quantify the biological targets through directly measuring the presence and/or the intensity of the fluorescence. CdTe/SiO<sub>2</sub> core-shell structured nanoparticles were labeled with prostate-specific antigen (PSA) detection antibodies for PSA detection. And the fluorescent signals were measured after the specific recognition between PSA and the QD labeled antibodies followed by a magnetic separation to remove unbound QDs. This system represents a typical fluorescent biosensor detecting the presence of QD labels [74]. This strategy design shows great flexibility for employing a variety of fluorescence detectors, e.g., fluorescence spectrometry and handheld UV lamp tests. Furthermore, such design enables not only target quantification but also imaging multiple targets with different QD labels [75].

**Imaging.** QDs have also demonstrated their applicability in biomedical imaging, which is an important tool in diagnosis, visualization, treatment and prognosis of diseases [76]. QDs emit in the visible and near infrared ray wavelengths, with high brightness and excellent photostability, suitable for morphological studies. A representative examples of such applications encapsulated QDs in virus-like particles as theranostic platforms to image viral behavior in living cells [77]. Furthermore, multifunctional SV40 virus-like particles was constructed encapsulating QDs bearing peptides recognizing early, developmental, and late stages of atherosclerosis, respectively, in live mice [78].

### *3.2.2 Labeling type*

One of essential challenges to apply QDs in biosensors is immobilization of target recognition biomolecules onto the surface of QDs via stable bonding. In this part, methods for preparing QD-biomolecule conjugates will be presented and modified QDs applied as labels in biosensors are also summarized. Roughly, there are 4 strategies to prepare the QD-based bioconjugates:

1. Direct binding: proteins and nucleic acids can be immobilized on the QDs surface directly through interactions between the thiol-groups or imidazole-groups with the metal component of QDs, e.g., alkylthiol terminated DNAs are linked with QDs surface directly via dative thiol bond [79].
2. Conjugation via ligands: QDs can be functionalized firstly by ligands, such as carboxyl groups, hydroxyl groups and amino-groups, then covalently bond to biomolecules [80].
3. Conjugation via functional shell: QDs are capped with silane shell [81] or copolymers [82], then bond to biomolecules by the functional groups on the outer shell.

4. Conjugation via specific biological affinity: some types of biological affinity can be used to bond the QDs with biomolecules strongly and specifically, such as biotin-streptavidin interaction [83].

### 3.3 Upconversion fluorescent materials

Upconversion fluorescent materials are emerging fluorescent nanoparticles that can convert low frequent exciting light into high frequent emitting light by absorbing two-photons or multi-photons. The luminous mechanism of upconversion nanoparticles (UCNPs) is anti-stokes, which is opposite with the most fluorescent materials, including organic fluorescent dyes, quantum dots, fluorescent proteins, metal complexes, etc [84]. Because of the distinctive luminescence mechanism, UCNPs have some unique advantages, which make up the disadvantage of above other dyes. Firstly, UCNPs have improved biological tissue penetration. Secondly, UCNPs can reduce light damage on biological samples. Thirdly, UCNPs can effectively avoid the disturbance of autofluorescence from biological samples. Therefore, UCNPs have wide applications in biosensing and imaging [85]. The sensing principle of UCNPs-based probe is widely based on fluorescence resonance energy transfer (FRET) between UCNPs (donor) and other down-conversion fluorophores (acceptor). The reaction between UCNPs-based probe and the target biomolecules will trigger or hinder the FRET process, causing the quenching and enhancement of fluorescence for detection.

## 4. Dyes in electrochemical biosensors

Electrochemical biosensor is capable of providing specific quantitative or semi-quantitative analytical information using electrochemical transduction elements, e.g., charge-transfer complexes. Low-cost, energy efficient, portable, easy fabrication, and real-time sensing are major advantages of electrochemical biosensing platforms. Among the electrical signal molecules, there are several types of dyes with electrochemical activity, and they will be introduced in this part. In addition, the electrochemical signals generation mechanisms are explained and applications of these dyes as labels in the biosensors are also displayed.

### 4.1 Organic dye molecules

Methylene blue (MB) is a kind of derivative of phenothiazine and widely used as a redox indicator and electron transfer medium in electrochemical analysis. For a typical DNA detection using MB labels, the distance between the MB and the electrode surface is adjusted by the change of conformation of the DNA probes labeled with MB, so that the peak current or the change in impedance can indicate the presence of the target DNA and quantitative concentration. This method is simple and versatile, however easy to be influenced by the solution environment. Despite MB, other organic dyes, such as gentian violet, ethyl green, Hoechst 33258 are also utilized in the electrochemical works. They are not as popular as MB, but show good performance in some biosensors.

### 4.2 Organometallic complexes

Organometallic complexes consist of centrally located metal atoms or ions and completely or partly coordinated organic ligands. The organometallic complexes with transition metals have the advantages of strong redox signal, good chemical

stability, low toxicity, and high structural flexibility. They interact with biomolecules via the Intermolecular interaction force and electrostatic interaction.

Ferrocene (Fc), is a yellow organometallic complexes with transition metal (Fe) and aromatic ligands (cyclopentadiene rings). Because Fc has two freely rotating cyclopentadiene rings, it can be labeled with the biomolecules, such as DNA via hydrophobic interactions. As an electrical signal molecule, in the combination of bio-receptors and target molecules, Fc generates electrical signals mainly by adjusting the distance between the Fc and the electrode surface to realize the change of electrical signal and achieve the purpose of detection.

K<sub>3</sub>[Fe(CN)<sub>6</sub>]/K<sub>4</sub>[Fe(CN)<sub>6</sub>], is a pair of dyes with bright red and yellow color, respectively. Mainly, they are used as electron transfer agents in amperometric biosensors, to replace the natural electron transfer agents of the enzymes. In the commercial blood glucose meters, the glucose in the blood reacts with glucose oxidase and K<sub>3</sub>[Fe(CN)<sub>6</sub>] fixed on the surface of the test strip to produce gluconic acid and K<sub>4</sub>[Fe(CN)<sub>6</sub>]. Applying a constant working voltage to the test strip, K<sub>4</sub>[Fe(CN)<sub>6</sub>] is oxidized to K<sub>3</sub>[Fe(CN)<sub>6</sub>], generating an oxidation current that is proportional to the glucose concentration.

### 4.3 Nanomaterials

#### 4.3.1 Quantum dots

One of the most commonly used electrochemical biosensor is cadmium selenide (CdSe) QDs, which employ as electrical signal molecules for the labeling of nucleic acid strands [86]. The Pb<sup>2+</sup> cleavage ribozyme sequence was modified on the surface of the magnetic beads, and designed an electrochemical biosensor for detecting Pb<sup>2+</sup> by using rolling circle amplification reaction and a signal probe labeled with CdS QDs [87]. Based on Ni<sup>2+</sup> cleavage ribozyme and CdSe QDs, The Ni<sup>2+</sup> was detected and the detection limit was 6.67 nmol/L [88]. As electrical signal molecules, QDs have versatility and low background signal, which has great application prospects.

#### 4.3.2 Graphene quantum dots

Graphene quantum dots (GQDs) are actually sheets of graphene with dimensions less than 100 nm with sp<sup>2</sup> hybridized honeycomb structures, and their shapes are mostly circular and elliptical, but square and hexagonal QDs are also available. Basically, GQDs are characterized as graphene-like, consisting of C, O, and H as well as carbonyl, carboxyl, hydroxyl, and epoxy groups. GQDs can bind to ssDNA through  $\pi$ - $\pi$  interactions, but it has no such effect on double-stranded DNA. Park et al. used GQDs as electrical signal substances to detect the Hg<sup>2+</sup> concentration by measuring the current generated during the electrochemical reduction of GQDs [89].

#### 4.3.3 Metal-organic frameworks

Metal-organic frameworks (MOFs) are crystalline materials with an infinitely regular and infinitely expanding periodic network structure formed by the self-assembly of metal ions and organic ligands through coordination bonds, covalent bonds, and weak intermolecular bonds ( $\pi$ - $\pi$  stacking, van der Waals forces, hydrogen bonding, and other electrostatic interactions, etc.) [90]. MOFs are nanomaterials with good stability, large porosity, and specific surface area that are of great interest in gas storage, drug delivery, and sensors. Due to the intrinsic peroxidase

catalytic activity, MOFs can also be used in electrochemical biosensors. Xu et al. constructed a  $\text{Pb}^{2+}$  electrochemical biosensor based on the MOFs prepared based on Fe [91], and AgPt nanoparticles are employed to increase its electrical conductivity and electrocatalytic activity, and the obtained sensitivity approaches 0.032 pmol/L. However, even though MOFs have enzymatic activity to improve sensitivity, their synthesis process is very complicated, and the characterization of the modification process is also very critical, so it is not suitable for routine use.

## 5. Conclusion

Investigation and evaluation of dyes play a vital role in the process of introduction novel labels and their corresponding sensing methods, which signify opportunities for the development of biosensors. This chapter highlights the utilization of dyes as biosensing labels and some most important sensing mechanisms for biological, biotechnological, and biomedical applications. These designs and applications have been much attracted for in vivo and in vitro analysis due to their high sensitivity and selectivity, fast response, biocompatibility, etc. Further developments in novel synthetic approaches of functional nanomaterials and sensing strategies will accelerate the discovery of unique properties of dyes, which will further improve their applications towards future biosensing platforms.

## Acknowledgements

The authors are grateful to ÅForsk Foundation (grant number, 20-280), Formas (grant number, 2019-01583), STINT (grant number, IB2020-8594) and I Bergh scholarship. Qilu young scholar program of Shandong University (grant number, 11500082063141) is also acknowledged for the financial support.

## Conflict of interest

The authors declare no conflict of interest.

IntechOpen

### Author details

Hu Li<sup>1,2</sup>, Yuanyuan Han<sup>3</sup>, Haiyan Zhao<sup>4</sup>, Hassan Jafri<sup>5</sup> and Bo Tian<sup>6\*</sup>

1 Shandong Technology Centre of Nanodevices and Integration,  
School of Microelectronics, Shandong University, Jinan, China

2 Department of Materials Science and Engineering, Uppsala University, Uppsala,  
Sweden

3 College of Biology, Hunan University, Changsha, China


4 College of Science, Hebei University of Science and Technology, Shijiazhuang,  
China

5 Faculty of Engineering and Technology, Mirpur University of Science and  
Technology, Kashmir, Pakistan

6 Department of Biomedical Engineering, Central South University, Changsha,  
China

\*Address all correspondence to: tianbo@csu.edu.cn

### IntechOpen

© 2021 The Author(s). Licensee IntechOpen. This chapter is distributed under the terms of the Creative Commons Attribution License (<http://creativecommons.org/licenses/by/3.0>), which permits unrestricted use, distribution, and reproduction in any medium, provided the original work is properly cited. 



## References

- [1] Clark Jr. LC, Lyons C. ELECTRODE SYSTEMS FOR CONTINUOUS MONITORING IN CARDIOVASCULAR SURGERY. *Annals of the New York Academy of Sciences*. 1962;102:29-45. DOI:<https://doi.org/10.1111/j.1749-6632.1962.tb13623.x>
- [2] Mosbach K, Danielsson B. An enzyme thermistor. *Biochimica et Biophysica Acta (BBA) - Enzymology*. 1974;364:140-5. DOI:[https://doi.org/10.1016/0005-2744\(74\)90141-7](https://doi.org/10.1016/0005-2744(74)90141-7)
- [3] Völkl K-P, Opitz N, Lübbers DW. Continuous measurement of concentrations of alcohol using a fluorescence-photometric enzymatic method. *Fresenius' Zeitschrift für analytische Chemie*. 1980;301:162-3. DOI:10.1007/BF00467800
- [4] Guilbault GG. Determination of formaldehyde with an enzyme-coated piezoelectric crystal detector. *Analytical Chemistry*. 1983;55:1682-4. DOI:10.1021/ac00261a010
- [5] Liedberg B, Nylander C, Lunström I. Surface plasmon resonance for gas detection and biosensing. *Sensors and Actuators*. 1983;4:299-304. DOI:[https://doi.org/10.1016/0250-6874\(83\)85036-7](https://doi.org/10.1016/0250-6874(83)85036-7)
- [6] Thevenot DR, Toth K, Durst RA, Wilson GS. Electrochemical biosensors: recommended definitions and classification. *Pure and applied chemistry*. 1999;71:2333-48.
- [7] Turner, A.P.F., Karube, I., and Wilson GS, editors. *Biosensors: Fundamentals and Applications*. Oxford: University Press; 1987. 770 p. 2011. 1132 p.
- [8] Doering WE, Nie S. Spectroscopic Tags Using Dye-Embedded Nanoparticles and Surface-Enhanced Raman Scattering. *Analytical Chemistry*. 2003;75:6171-6. DOI:10.1021/ac034672u
- [9] Wu D-Y, Li J-F, Ren B, Tian Z-Q. Electrochemical surface-enhanced Raman spectroscopy of nanostructures. *Chemical Society Reviews*. 2008;37:1025-41. DOI:10.1039/B707872M
- [10] Qian X, Peng X-H, Ansari DO, Yin-Goen Q, Chen GZ, Shin DM, et al. In vivo tumor targeting and spectroscopic detection with surface-enhanced Raman nanoparticle tags. *Nature Biotechnology*. 2008;26:83-90. DOI:10.1038/nbt1377
- [11] Fleischmann M, Hendra PJ, McQuillan AJ. Raman spectra of pyridine adsorbed at a silver electrode. *Chemical Physics Letters*. 1974;26:163-6. DOI:[https://doi.org/10.1016/0009-2614\(74\)85388-1](https://doi.org/10.1016/0009-2614(74)85388-1)
- [12] Le Ru EC, Etchegoin PG, Meyer M. Enhancement factor distribution around a single surface-enhanced Raman scattering hot spot and its relation to single molecule detection. *The Journal of Chemical Physics*. 2006;125:204701. DOI:10.1063/1.2390694
- [13] Zhao Y, Liu X, Lei DY, Chai Y. Effects of surface roughness of Ag thin films on surface-enhanced Raman spectroscopy of graphene: spatial nonlocality and physisorption strain. *Nanoscale*. 2014;6:1311-7. DOI:10.1039/C3NR05303B
- [14] Su J-P, Lee Y-T, Lu S-Y, Lin JS. Chemical mechanism of surface-enhanced raman scattering spectrum of pyridine adsorbed on Ag cluster: Ab initio molecular dynamics approach. *Journal of Computational Chemistry*. 2013;34:2806-15. DOI:<https://doi.org/10.1002/jcc.23464>
- [15] Zhang L, Mazouzi Y, Salmain M, Liedberg B, Boujday S. Antibody-Gold Nanoparticle Bioconjugates for Biosensors: Synthesis, Characterization and Selected Applications. *Biosensors*

- and Bioelectronics. 2020;165:112370. DOI:<https://doi.org/10.1016/j.bios.2020.112370>
- [16] Duan N, Shen M, Qi S, Wang W, Wu S, Wang Z. A SERS aptasensor for simultaneous multiple pathogens detection using gold decorated PDMS substrate. *Spectrochimica Acta Part A: Molecular and Biomolecular Spectroscopy*. 2020;230:118103. DOI:<https://doi.org/10.1016/j.saa.2020.118103>
- [17] Panikar SS, Banu N, Haramati J, Gutierrez-Silerio GY, Bastidas-Ramirez BE, Tellez-Bañuelos MC, et al. Anti-fouling SERS-based immunosensor for point-of-care detection of the B7–H6 tumor biomarker in cervical cancer patient serum. *Analytica Chimica Acta*. 2020;1138:110-22. DOI:<https://doi.org/10.1016/j.aca.2020.09.019>
- [18] Zhu A, Ali S, Xu Y, Ouyang Q, Chen Q. A SERS aptasensor based on AuNPs functionalized PDMS film for selective and sensitive detection of *Staphylococcus aureus*. *Biosensors and Bioelectronics*. 2021;172:112806. DOI:<https://doi.org/10.1016/j.bios.2020.112806>
- [19] Quesada-González D, Merkoçi A. Nanoparticle-based lateral flow biosensors. *Biosensors and Bioelectronics*. 2015;73:47-63. DOI:<https://doi.org/10.1016/j.bios.2015.05.050>
- [20] Bhatt N, Huang P-JJ, Dave N, Liu J. Dissociation and Degradation of Thiol-Modified DNA on Gold Nanoparticles in Aqueous and Organic Solvents. *Langmuir*. 2011;27:6132-7. DOI:10.1021/la200241d
- [21] Elghanian R, Storhoff JJ, Mucic RC, Letsinger RL, Mirkin CA. Selective Colorimetric Detection of Polynucleotides Based on the Distance-Dependent Optical Properties of Gold Nanoparticles. *Science*. 1997;277:1078 LP – 1081. DOI:10.1126/science.277.5329.1078
- [22] Liu G, Lu M, Huang X, Li T, Xu D. Application of Gold-Nanoparticle Colorimetric Sensing to Rapid Food Safety Screening. *Sensors (Basel, Switzerland)*. 2018;18:4166. DOI:10.3390/s18124166
- [23] Huang J, Shangguan J, Guo Q, Ma W, Wang H, Jia R, et al. Colorimetric and fluorescent dual-mode detection of microRNA based on duplex-specific nuclease assisted gold nanoparticle amplification. *Analyst*. 2019;144:4917-24. DOI:10.1039/C9AN01013K
- [24] Zagorovsky K, Chan WCW. A Plasmonic DNAzyme Strategy for Point-of-Care Genetic Detection of Infectious Pathogens. *Angewandte Chemie International Edition*. 2013;52:3168-71. DOI:<https://doi.org/10.1002/anie.201208715>
- [25] Li J, Liu Q, Xi H, Wei X, Chen Z. Y-Shaped DNA Duplex Structure-Triggered Gold Nanoparticle Dimers for Ultrasensitive Colorimetric Detection of Nucleic Acid with the Dark-Field Microscope. *Analytical Chemistry*. 2017;89:12850-6. DOI:10.1021/acs.analchem.7b03391
- [26] Posthuma-Trumpie GA, Wichers JH, Koets M, Berendsen LBJM, van Amerongen A. Amorphous carbon nanoparticles: a versatile label for rapid diagnostic (immuno)assays. *Analytical and bioanalytical chemistry*. 2012;402:593-600. DOI:10.1007/s00216-011-5340-5
- [27] Blažková M, Rauch P, Fukal L. Strip-based immunoassay for rapid detection of thiabendazole. *Biosensors and Bioelectronics*. 2010;25:2122-8. DOI:<https://doi.org/10.1016/j.bios.2010.02.011>

- [28] Yang Y, Li M, Tang A, Liu Y, Li Z, Fu S. Preparation of Covalent and Solvent-resistance Colored Latex Particles and Its Application on Cotton Fabric. *Fibers and Polymers*. 2020;21:1685-93. DOI:10.1007/s12221-020-9990-9
- [29] Rembaum A, Dreyer WJ. Immunomicrospheres: reagents for cell labeling and separation. *Science*. 1980;208:364 LP – 368. DOI:10.1126/science.6768131
- [30] Garcia VS, Guerrero SA, Gugliotta LM, Gonzalez VDG. A lateral flow immunoassay based on colored latex particles for detection of canine visceral leishmaniasis. *Acta Tropica*. 2020;212:105643. DOI:<https://doi.org/10.1016/j.actatropica.2020.105643>
- [31] Matsumura Y, Enomoto Y, Takahashi M, Maenosono S. Metal (Au, Pt) Nanoparticle–Latex Nanocomposites as Probes for Immunochromatographic Test Strips with Enhanced Sensitivity. *ACS Applied Materials & Interfaces*. 2018;10:31977-87. DOI:10.1021/acsami.8b11745
- [32] Borisov SM, Wolfbeis OS. Optical Biosensors. *Chemical Reviews*. 2008;108:423-61. DOI:10.1021/cr068105t
- [33] Shen J, Li Y, Gu H, Xia F, Zuo X. Recent Development of Sandwich Assay Based on the Nanobiotechnologies for Proteins, Nucleic Acids, Small Molecules, and Ions. *Chemical Reviews*. 2014;114:7631-77. DOI:10.1021/cr300248x
- [34] Hurley LH, Reynolds VL, Swenson DH, Petzold GL, Scathill TA. Reaction of the antitumor antibiotic CC-1065 with DNA: structure of a DNA adduct with DNA sequence specificity. *Science*. 1984;226:843 LP – 844. DOI:10.1126/science.6494915
- [35] Wang J, Liu B. Highly sensitive and selective detection of Hg<sup>2+</sup> in aqueous solution with mercury-specific DNA and Sybr Green I. *Chemical Communications*. 2008;4759-61. DOI:10.1039/B806885B
- [36] Bhasikuttan AC, Mohanty J, Pal H. Interaction of Malachite Green with Guanine-Rich Single-Stranded DNA: Preferential Binding to a G-Quadruplex. *Angewandte Chemie International Edition*. 2007;46:9305-7. DOI:<https://doi.org/10.1002/anie.200703251>
- [37] Maniatis T, Jeffrey A, Kleid DG. Nucleotide sequence of the rightward operator of phage lambda. *Proceedings of the National Academy of Sciences*. 1975;72:1184 LP – 1188. DOI:10.1073/pnas.72.3.1184
- [38] Li H, Liu J, Fang Y, Qin Y, Xu S, Liu Y, et al. G-quadruplex-based ultrasensitive and selective detection of histidine and cysteine. *Biosensors and Bioelectronics*. 2013;41:563-8. DOI:<https://doi.org/10.1016/j.bios.2012.09.024>
- [39] Day HA, Pavlou P, Waller ZAE. i-Motif DNA: Structure, stability and targeting with ligands. *Bioorganic & Medicinal Chemistry*. 2014;22:4407-18. DOI:<https://doi.org/10.1016/j.bmc.2014.05.047>
- [40] Tyagi S, Kramer FR. Molecular Beacons: Probes that Fluoresce upon Hybridization. *Nature Biotechnology*. 1996;14:303-8. DOI:10.1038/nbt0396-303
- [41] Zeng R, Luo Z, Su L, Zhang L, Tang D, Niessner R, et al. Palindromic Molecular Beacon Based Z-Scheme BiOCl-Au-CdS Photoelectrochemical Biodetection. *Analytical Chemistry*. 2019;91:2447-54. DOI:10.1021/acs.analchem.8b05265
- [42] Masuko M, Ohtani H, Ebata K, Shimadzu A. Optimization of



- excimer-forming two-probe nucleic acid hybridization method with pyrene as a fluorophore. *Nucleic acids research*. 1998;26:5409—5416. DOI:10.1093/nar/26.23.5409
- [43] Kolpashchikov DM. Binary Probes for Nucleic Acid Analysis. *Chemical Reviews*. 2010;110:4709-23. DOI:10.1021/cr900323b
- [44] Svanvik N, Westman G, Wang D, Kubista M. Light-Up Probes: Thiazole Orange-Conjugated Peptide Nucleic Acid for Detection of Target Nucleic Acid in Homogeneous Solution. *Analytical Biochemistry*. 2000;281:26-35. DOI:https://doi.org/10.1006/abio.2000.4534
- [45] Fang X, Cao Z, Beck T, Tan W. Molecular Aptamer for Real-Time Oncoprotein Platelet-Derived Growth Factor Monitoring by Fluorescence Anisotropy. *Analytical Chemistry*. 2001;73:5752-7. DOI:10.1021/ac010703e
- [46] Jhaveri SD, Kirby R, Conrad R, Maglott EJ, Bowser M, Kennedy RT, et al. Designed Signaling Aptamers that Transduce Molecular Recognition to Changes in Fluorescence Intensity. *Journal of the American Chemical Society*. 2000;122:2469-73. DOI:10.1021/ja992393b
- [47] Wang H, Wang Y, Jin J, Yang R. Gold Nanoparticle-Based Colorimetric and “Turn-On” Fluorescent Probe for Mercury(II) Ions in Aqueous Solution. *Analytical Chemistry*. 2008;80:9021-8. DOI:10.1021/ac801382k
- [48] Guilbault GG, editors. *Practical Fluorescence*, 2nd ed. Boca Raton: CRC Press; 2020. 826 p. DOI:10.1201/9781003066514
- [49] Alvarez-Pez JM, Ballesteros L, Talavera E, Yguerabide J. Fluorescein Excited-State Proton Exchange Reactions: Nanosecond Emission Kinetics and Correlation with Steady-State Fluorescence Intensity. *The Journal of Physical Chemistry A*. 2001;105:6320-32. DOI:10.1021/jp010372+
- [50] Haugland RP, editors. *Handbook of fluorescent probes and research products* [Internet]. 9th edition, EU version. Eugene (Or.) : Molecular probes; 2002. 966 p.
- [51] Song L, Hennink EJ, Young IT, Tanke HJ. Photobleaching kinetics of fluorescein in quantitative fluorescence microscopy. *Biophysical journal*. 1995;68:2588-600. DOI:10.1016/S0006-3495(95)80442-X
- [52] Jiao G-S, Han JW, Burgess K. Syntheses of Regioisomerically Pure 5- or 6-Halogenated Fluoresceins. *The Journal of Organic Chemistry*. 2003;68:8264-7. DOI:10.1021/jo034724f
- [53] Banks PR, Paquette DM. Comparison of Three Common Amine Reactive Fluorescent Probes Used for Conjugation to Biomolecules by Capillary Zone Electrophoresis. *Bioconjugate Chemistry*. 1995;6:447-58. DOI:10.1021/bc00034a015
- [54] Ceresole. M. Production of new red coloring matter. 1888;377360.
- [55] Poronik YM, Vygranenko K V, Gryko D, Gryko DT. Rhodols – synthesis, photophysical properties and applications as fluorescent probes. *Chemical Society Reviews*. 2019;48:5242-65. DOI:10.1039/C9CS00166B
- [56] Chen X, Pradhan T, Wang F, Kim JS, Yoon J. Fluorescent Chemosensors Based on Spiroring-Opening of Xanthenes and Related Derivatives. *Chemical Reviews*. 2012;112:1910-56. DOI:10.1021/cr200201z
- [57] Mishra A, Behera RK, Behera PK, Mishra BK, Behera GB. Cyanines during the 1990s: A Review. *Chemical Reviews*.



2000;100:1973-2012. DOI:10.1021/cr990402t

[58] Fabian J, Nakazumi H, Matsuoka M. Near-infrared absorbing dyes. Chemical Reviews. 1992;92:1197-226. DOI:10.1021/cr00014a003

[59] Zhu Z, Chao J, Yu H, Waggoner AS. Directly labeled DNA probes using fluorescent nucleotides with different length linkers. Nucleic Acids Research. 1994;22:3418-22. DOI:10.1093/nar/22.16.3418

[60] Ekimov A ~I., Onushchenko A ~A. *quantum* size effect in three-dimensional microscopic semiconductor crystals. Soviet Journal of Experimental and Theoretical Physics Letters. 1981;34:345.

[61] Kalyanasundaram K, Borgarello E, Duonghong D, Grätzel M. Cleavage of Water by Visible-Light Irradiation of Colloidal CdS Solutions; Inhibition of Photocorrosion by RuO<sub>2</sub>. Angewandte Chemie International Edition in English. 1981;20:987-8. DOI:<https://doi.org/10.1002/anie.198109871>

[62] Rossetti R, Nakahara S, Brus LE. Quantum size effects in the redox potentials, resonance Raman spectra, and electronic spectra of CdS crystallites in aqueous solution. The Journal of Chemical Physics. 1983;79:1086-8. DOI:10.1063/1.445834

[63] Murray CB, Norris DJ, Bawendi MG. Synthesis and characterization of nearly monodisperse CdE (E = sulfur, selenium, tellurium) semiconductor nanocrystallites. Journal of the American Chemical Society. 1993;115:8706-15. DOI:10.1021/ja00072a025

[64] Mal J, Nanchaiah Y V, van Hullebusch ED, Lens PNL. Metal chalcogenide quantum dots: biotechnological synthesis and applications. RSC Advances.

2016;6:41477-95. DOI:10.1039/C6RA08447H

[65] Zhu H, Song N, Lian T. Controlling Charge Separation and Recombination Rates in CdSe/ZnS Type I Core–Shell Quantum Dots by Shell Thicknesses. Journal of the American Chemical Society. 2010;132:15038-45. DOI:10.1021/ja106710m

[66] Chung Y-C, Yang C-H, Zheng H-W, Tsai P-S, Wang T-L. Synthesis and characterization of CdS<sub>x</sub>Se<sub>1-x</sub> alloy quantum dots with composition-dependent band gaps and paramagnetic properties. RSC Advances. 2018;8:30002-11. DOI:10.1039/C8RA06007J

[67] Li Y-F, Feng J, Sun H-B. Perovskite quantum dots for light-emitting devices. Nanoscale. 2019;11:19119-39. DOI:10.1039/C9NR06191F

[68] Chung S, Revia RA, Zhang M. Graphene Quantum Dots and Their Applications in Bioimaging, Biosensing, and Therapy. Advanced Materials. 2019;n/a:1904362. DOI:<https://doi.org/10.1002/adma.201904362>

[69] Medintz IL, Uyeda HT, Goldman ER, Mattoussi H. Quantum dot bioconjugates for imaging, labelling and sensing. Nature Materials. 2005;4:435-46. DOI:10.1038/nmat1390

[70] Cotta Ma. *quantum* Dots and Their Applications: What Lies Ahead? ACS Applied Nano Materials. 2020;3:4920-4. DOI:10.1021/acsanm.0c01386

[71] Ma F, Li C, Zhang C. Development of quantum dot-based biosensors: principles and applications. Journal of Materials Chemistry B. 2018;6:6173-90. DOI:10.1039/C8TB01869C

[72] Chern M, Toufanian R, Dennis AM. Quantum dot to quantum dot Förster resonance energy transfer: engineering materials for visual color change

sensing. *Analyst*. 2020;145:5754-67.  
DOI:10.1039/D0AN00746C

[73] Chan WCW, Nie S. Quantum Dot Bioconjugates for Ultrasensitive Nonisotopic Detection. *Science*. 1998;281:2016 LP – 2018. DOI:10.1126/science.281.5385.2016

[74] Zhao Y, Gao W, Ge X, Li S, Du D, Yang H. CdTe@SiO<sub>2</sub> signal reporters-based fluorescent immunosensor for quantitative detection of prostate specific antigen. *Analytica Chimica Acta*. 2019;1057:44-50. DOI:https://doi.org/10.1016/j.aca.2019.01.019

[75] Wu M, Zhang Z-L, Chen G, Wen C-Y, Wu L-L, Hu J, et al. Rapid and Quantitative Detection of Avian Influenza A(H7N9) Virions in Complex Matrices Based on Combined Magnetic Capture and Quantum Dot Labeling. *Small*. 2015;11:5280-8. DOI:https://doi.org/10.1002/smll.201403746

[76] Mateu MG. Assembly, Engineering and Applications of Virus-Based Protein Nanoparticles. *Advances in experimental medicine and biology*. 2016;940:83-120. DOI:10.1007/978-3-319-39196-0\_5

[77] Li F, Zhang Z-P, Peng J, Cui Z-Q, Pang D-W, Li K, et al. Imaging viral behavior in Mammalian cells with self-assembled capsid-quantum-dot hybrid particles. *Small (Weinheim an der Bergstrasse, Germany)*. 2009;5:718-26. DOI:10.1002/smll.200801303

[78] Sun X, Li W, Zhang X, Qi M, Zhang Z, Zhang X-E, et al. In Vivo Targeting and Imaging of Atherosclerosis Using Multifunctional Virus-Like Particles of Simian Virus 40. *Nano letters*. 2016;16:6164-71. DOI:10.1021/acs.nanolett.6b02386

[79] Banerjee A, Pons T, Lequeux N, Dubertret B. Quantum dots-DNA bioconjugates: synthesis to applications.

*Interface focus*. 2016;6:20160064. DOI:10.1098/rsfs.2016.0064

[80] Medintz IL, Konnert JH, Clapp AR, Stanish I, Twigg ME, Mattoussi H, et al. A fluorescence resonance energy transfer-derived structure of a quantum dot-protein bioconjugate nanoassembly. *Proceedings of the National Academy of Sciences of the United States of America*. 2004;101:9612 LP – 9617. DOI:10.1073/pnas.0403343101

[81] Feng H, ten Hove JB, Zheng T, Velders AH, Sprakel J. All-Aqueous Synthesis of Silica-Encapsulated Quantum Dots with Functional Shells. *European Journal of Inorganic Chemistry*. 2017;2017:5152-7. DOI:https://doi.org/10.1002/ejic.201700886

[82] Palui G, Aldeek F, Wang W, Mattoussi H. Strategies for interfacing inorganic nanocrystals with biological systems based on polymer-coating. *Chemical Society Reviews*. 2015;44:193-227. DOI:10.1039/C4CS00124A

[83] Díaz-González M, de la Escosura-Muñiz A, Fernandez-Argüelles MT, García Alonso FJ, Costa-Fernandez JM. Quantum Dot Bioconjugates for Diagnostic Applications. *Topics in Current Chemistry*. 2020;378:35. DOI:10.1007/s41061-020-0296-6

[84] Zhou J, Liu Q, Feng W, Sun Y, Li F. Upconversion Luminescent Materials: Advances and Applications. *Chemical Reviews*. 2015;115:395-465. DOI:10.1021/cr400478f

[85] Wang F, Banerjee D, Liu Y, Chen X, Liu X. Upconversion nanoparticles in biological labeling, imaging, and therapy. *Analyst*. 2010;135:1839-54. DOI:10.1039/C0AN00144A

[86] Fan H, Chang Z, Xing R, Chen M, Wang Q, He P, et al. An Electrochemical Aptasensor for Detection of Thrombin

based on Target Protein-induced Strand Displacement. *Electroanalysis*. 2008;20:2113-7. DOI:<https://doi.org/10.1002/elan.200804281>

[87] Tang S, Lu W, Gu F, Tong P, Yan Z, Zhang L. A novel electrochemical sensor for lead ion based on cascade DNA and quantum dots amplification. *Electrochimica Acta*. 2014;134:1-7. DOI:<https://doi.org/10.1016/j.electacta.2014.04.021>

[88] Yang Y, Yuan Z, Liu X-P, Liu Q, Mao C-J, Niu H-L, et al. Electrochemical biosensor for Ni<sup>2+</sup> detection based on a DNAzyme-CdSe nanocomposite. *Biosensors and Bioelectronics*. 2016;77:13-8. DOI:<https://doi.org/10.1016/j.bios.2015.09.014>

[89] Park H, Hwang S-J, Kim K. An electrochemical detection of Hg<sup>2+</sup> ion using graphene oxide as an electrochemically active indicator. *Electrochemistry Communications*. 2012;24:100-3. DOI:10.1016/j.elecom.2012.08.027

[90] Xu W, Zhou X, Gao J, Xue S, Zhao J. Label-free and enzyme-free strategy for sensitive electrochemical lead aptasensor by using metal-organic frameworks loaded with AgPt nanoparticles as signal probes and electrocatalytic enhancers. *Electrochimica Acta*. 2017;251:25-31. DOI:<https://doi.org/10.1016/j.electacta.2017.08.046>

[91] Rogez G, Massobrio C, Rabu P, Drillon M. Layered hydroxide hybrid nanostructures: a route to multifunctionality. *Chemical Society Reviews*. 2011;40:1031-58. DOI:10.1039/C0CS00159G

# Natural Dyes: From Cotton Fabrics to Solar Cells

*Indriana Kartini and Adhi Dwi Hatmanto*

## Abstract

This article will discuss natural dyes' role, from colouring the cotton fabrics with some functionality to harvesting sunlight in the dye-sensitized solar cells. Natural dye colourants are identical to the low light- and wash-fastness. Therefore, an approach to improving the colourant's physical properties is necessary. Colouring steps employing silica nanosol and chitosan will be presented. The first part will be these multifunctional natural dye coatings on cotton fabrics. Then, functionality such as hydrophobic surfaces natural dyed cotton fabrics will be discussed. Natural dyes are also potential for electronic application, such as solar cells. So, the second part will present natural dyes as the photosensitizers for solar cells. The dyes are adsorbed on a semiconductor oxide surface, such as  $\text{TiO}_2$  as the photoanode. Electrochemical study to explore natural dyes' potential as sensitizer will be discussed, for example, natural dyes for *Batik*. Ideas in improving solar cell efficiency will be discussed by altering the photoanode's morphology. The ideas to couple the natural dyes with an organic-inorganic hybrid of perovskite and carbon dots are then envisaged.

**Keywords:** natural dyes, cotton fabrics, hydrophobic, multifunctional textiles, dye-sensitized solar cells

## 1. Introduction

Technology is a means to achieve enhanced goals towards advancing human civilization, as is textile dyeing technology. Dyeing is an integral part of the wet textile processing process, which involves massive amounts of chemicals, both in type and quantity. Recently, the development of the concept of eco-fashion or sustainable textiles has led to the development of dyeing technology using natural dyes that care about aspects of water pollution, the sustainability of raw materials and processed products, biodegradability and other environmentally friendly attributes [1]. Human awareness of a healthy environment has revived interest in products that use natural dyes.

Eco-fashion or Sustainable Fashion as a trend against fast fashion is part of a developing design philosophy to create a system that can support and counteract the impact of human activities on the environment. The focus of eco-fashion is not only on the aspects of the materials used and the environment affected by it but also on the wearer's health and the durability of the clothes. An example is the use of natural pesticide-free materials, the use of materials that can be recycled, clothes that are made to last longer and are not easily damaged, to cover the welfare



guarantee for fashion workers. Conventional clothing production is known to involve many resources and produce hazardous waste for the environment. Three criteria attached to environmentally friendly textile creation products include less toxic chemicals, less land or water, and reduction of greenhouse gases. The advantages of nano-sized materials promise exploration opportunities for new technologies with achievements beyond those achieved in computers and biotechnology in recent decades.

The advantage of using natural dyes lies in the smoothness and softness of the colour. This product is highly valued and maintained because it reflects the beauty, prestige, and cultural structures whose existence cannot be replaced by synthetic dyes. However, despite the advantages of natural dyes, several shortcomings of natural dyes have made *Batik* (traditional Indonesia fabrics) craftsmen still reluctant to change their *Batik* dyes from synthetic dyes to natural dyes. Among them are the high price, limited availability, long manufacturing process, and low colour resistant to light or washing.

Natural dyes that are currently often used for *Batik* production besides indigo blue are *Tingi* (*Ceriops tagal*) natural dyes. This dye is obtained from the extraction of the bark of the *Tingi* tree, a type of mangrove plant, which has a high tannin content and is used as a dye for *Batik* and tanners. This dye gives the distinctive brown colour of *Batik*. Like most other natural dyes, *Tingi* natural dyes also have a low degree of fastness to washing. So it requires treatment to increase its fastness to washing. Efforts to increase the colour resistance to washing of cotton fabrics coloured by *Tingi* natural dyes will be discussed in the next section. Afterward, works to attach hydrophobic functionality to result in a multifunctional textiles will be described.

Nanotechnology is a technology related to materials or systems at the nanometer scale ( $1\text{ nm} = 10^{-9}\text{ m}$ ). Unusual changes, which cannot be predicted using classical mechanical models, will be obtained at the nanometer scale, such as changes to electronic properties, mechanical properties, magnetic properties, optical properties and chemical reactivity. The potential for a revival of natural dyes can occur through treaties with nanotechnology.

One of the breakthroughs in photovoltaic technology was the photovoltaic cell's invention based on the photoelectrochemical concept employing nanomaterial by a group of Swiss researchers [2], which became popular as dye-sensitized solar cells (DSSC). The solar cell is composed of a thin layer of semiconductor material, such as titanium dioxide or titania ( $\text{TiO}_2$ ), which has a porous structure, a complex ruthenium (Ru) compound as a sensitizer, and an electrolyte system for the redox pair of iodine compounds. The ruthenium dye complex has a role in absorbing solar radiation, which will generate the dye's electron system so that it flows into the semiconductor material and is connected to a circuit to generate an electric current. The excited electrons from the dye are immediately replaced by the electrons produced from the electrolyte redox pair system,  $\text{I}^-/\text{I}_3^-$ . The natural mechanisms of photosynthesis inspire technology to harvest and use continuous sunlight as a source of energy for all life on earth. Harvesting sunlight ultimately requires the sensitizer to have an absorption character like a black body. So far, ruthenium complex dye as a DSSC photosensitizer has produced a conversion efficiency of  $\sim 10\%$  [2]. However, ruthenium is not environmentally friendly. Therefore environmentally friendly sensitizers need to be sought. This environmental demand raises the potential of natural dyes as solar cell sensitizers.

Natural sources of natural dyes for sensitizers are directed to plants that have no potential as a food source and have a large percentage of active colouring agents. Several natural dyes that can be used as solar cell sensitizers have been identified to contain tannins, anthocyanins, betalains, flavonoids, and carotenoids [3]. *Batik's*

natural dyes used for production, mostly are rich of tannins. Potential of this natural dyes will be explored in the fourth section. Finally, some ideas to improve the performance of the natural dyes solar cell will be envisaged in the concluding remarks.

## 2. Improving the wash-fastness of the natural dyed cotton fabrics

The wood of the *tingi* tree (**Figure 1**) is usually used as firewood. The bark is used as a dye for *Batik* and tanners because of its high tannin content. According to Kasmudjiastuti [4] the tannin content in the bark reaches as high as 26%. The *tingi* bark gives a reddish brown colour with a large enough tannin content. The availability of *tingi* bark as a raw material is very abundant in Indonesia. According to Nazir [5] tannins from *Tingi* dyes fall into the category of condensation tannins, with 26% more tannins than other woody plants such as Avaram, Hemlock, Oak, and Chestnut. Kasmudjiastuti [4] characterised the extract of *tingi* tree wood, resulting in that *tingi* wood contains 70.91% of tannins which are included in procyanidin condensation tannins. However, natural dyes derived from plant extraction have a weakness in their fastness resistance to washing processes and exposure to light. Modification of the dye composition can increase the dye fastness [6].

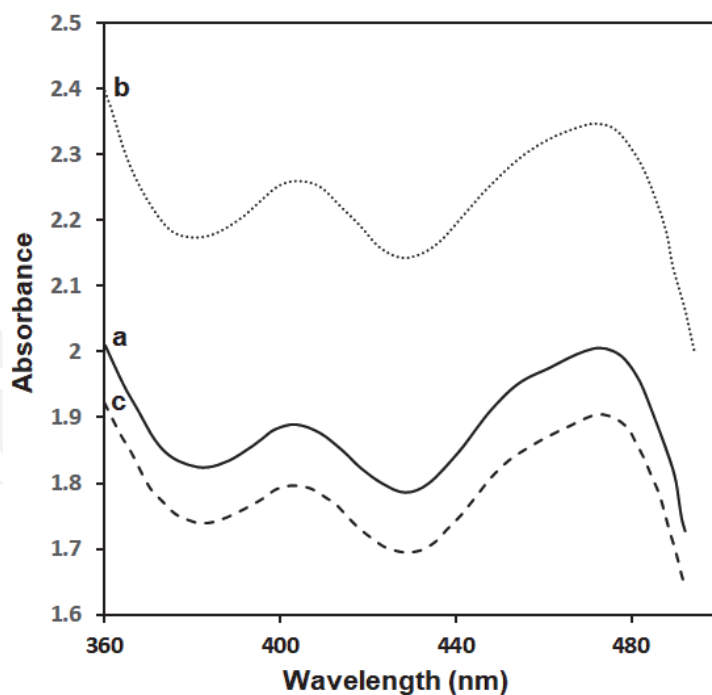
Dipping the dyed cotton into silica nanosols using the sol-gel method can improve the fastness resistance of a synthetic dye of malachite green b (MG) on cotton fabrics [7, 8]. The hydrogen interaction that occurs between the hydroxyl groups on the cellulose fibers and the hydroxyl groups from the silica sol probably made the silica-MG nanosols to be firmly coated on cotton fabrics. The thin silicon dioxide layer forms a layer that is resistant to heat, light, chemical processes and microbial attack. The oxide thin layer can improve the properties of mechanical strength and resistance to abrasion [7].

The silica nanosol was prepared using the sol gel method with tetraethylortosilicate (TEOS) as a precursor for Si. This process was carried out in an acidic solution of pH 3-4 using HCl as the catalyst and pH regulator [8]. **Figure 2** showed UV-Vis spectra of the *Tingi* extract in water and the mixture of silica nanosol and *Tingi* extract in volume ratio of 1:4 and 1:40. The maximum absorbance of the natural dye is at 473 nm and did not show any shifting after mixing with nanosol silica indicating no structure changes in the dye and the sols. The infrared spectra of the corresponding dried-powder of the mixture dye sols confirmed this, as implied in **Figure 3**. The more the dyes in the mixture sols, the weaker the peaks for Si-O-Si, at around  $1080\text{ cm}^{-1}$ .

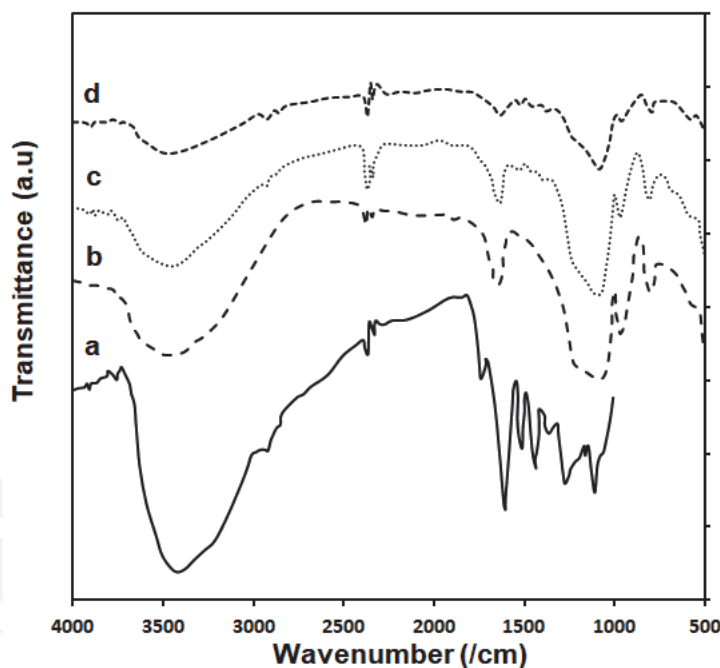
The dyeing process on the fabric was done by using the dip coating method, which is the direct immersion of the cloth in a solution mixture of silica sol and the



**Figure 1.**  
The Tingi tree (left) and its corresponding bark for the natural dye's resource (right).



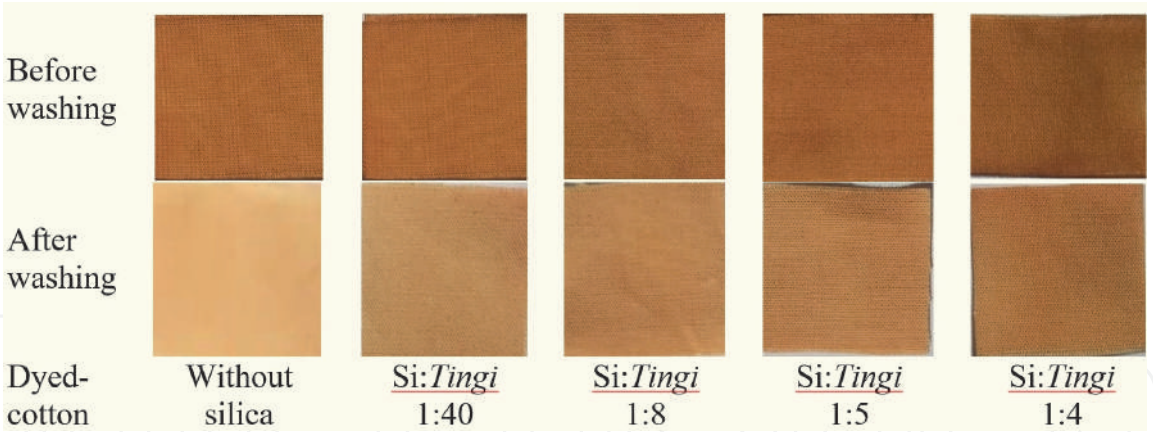
**Figure 2.**  
Electronic spectra of: a. Tingi extract, and silica sol-Tingi extract of: b. 1:4, c. 1:40 by volume.



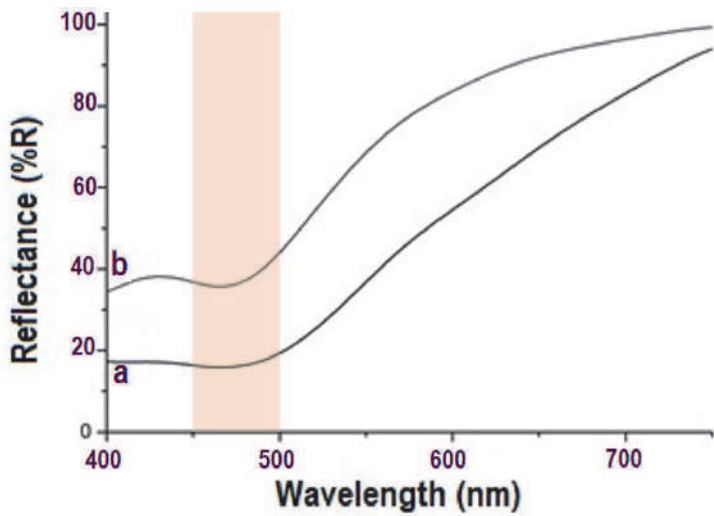
**Figure 3.**  
Infrared spectra of: a. Tingi extract powder, dried-powder of: b. silica sol, and silica sol-extract Tingi of: c. 1:4, d. 1:40.

dye extract. The variation of the volume ratio of the silica-dye sol was 1:40; 1:8; 1:5; and 1:4 with a total volume of 50 mL. The photos of the dyeing products are displayed in **Figure 4**. The strong dark brown colours are the dominant colour. The colour strength changed as the sols composition changed, with the strongest observed for fabric coloured by 1:4 mixture sols of Si-Tingi extract. At other compositions, the colour are almost the same.

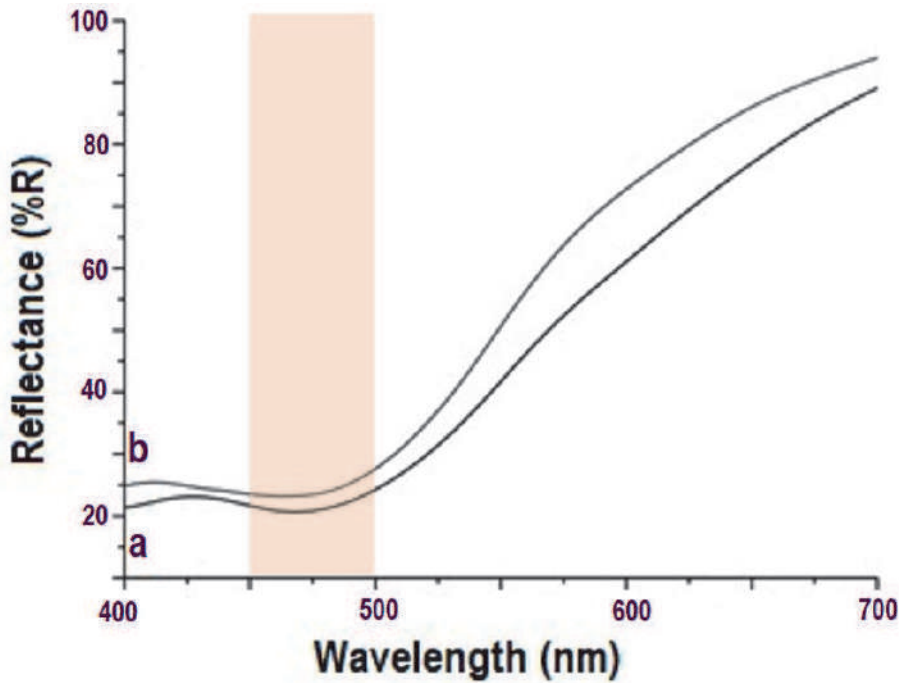
The wash-fastness of the dyed fabrics were tested by immersing the testing samples in 1% SDS (sodium dodecyl sulphate) solution (in water) at room



**Figure 4.**  
*Dyed cotton fabrics before and after washing under indoor illumination.*



**Figure 5.**  
*Reflectance spectra of dyed-cotton without silica coating: a. before washing, b. after washing.*



**Figure 6.**  
*Reflectance spectra of dyed-cotton with 1:4 silica coating: a. before washing, b. after washing.*



temperature for 1 h [7, 8]. Compared to cotton cloth without the addition of silica nanosol, the mixture composition of silica nanosol-dye can increase the wash-fastness resistance of the dye over the washing process. The  $\text{SiO}_2$ -*Tingi* nanosol ratio of 1: 4 gave the best results, where the colour after the washing process only changed very little when compared to the dyed cotton without nanosol  $\text{SiO}_2$ . The leaching degree calculated from the reflectance data was 3.18%.

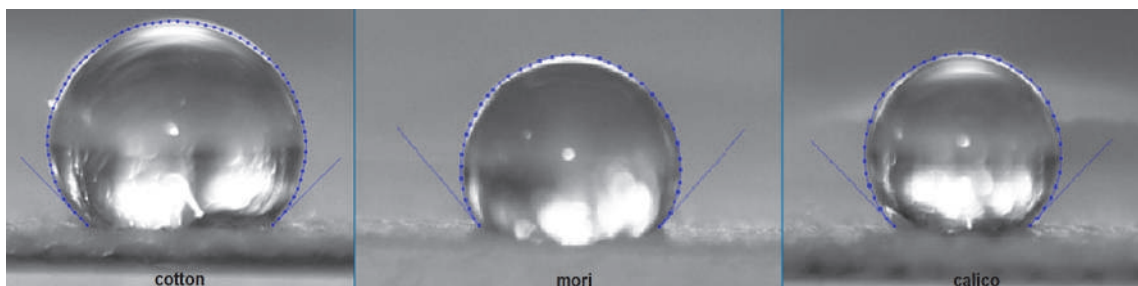
**Figures 5 and 6** showed the reflectance spectra to confirm the effect of nanosol silica in the mixture of dye sols. It can be seen that the reflectance difference for fabrics dyed with silica nanosols is relatively smaller than those without silica. Just recently, similar effect can also be obtained by using chitosan coating on the dyed-cotton [9]. It is envisaged that chitosan structure may provide more functional groups for hydrogen bonding with either cellulose of the cotton fabrics or the dye (represented by procyanidin as the active dye for the *Tingi* extract). Therefore, the mixture of chitosan and dye solutions resulted in lower leaching degree to SDS than that of the dye itself. Leaching degree as low as 6.24% has been achieved for dyeing process using a mixture of chitosan and *Tingi* extract [9].

### 3. Hydrophobic surfaces on natural dyed cotton fabrics

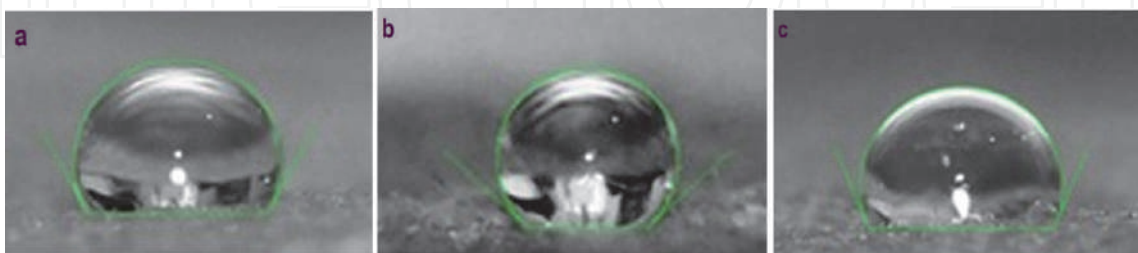
*Batik* is a work of art with distinctive patterns and motifs on the fabric. The *Batik* cloth used is a cloth that has gone through a pre-treatment preparation process in the textile industry. The pre-treatment process gives a different character to the *Batik* cloth, the *Batik* fabrics commonly used are calico, cotton, and mori. *Batik* fabrics, which are natural textiles, are generally made of cellulose (cotton) and protein (silk) so they are considered more susceptible to microbial attack than synthetic fibers because the porous structure and the constituent polymers are hydrophilic so they are easy to absorb moisture [10]. Fabric surface engineering of *Batik* material needs to be done so that the fabric surface becomes hydrophobic and indirectly provides antimicrobial properties. Topographical engineering of micro-structure and chemical properties on the surface of the fabric was carried out using the sol-gel method.

So far, the surface preparation of hydrophobic fabrics has been done using fluorocarbons which are known to be compounds with low surface energy. Hayn et al. [11] conducted coating of fluorosilane compound (FS) on a nylon-cotton blend fabric resulting in a water contact angle of  $148^\circ$ . However, the use of fluorinated compounds which are commonly used as hydrophobic agents is now starting to be abandoned due to adverse effects such as pollution caused by high toxicity, bioaccumulation in living things and the costs used are also relatively expensive [12]. This has led to research using non-fluorine compounds which are more environmentally friendly. One of them is the compounds of the alkylsilane group which are known to have low surface energy, for example trimethylchlorosilanes (TMCS), octadecyltrichlorosilanes (ODTCS), cetyltrimethoxysilanes (CTMS), and hexadecyltrimethoxysilanes (HDTMS) [13]. Here, we used HDTMS as the hydrophobic agent.

Three types of fabrics commonly used for *Batik* are cotton, *mori* and calico. The three types of clothes are batik fabrics which are differentiated based on the fabrication process. Calico cloth is a cellulose-based cloth that does not go through a pre-treatment process, while cotton and *mori* fabrics go through a pre-treatment process. Therefore, there are differences in fabric properties that will affect the interaction with silica nanosols and HDTMS. **Figure 7** shows the water contact angle obtained from the surface of the three types of *Batik* common fabrics. Cotton and calico clothes resulted in similar basic water contact angle, so similar hydrophobicity. Therefore, for further testing using *Tingi* dyed fabrics, we used cotton.



**Figure 7.**  
The water contact angle on different types of Batik's fabrics: cotton  $135.8^\circ$ , mori  $133.9^\circ$ , and calico  $136.2^\circ$ .



**Figure 8.**  
The water contact angle on cotton fabrics dyed by: a. Tingi extract ( $120.1^\circ$ ), b. Tingi-silica nanosol mixture ( $134.7^\circ$ ), C. tingi and silica nanosol layer by layer ( $114.7^\circ$ ).

**Figure 8** displays the water contact angle of *Tingi*-dyed fabrics with and without silica nanosols coated by HDTMS. The mixture nanosol coated cloth showed the best hydrophobicity properties with the greatest water contact angle value of  $134.7^\circ$ , while the fabric coated layer by layer gave the lowest hydrophobicity. This could be due to the weak interaction between HDTMS and the dye molecules. The layer by layer coatings on cotton fabrics were performed in the sequence of silica nanosol, the dye, and the HDTMS.

Our recent results for chitosan coating mixture have shown improved water contact angle after leaching test using natural detergent (*Sapindus rarak*). Saponin in the *Sapindus rarak* which also classified as the low surface energy compound is presumably responsible for this enhanced hydrophobicity. A ten percent improvement was achieved for the fabrics dyed by a mixture of chitosan-*Tingi* extract dye, resulted in water contact angle of  $107.83^\circ$  [9]. Further studies are still required to explore the potential of *Sapindus rarak* as the co-hydrophobic agent to obtain a hydrophobic *Batik* fabrics.

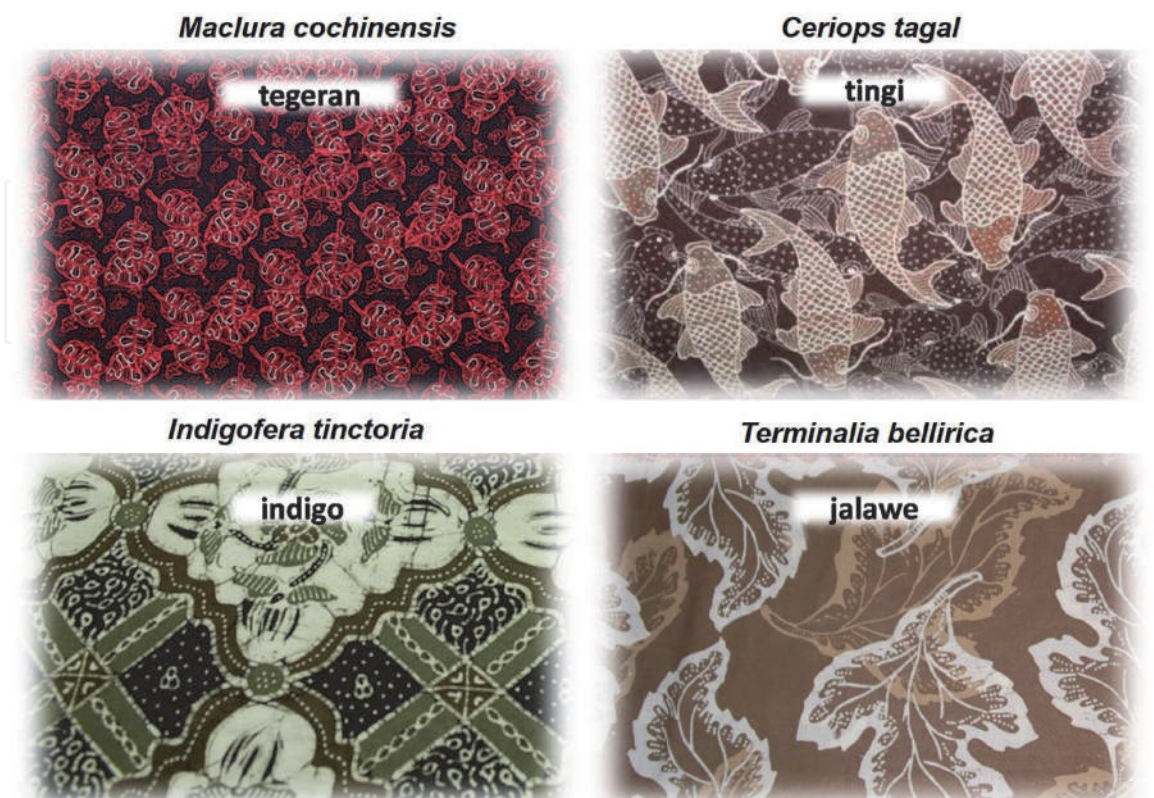
#### 4. Natural dyes for dye-sensitized solar cells: *Batik* and Algae's extract

A dye-sensitized solar cell (DSSC) is one promising alternative to conventional semiconductor silicon-based solar cells due to its low-cost and moderate efficiency. DSSC is typically constructed of  $\text{TiO}_2$  (titania) nanoparticles film sensitized with a monolayer of dye molecules as the photoanode. Upon light illumination, the photo-excited dye molecules inject the electrons. Then, the electrons transport through the photoanode to the counter electrode (e.g., fluorine-doped tin oxide (FTO)). These electrons are collected at the counter electrode through an external load and further shuttled back to the oxidized dye molecules via redox reactions of  $\text{I}^-/\text{I}_3^-$  redox couple in the electrolyte. The dye molecules are critical to the overall device performance since they determine the amount of solar energy absorbed by the device. The efficiencies of the sensitizers are related to some essential criteria. The HOMO



potential of the dye should be sufficiently positive compared to the electrolyte redox potential for efficient dye regeneration. The dye's LUMO potential should be negative enough to match the potential of the conduction band edge of the  $\text{TiO}_2$ . Its orbitals should be located at the acceptor part of the dye to provide efficient electron injection. The common dyes in DSSCs are based on ruthenium metal-ligand complexes (e.g. N3 and N719 dyes). However, the limited availability of ruthenium and the low stability of ruthenium-based dyes could hinder the commercialization of DSSCs. On the other hand, natural dyes are promising sensitizers for DSSC application because of their high extinction coefficient and variable chemical structures for strong and broad absorption of solar energy. In addition to the consideration of environmental aspects, natural dyes can also be extracted easily through water, methanol, or ethanol extraction process directly from the bark, roots, flowers, or leaves, so that they are cost-effective in comparison to the manufactured Ru dyes [14, 15].

Some natural dyes, including dyes extracted from the bark of *Tingi* (*Ceriops tagal*, CT) and *Tegeran* (*Maclura cochinchensis*, MC), the dried fruit of *Jalawe* (*Terminalia bellirica*(*gaertn*)*roxb*, TB), as well as the leaves of Indigo (*Indigofera tinctoria*, IT), are commonly used in the production of *Batik* (**Figure 9**), a technique of wax-resist dyeing applied to whole cloth originated from Java Island in Indonesia. The bark of CT is silvery-grey to orangeish-brown, smooth with occasional pustular lenticels, containing 23-40% tannin. Like CT, the smooth, lenticellate, and yellowish-brown bark of MC contains a high amount of tannin. The dried fruit of TB is yellowish-brown with flavonoids, sterols, and tannins content [16], while the IT dye contains 2,2'-Bis(2,3-dihydro-3-oxoindolyliden), known as Indigotin, with a dark blue colour. Since all of those “Batik” natural dyes are able to absorb light, the possibility of using them as photosensitizers for DSSC will then become interesting and important to be further investigated. Considering that the energy level of the photosensitizers will strongly affect the electron transport in DSSC, in this study, the absorption spectra and electrochemical properties of the *Batik* natural dyes were

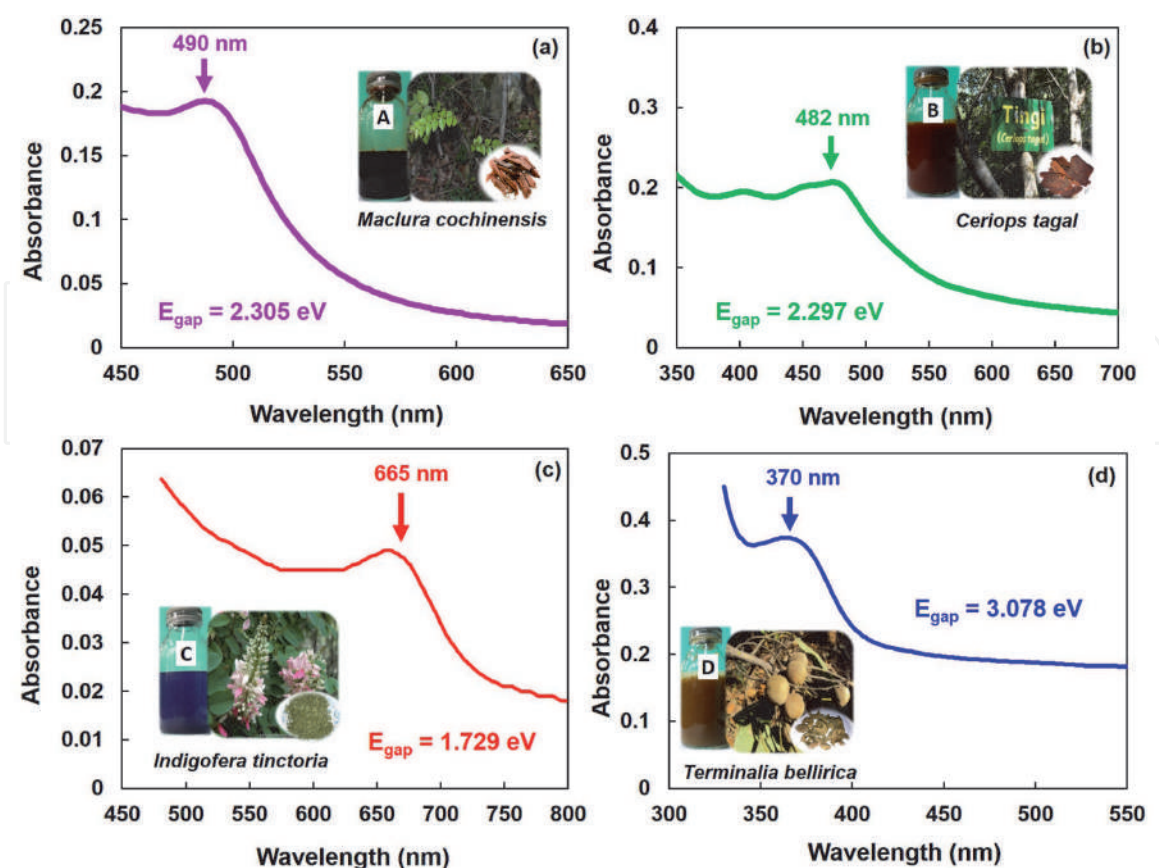


**Figure 9.**  
Batik with some Indonesian natural dyes.

presented and discussed. Both data were used to construct the energy of the highest occupied molecular orbitals (HOMO) and lowest unoccupied molecular orbitals (LUMO) of the corresponding natural dyes to reveal their potential as a light harvester for DSSC.

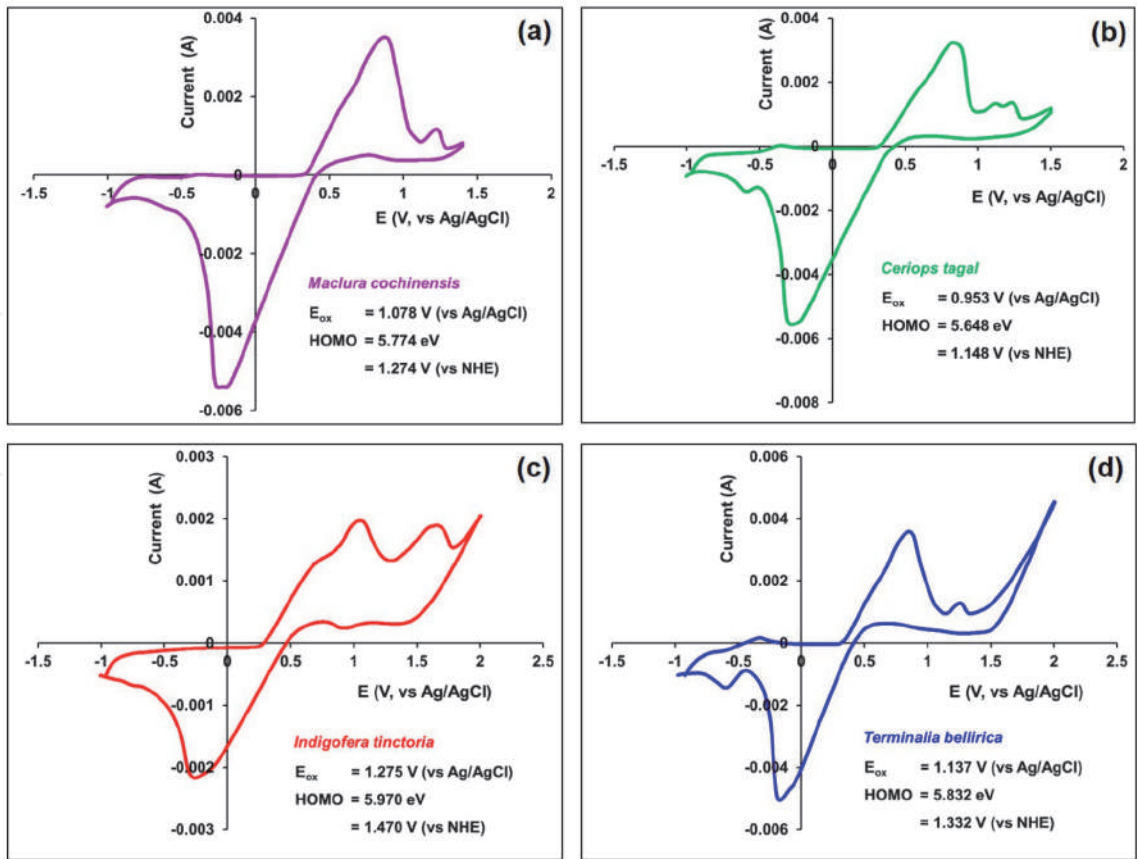
The construction of schematic energy diagrams in DSSC requires some information regarding the HOMO and LUMO energy levels of the photosensitizer that are determined from its absorption spectra and electrochemical properties. The electronic spectra of the *Batik* natural dye extracts were determined using the UV-Vis spectrophotometry method in the range of 300 to 800 nm, as shown in **Figure 10**. The bark of *MC* and *CT*, as well as the dried fruit of *TB*, were extracted by heating in distilled water, while the *IT* dye was prepared by dissolving a commercial Indigo paste directly in ethanol. The dye extracted from the bark of *MC* shows a single absorption at 490 nm, while several absorptions in the range of 450-500 nm (with the highest peak at 482 nm) were observed from the dye extracted from the bark of *CT*. Both dyes extracted from *IT* and *TB* show a single absorption peak respectively at 665 and 370 nm. The energy band gap of materials was then determined by using the absorption edge of the spectrum. The absorption edge of *MC*, *CT*, *IT*, and *TB* were obtained at observed at 538, 540, 718, and 403 nm, respectively, which attributed to the bandgap energy ( $E_{\text{gap}}$ ) of 2.305, 2.297, 1.729, and 3.078 eV. These  $E_{\text{gap}}$  values, together with the  $E_{\text{HOMO}}$  (determined from cyclic voltammetry analysis), were then used to calculate the LUMO energy level.

The electrochemical properties of all *Batik* natural dyes were studied by cyclic voltammetry method using Pt as the working electrode, Pt-wire as the auxiliary electrode, and Ag/AgCl as the reference electrode, with the addition of  $\text{I}^-/\text{I}_3^-$  redox couple as supporting electrolyte. The cyclic voltammograms of all four dyes are shown in **Figure 11**. All cyclic voltammograms results show combined peaks characteristic to



**Figure 10.**  
 UV-Vis absorption spectra of four Batik natural dyes: (a) *Maclura cochinchensis* (MC), (b) *Ceriops tagal* (CT), (c) *Indigofera tinctoria* (IT), (d) *Terminalia bellirica* (TB).





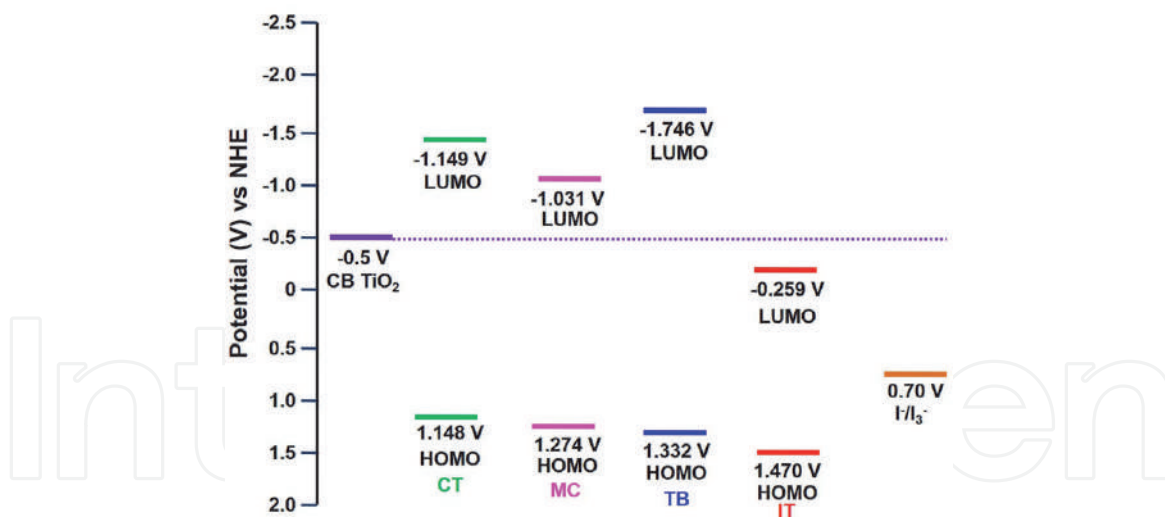
**Figure 11.** Cyclic voltammograms of four Batik natural dyes: (a) *Maclura cochinchensis* (MC), (b) *Ceriops tagal* (CT), (c) *Indigofera tinctoria* (IT), (d) *Terminalia bellirica* (TB).

oxidation and reduction potential of the reference electrolyte and the natural dyes. The HOMO energy level of the dyes was then calculated from the onset anodic potential of the cyclic voltammograms. The onset anodic potential ( $E_{ox}$ ) is a cross-section of the baseline and the oxidation peak of the dye [17].  $Fe(CN)_6^{4-}/Fe(CN)_6^{3-}$  redox couple was used as an external standard to calculate the  $E_{HOMO}$  of the natural dyes. The onset anodic potential of MC, CT, IT, and TB were observed respectively at 1.078, 0.953, 1.275, and 1.137 V, which are attributable to the  $E_{HOMO}$  of 1.274, 1.148, 1.470, and 1.332 V (vs NHE), respectively. The  $E_{LUMO}$  was then calculated based on the bandgap energy and the  $E_{HOMO}$  of the dyes. They are  $-1.031$ ,  $-1.149$ ,  $-0.259$ , and  $-1.746$  V (vs NHE), respectively for MC, CT, IT, and TB. The half-wave redox potential ( $E_{p/2}$ ) of  $I^-/I_3^-$  redox couple that was used as supporting electrolyte was observed at around 0.478 V vs. Ag/AgCl or 0.701 V vs. NHE. The values of  $E_{gap}$ ,  $E_{HOMO}$ , and  $E_{LUMO}$  of all Batik natural dyes were summarized in Table 1.

Figure 12 shows a schematic energy level diagram of DSSC using Batik natural dyes as photosensitizer and  $I^-/I_3^-$  a couple as redox electrolyte. All the HOMO levels of the dyes are sufficiently more positive than the half-wave redox potential

Dyes	Absorption Edge (nm)	$E_{gap}$ (V)	HOMO (V vs. NHE)	LUMO (V vs. NHE)
MC	538	2.305	1.274	$-1.031$
CT	540	2.297	1.148	$-1.149$
IT	718	1.729	1.470	$-0.259$
TB	403	3.078	1.332	$-1.746$

**Table 1.** The values of  $E_{gap}$ ,  $E_{HOMO}$ , and  $E_{LUMO}$  of the four Batik natural dyes.



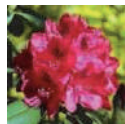

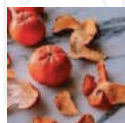
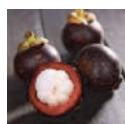
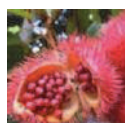



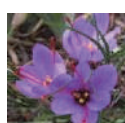
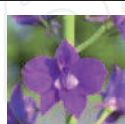



**Figure 12.**






Schematic energy level diagram of DSSC using Batik natural dyes as photosensitizer and  $I^-/I_3^-$  couple as redox electrolyte.

of  $I^-/I_3^-$  couple, suggesting an efficient regeneration of the oxidized dye by the  $I^-/I_3^-$  redox couple as the hole transport material. Meanwhile, the LUMO level of the dyes is sufficiently more negative than the conduction band edge of the  $TiO_2$  ( $E_{CB}$ ), except for IT, which ensure the necessary driving force for electron injection from the excited state of the dye into the conduction band of  $TiO_2$  semiconductor [18, 19]. Therefore, in this DSSC system, we can expect that the *Batik* natural dyes would be regenerated by  $I^-/I_3^-$  redox couple and allow the electron injection to the semiconductor and complete the electron flow through an external circuit. **Table 2** lists the solar cell parameters of some *Batik* dyes. The order of efficiency of the solar cell corresponds to the ease of electron injection from the dyes into the conduction band of  $TiO_2$ . Thermodynamically, the LUMO of MC to the conduction band of  $TiO_2$  is closer than the LUMO of CT and TB (**Figure 12**). Thus, facilitating the electron injection from the dyes to the semiconductor oxide. However, the cell efficiency is still low. It is probably due to the poor cell construction as indicated by the low values for all solar parameters (**Table 2**).

Kay and Gratzel [27] has studied photosensitization of  $TiO_2$  solar cells with chlorophyll derivatives and related natural porphyrins. Mechanism for sensitization has been revealed [28]. Here, spectral sensitization of  $TiO_2$  films with natural chlorophylls extracted from algae is reported. The crude chlorophylls extracts are obtained by methanol extraction of the dried algae. The algae were harvested from Krakal beach, Yogyakarta on September 2007. They were washed with water and air-dried before use. **Figure 13** shows the absorption spectra of some chlorophylls extracted from algae and the corresponding sensitized titania film.

Based on the UV-Vis absorption spectra of the algal methanol extract in **Figure 13**, it appears that the spectra show the two main absorption characters in the visible light region, around 416-422 nm and 660-666 nm. These results are consistent with the results of Kay and Gratzel [27] who have extracted chlorophyll a and b from spinach using methanol as a solvent. The visible light absorption ability of each algal methanol extract can be assessed by determining the solution's light absorption coefficient. In this study, the light absorption coefficient was determined by measuring the uptake of algae methanol extract at different concentrations. Then the absorption coefficient can be determined by applying the Lambert-Beer law ( $A = a.b.c$ , where  $A$  is the absorbance,  $a$  is the absorption coefficient,  $b$  is the thickness of the sample and  $c$  is the concentration of the solution). The concentration of algae extract that is not a pure isolated chlorophyll extract is expressed in

Dye Sources		Active Ingredients	J <sub>sc</sub> (mA.cm <sup>-2</sup> )	V <sub>oc</sub> (V)	FF	η (%)	Ref.
	Rhododendron	carotenoid	1.61	0.585	0.609	0.57	[20]
	Yellow rose	carotenoid	0.74	0.609	0.571	0.26	[20]
	Tangerine peel	flavonoid	0.74	0.592	0.631	0.28	[20]
	Mangosteen pericarp	anthocyanin	2.69	0.686	0.633	1.17	[20]
	Achiote seed	bixin	1.10	0.57	0.59	0.37	[21]
	Chrysanthemum	xanthophyll	0.09	0.31	0.26	0.01	[22]
	Pomegranate leaf	chlorophyll	2.05	0.56	0.52	0.597	[23]
	Mulberry	anthocyanin	1.89	0.555	0.49	0.548	[23]
	Saffron petal	anthocyanin	2.77	0.36	0.52	0.52	[24]
	<i>Consolida orientalis</i>	delphinidin	0.56	0.60	0.53	0.18	[25]
	<i>Adonis flammea</i>	astaxanthin	0.40	0.59	0.66	0.16	[25]
	<i>Salvia sclarea</i>	eupatilin	0.10	0.37	0.54	0.02	[25]
	Green algae	chlorophyll	0.13	0.41	0.21	0.01	[26]

Dye Sources		Active Ingredients	J <sub>sc</sub> (mA.cm <sup>-2</sup> )	V <sub>oc</sub> (V)	FF	η (%)	Ref.
	<i>Maclura cochinchensis</i> (MC)*	phenolic	0.0064	0.10	0.38	0.0100	this work
	<i>Ceriops tagal</i> (CT)*	phenolic	0.0032	0.07	0.21	0.0020	this work
	<i>Terminalia bellerica</i> (TB)*	phenolic	0.0064	0.10	0.31	0.0080	this work
	<i>Sargassum mcclurei</i> Setchell (SM)†	chlorophyll	3 × 10 <sup>-5</sup>	0.06	0.25	0.0009	this work
	<i>Hypnea esperi</i> Bory (HE)†	chlorophyll	0.013	0.055	0.31	0.0044	this work

\*P<sub>input</sub> = 25.6 mW/cm<sup>2</sup>, vapor deposited Au counter electrode.  
†P<sub>input</sub> = 50.0 mW/cm<sup>2</sup>, vapor deposited Au counter electrode.

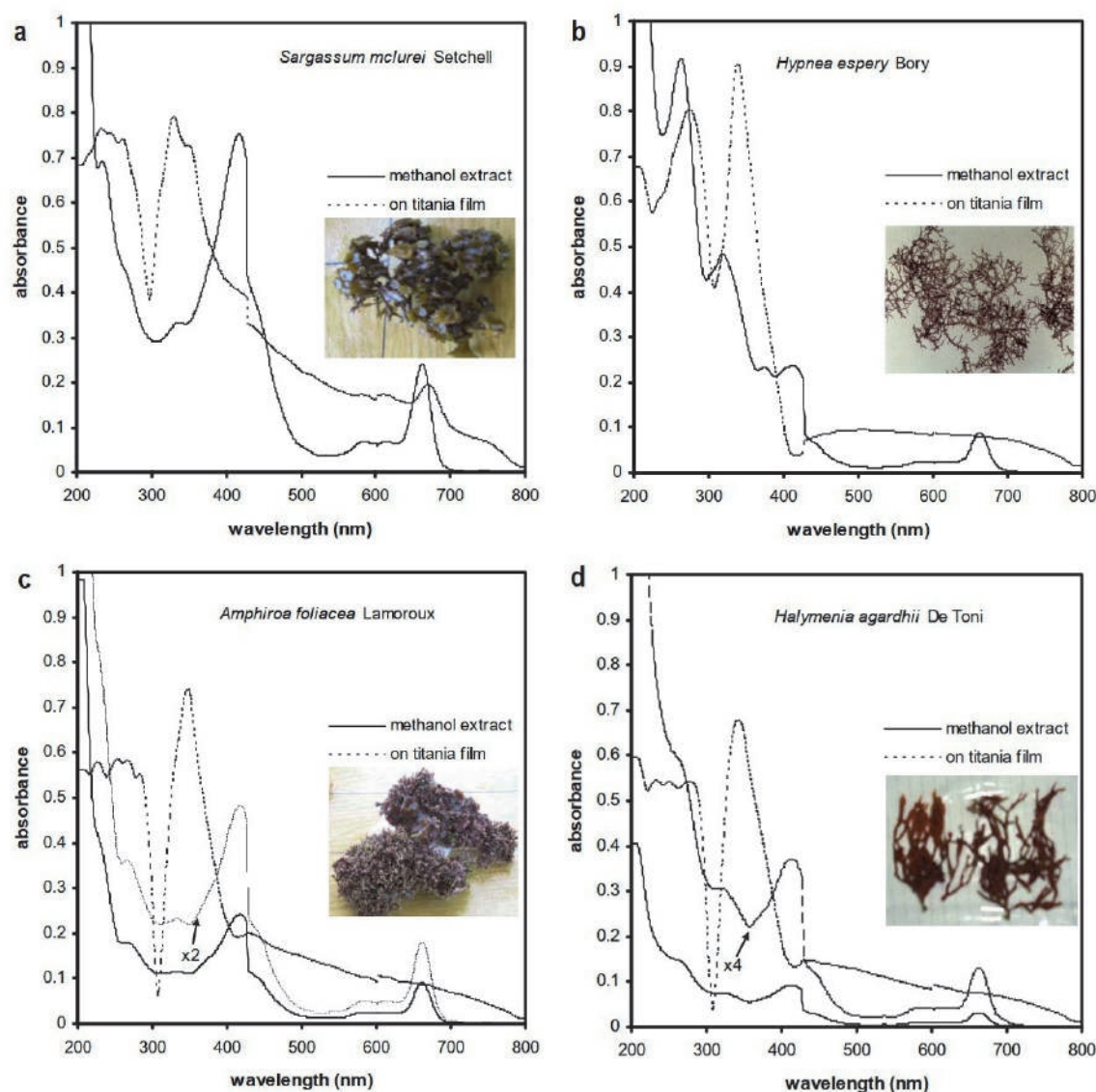
**Table 2.**  
Photoelectrochemical parameters of DSSC with Batik and other natural dyes.

the weight concentration of the extract against the volume of solvent (mg/L), so that *a* is also expressed in mg<sup>-1</sup> mL cm<sup>-1</sup>. It appears that the methanol extract of the algae *Sargassum mcclurei* Setchell (SM) has the greatest ability to absorb visible light (*a* = 0.027), while the algae *Hypnea esperi* Bory (HE) has the ability to absorb less light (*a* = 0.006). The value of *a* is characteristic and expresses the intrinsic property of a chemical species to absorb light at a particular wavelength. Based on the electronic spectra of the algae's methanol extract in **Figure 13**, it can be confirmed that chlorophyll *a* is the main component of the algae's extracts. The concentration of chlorophyll *a* (*Ca*) can be calculated using the equation  $Ca = 12.7 \cdot A_{663} - 2.69 \cdot A_{646}$  [29]. It turns out that the value of *a* is in line with the chlorophyll concentration (*Ca*) contained in the algae methanol extract. The *Ca* algae SM and HE were 2.59 and 0.96 mg/L, respectively. While, the *Ca* of extract HA and AF were 0.35 and 0.98 mg/L, respectively. Algae SM has green leaves, but the others are brown to red. Based on the character of visible light absorption and the *Ca*, the algae SM has the best character as a DSSC sensitizer. Two dye extracts of SM and HE were set for I-V measurement. The extract of *Hypnea esperi* Bory is chosen for I-V testing due to its rich spectra absorption from UV to visible region compared to the other two algae. **Table 2** presents the solar cell parameters as the results from SM and HE solar cells. It is confirmed that SM resulted in better solar cell parameters compared to HE as predicted.

The absorption spectra of four methanol extract dyes of algae as adsorbed on TiO<sub>2</sub> surface, depicted in **Figure 13**, are all relatively broadened forward to both red and blue sides of visible region compared to their respective spectra in methanol solution. These indicate pronounced aggregation occurred as the dyes adsorbed on



TiO<sub>2</sub> surface. However, the absorption pattern of SM is quite different. The electronic absorption of methanol extract of SM exhibits similar pattern to its respective spectra on TiO<sub>2</sub> surfaces. Two main peaks of chlorophyll *a* are still observed. The Soret band experienced hypsochromic shift (blue-shifted), while the Qy band was red-shifted. This indicates that chlorophyll *a* of SM adsorbed on the TiO<sub>2</sub> surface with limited aggregation [30, 31]. Absorption spectrum in the visible region resembles the absorption spectra of chlorophyll *a* in a mixture of methanol or ethanol-water upon completion of transition of monomer into aggregates [32]. A weak shoulder around 445 nm, close to the Soret band is also observed. This may ascribe to the presence of chlorophyllin *b* [33]. Chlorophyllin is chlorophyll derivative in which the cyclopentanone ring is opened as well as the carbonyl of the phytol ester bond [33]. Compared to the parent chlorophyll, the Qy band of chlorophyllin is much weaker than the Soret band. The presence of chlorophyllin affects mainly the intensity of the Qy bands of the crude extracts of algae. In general, the Qy bands of chlorophyll contained in methanol extracts of algae are slightly lower related to the synthetic chlorophyll *a* presented in the previous reference [33]. The presence of chlorophyllin as observed in **Figure 13** is predicted to facilitate aggregation due to intermolecular bonding induced by the –COOH groups. Efficient photosensitization



**Figure 13.**

The electronic absorption of methanol extract of algae adsorbed on titania film and their corresponding solution spectra of: a. *Sargassum mclurei* Setchell (SM) b. *Hypnea espery* Bory (HE), c. *Amphiroa foliacea* Lamoroux (AF), and d. *Halymenia agardhii* De Toni (HA).

may result from efficient electron injection through the bonding formed between  $\text{TiO}_2$  and the pigment. Large difference in the photocurrent density of the SM and HE cells rather than in photovoltage suggesting that the solar cell performance of the cells are influenced by the efficiency of the electron injection from the sensitizers into  $\text{TiO}_2$  [34].

Natural dyes can be used as a sensitizer, which will require making and purifying dyes more efficiently and rapidly in order to lower production costs, reduce the risk of solar cell toxicity, and use an environmentally sustainable manufacturing method. Some also can be extracted from fruit waste [20, 21], thus it is green technology. Improved efficiency are still intensively researched by employing a cocktail of dyes [20–26, 35], adsorbed dyes on clay [36], optimizing solvent extraction [37]. Amongst, combination of dyes has shown two to three times increased efficiency, while the use of clay has decreased the cell efficiency. It has been shown that  $\text{TiO}_2$  is still superior compared to  $\text{ZnO}$  semiconductor as the photoanode materials [38]. Therefore, discussion will focus on the improvement of natural dyes PEC solar cells due to the use of nanostructured titania.  $\text{TiO}_2$  has band gap energy ( $E_g$ ) in the range of 3.0–3.2 eV. The crystalline phase of  $\text{TiO}_2$  found in nature includes anatase, rutile, brookite, and  $\text{TiO}_2$ -B. Among all the crystalline  $\text{TiO}_2$  phases, anatase is the most photoactive crystalline phase. The energy of the upper  $\text{TiO}_2$  band gap is 3.2 eV, higher than rutile (3.0 eV). The width of the  $\text{TiO}_2$  band gap gives the nature of photostability due to the electron recombination.

The next strategy is to take advantage of the sophistication of nanotechnology, namely utilizing the features of 1D nanostructures such as nanofibers, nanotubes, nanorods; which allows a toll path for electrons from the sensitizer to the back contact of the titania photoanode [39, 40]. The  $\text{TiO}_2$  nanorod photoanode gave a value of  $V_{oc}$  0.802 V,  $I_{sc}$  7.01 mA and efficiency of 2.9% [41], whereas  $\text{TiO}_2$  nanowire produced  $V_{oc}$  0.752 V,  $I_{sc}$  3.73 mA and efficiency of 1.81% [42]. The  $\text{TiO}_2$  nanotube photoanode gave characteristic values of  $V_{oc}$  0.846 V,  $I_{sc}$  ~9.63 mA and efficiency of 4.03% [43]. Bijarbooneh et al. [44] used mesoporous  $\text{TiO}_2$  nanofibers and obtained  $V_{oc}$  0.76 V,  $I_{sc}$  15.23 mA and were able to increase energy efficiency from 7.28% to 8.14%. The cell performance of nanotubes titania was three-times higher than that constructed from nanoparticle titania (P25) using mangosteen pericarp ethanol extract as the sensitizer [45]. These studies encourage the use of 1D nanostructured  $\text{TiO}_2$  to improve performance of the natural dyes solar cells.

Another possibility to improve the natural dyes solar cells is the invention of perovskite material for hybrid DSSCs. Methylammonium lead (II) iodide ( $\text{MAPbI}_3$ ) is a perovskite material where the A cation is the organic  $\text{CH}_3\text{NH}_3^+$  cation, B is the  $\text{Pb}^{2+}$  metal cation, and X is the halide anion such as  $\text{I}^-$ . Since having a band gap energy of 1.55 eV, which is equivalent to the absorption at a wavelength of 800 nm, this material is potential as visible light absorber. The solar cells efficiency with perovskite structure has achieved up to 25.2% [46]. This high conversion efficiency provides the opportunity to be combined with natural dye sensitised solar cells. Dey et al. [47] has shown that a perovskite and carotene dye layers resulted in a conversion efficiency of up to 5.01%, which was almost ten times than that of solar cells using carotene alone [20]. This new perovskite material feature is expected to be another way to the revival of natural dyes as solar cell sensitizers. However, the presence toxic elements of lead in the perovskite could be a challenge for sustainability.

Recent computational study has shown potential of nanohybrid of graphene quantum dots (GQD), a one type of carbon dots, with porphyrin as the solar cell [48]. It was found that the electron transfer from porphyrin to GQD is faster for larger size of GQD. Nanocomposite carbon dots-polymer [49] has also resulted promising results for quasi solid state solar cells. The carbon dot in the electrolyte

composition resulted in improved efficiency up to 6.05% by absorbing unused higher energy of visible light. These findings pave a way to more efficient green natural dyes solar cells.

Our fast-moving time demands creating and innovating science and technology in natural dye's application. Intrinsic properties of the natural dyes of having rich antioxidant are rendering the potential for multifunctional antibacterial textiles. The soft and shady colour of natural dye dyed fabrics with low impact on the environment also drive the fashion industry into the more sophisticated functions of sustainable fashion. It is not only for textile colouring but also for bringing prestige and dignity. The more sophisticated natural dyes function as photosensitisers for photodynamic therapy (PDT) requires intensive purification [50, 51]. Advanced nanotechnology may direct the applications to the photochromic and sensor materials [52, 53].

## 5. Concluding remarks

Some works on the use of natural dyes for textiles have been presented. The use of natural dyes supports the shifting paradigm in the world fashion to the sustainable fashion. Although, past researches have endorsed essential growth in the application of the natural dyes for fabrics, but still there are a number of technical challenges of natural dye application that must be overcome. The composite formation with green resources such as chitosan, silica may result in enhance dyeing performance to cotton fabrics. Functional such as hydrophobic surface may also be introduced by using natural ingredients such as *Sapindus rarak*.

This work also presents the investigation of the absorption and electrochemical properties of four *Batik* natural dyes to be considered as environmentally friendly photosensitisers for dye-sensitised solar cells. All *Batik* natural dyes extract exhibit absorption peaks in the visible wavelength ensuring their sunlight harvesting ability and HOMO-LUMO energy levels ideal for DSSC. It is noteworthy to blend all the *Batik* dyes to obtain superposition of absorption spectra covering a visible light region from 350 to 800 nm, thus resulting in more efficient panchromatic dyes as required for DSSC. Most of the HOMO-LUMO of the *Batik* dyes have satisfied the thermodynamic requirement as a sensitizer to allow electron transport in DSSC.

Natural dye solar cell technology is still promising as an alternative green and renewable energy. Improved efficiency could be sought through the application of 1D nanostructured titania, the hybrid formation with perovskite organic-inorganic hybrid, and graphene quantum dots or carbon dots. Both, the organometallic perovskite halide and the carbon dots can be used as the co-sensitizer for the realisation of the more efficient natural dyes solar cells.

## Acknowledgements

The authors acknowledged financial supports from The Ministry of Research, Technology, and Higher Education of the Republic Indonesia (Ristekbrin) through the National Competitive Research Grant (PD 2020), International Foundation for Science (IFS) Sweden, and Universitas Gadjah Mada – Science Techno Cluster & Departmental research grants. Special thanks also to Alfi Fatihah and Stepanus Fredi Manurung for some experimental works on textile.

IntechOpen

### Author details

Indriana Kartini<sup>1\*</sup> and Adhi Dwi Hatmanto<sup>2</sup>

1 Department of Chemistry and Indonesia Natural Dye Institute, Universitas Gadjah Mada, Yogyakarta, Indonesia

2 Department of Chemistry, Universitas Gadjah Mada, Yogyakarta, Indonesia

\*Address all correspondence to: [indriana@ugm.ac.id](mailto:indriana@ugm.ac.id)

### IntechOpen

© 2021 The Author(s). Licensee IntechOpen. This chapter is distributed under the terms of the Creative Commons Attribution License (<http://creativecommons.org/licenses/by/3.0>), which permits unrestricted use, distribution, and reproduction in any medium, provided the original work is properly cited. 



## References

- [1] Bechtold T, Mahmud-Ali A, Komboonchoo S. Sustainable dyes from agrifood chain co-products. In: Waldron KW, Moates GK, Faulds CB, editors. Total Food: Sustainability of Agri-Food Chain. RSC Publishing, Cambridge: UK; 2009. p. 211-218. DOI: 10.1039/9781849730785-00211
- [2] O'Regan B., Gratzel M. A low-cost, high-efficiency solar cell based on dye-sensitized colloidal TiO<sub>2</sub> film. Nature. 1991;353: 737-739. DOI: 10.1038/353737a0
- [3] Tennakone K, Kumara GRRA, Kumarasinghe AR, Sirimanne PM, Wijayantha KGU. Journal of Photochemistry and Photobiology A. 1996;94(2-3):217-220. DOI: 10.1016/1010-6030(95)04222-9
- [4] Kasmudjiastuti E. Characterization of Tingi (*Ceriops Tagal*) Bark As Vegetable Tanning Material. Journal of Leather, Rubber, and Plastics. 2014;30(2):71-78. DOI: 10.20543/mkpk.v30i2.128
- [5] Nazir F. Mangrove studies: A source of tanning material. Reviews the used of mangrove as an ecologically friendly tanning material. Leather International. 2008;June.
- [6] Mahltig B, Textor T. Combination of silica sol and dyes on textiles. Journal of Sol-Gel Science and Technology. 2006; 39:111-118. DOI: 10.1007/s10971-006-7744-9
- [7] Mahltig B, Böttcher H, Rauch K, Dieckmann U, Nitsche R, Fritz T. Optimized UV Protecting Coatings by Combination of Organic and Inorganic UV Absorbers. Thin Solid Films. 2005; 485: 108-114. DOI: 10.1016/j.tsf.2005.03.056
- [8] Kartini I, Ilmi I, Kamariah, Kunarti ES. Wash fastness improvement of malachite green-dyed cotton fabrics coated with nanosol composites of silica-titania. Bulletin of Material Science. 2014;37(6):1419-1426. DOI: 10.1007/s12034-014-0091-5
- [9] Kartini I, Halimah SN, Rahayuningsih E. Enhanced wash-fastness of cotton fabric dyed with a composite of chitosan-natural dyes extract of *Ceriops tagal*. In: IOP Conference Series: Materials Science and Engineering. International Conference on Chemical and Material Engineering (ICCMME 2020); 6th-7th October 2020; Semarang; Indonesia: 2021;1053: 012022. DOI: 10.1088/1757-899X/1053/1/012022
- [10] Ye W, Leung MF, Xin JH, Pei LZ. Novel core-shell particles with poly(n-butyl acrylate) cores and chitosan shells as an antibacterial coating for textiles. Polymer. 2005;46:10538-10543. DOI: 10.1016/j.polymer.2005.08.019
- [11] Hayn RA, Owens JR, Boyer SA, McDonald RS, Lee HJ. Preparation of highly hydrophobic and oleophobic textile surfaces using microwave-promoted silane coupling. Journal of Material Science. 2011;46:2503-2509. DOI: 10.1007/s10853-010-5100-5
- [12] Prusty A, Gogoi N, Jassal M, Agrawal AK. Synthesis and Characterization of Non-fluorinated Copolymer Emulsions for Hydrophobic Finishing of Cotton Textiles. Indian Journal of Fibre Textile Research. 2010; 35:264-271. DOI: -
- [13] Gao L, McCarthy J. The "Lotus Effect": Two Reasons Why Two Length Scales of Topography are Important, Langmuir. 2006;22(7): 2966-2967. DOI: 10.1021/la0532149
- [14] Sharma G, Zervaki G, Angaridis P, Vatikioti A, Gupta K, Gayathri T, Nagarjuna P, Singh SP,

- Chandrasekharam M, Banthiya A. Stepwise co-sensitization as a useful tool for enhancement of power conversion efficiency of dye-sensitized solar cells: the case of an unsymmetrical porphyrin dyad and a metal-free organic dye. *Org. Electron.* 2014;15(7):1324–1337. DOI: 10.1016/j.arabjc.2021.103080
- [15] Ludin NA, Mahmoud AA-A, Mohamad AB, Kadhun AAH, Sopian K, Karim NSA. Review on the development of natural dye photosensitizer for dye sensitized solar cells. *Renewable and Sustainable Energy Reviews.* 2014;31: 386–396. DOI: 10.1016/j.rser.2013.12.001
- [16] Khan AU, Hassan A, Gilani. Pharmacodynamic evaluation of *Terminalia bellirica* for its anti-hypertensive effect. *Journal of Food and Drug Analysis.* 2008;16:6-14. DOI: 10.38212/2224-6614.2355
- [17] Schlaf R, Schroeder PG, Nelson MW, Parkinson BA, Merritt CD, Crisafulli LA, Murata H, Kafafi ZH. Determination of interface dipole and band bending at the Ag/tris (8 hydroxyquinolino) gallium organic Schottky contact by ultraviolet photoemission spectroscopy. *Surface Science.* 2000;450:142-152. DOI: 10.1016/S0039-6028(00)00232-6
- [18] Wu TY, Tsao MH, Chen FL, Su SG, Chang CW, Wang HP, Lin YC, Sun IW. Synthesis and characterization of three organic dyes with various donors and rhodamine ring acceptor for using in dye-sensitized solar cells. *Journal of The Iranian Chemical Society.* 2010;7:707–720.
- [19] Jolly D, Pelleja L, Narbey S, Oswald F, Chiron J, Clifford J, Palomares E, Demadrille R. Robust organic dye for dye sensitized solar cells based on iodine/iodide electrolytes combining high efficiency and outstanding stability. *Scientific Reports.* 2014;4(4033):1–7.
- [20] Zhou H, Wu L, Gao Y, Ma T. Dye-sensitized solar cells using 20 natural dyes as sensitizers. *Journal of Photochemistry and Photobiology.* 2011; 219:188-194. DOI: 10.1016/j.jphotochem.2011.02.008
- [21] Gomez-Ortiz NM, Vazquez-Maldonado IA, Perez-Espadas AR, Mena-Rejon GJ, Azamar-Barrios JA, Oskam G. Dye-sensitized solar cells with natural dyes extracted from achiote seeds. *Solar Energy Materials and Solar Cells.* 2010;94:40-44. DOI: 10.1016/j.solmat.2009.05.013
- [22] Kartini I, Dwitasari L, Wahyuningsih TD, Chotimah. The Sensitization of Xanthophylls-Chlorophyllin Mixtures on Titania Solar Cells. *International Journal of Science and Engineering.* 2015;8(2):109-114. DOI: 10.12777/ijse.8.2.109-114
- [23] Chang H, Lo YJ. Pomegranate leaves and mulberry fruit as natural sensitizers for dye-sensitized solar cells. *Solar Energy.* 2010;84:1833-1837. DOI: 10.1016/j.solener.2010.07.009
- [24] Hosseinneshad M, Rouhani S, Gharanjig K. Extraction and application of natural pigments for fabrication of green dye-sensitized solar cells. *Opto-Electronics Review.* 2018;26:165-171. DOI: 10.1016/j.opelre.2018.04.004
- [25] Hamadani M, Safaei-Ghomi J, Hosseinpour M, Masoomi R, Jabbari V. Uses of new natural dye photosensitizers in fabrication of high potential dye-sensitized solar cells (DSSCs). *Materials Science in Semiconductor Processing.* 2014;27: 733-739. DOI: 10.1016/j.mssp.2014.08.017
- [26] Taya SA, El-Agez TM, El-Ghamri HS, Abdel-Latif MS. Dye-sensitized solar cells using fresh and dried natural dyes. *International Journal of Materials Science and Applications.* 2013;2:37-42. DOI: 10.11648/j.ijmsa.20130202.11

- [27] Kay A, Gratzel M. Artificial Photosynthesis. I. Photosensitization of TiO<sub>2</sub> Solar Cells with Chlorophyll Derivatives and Related Natural Porphyrins. *Journal of Physical Chemistry*. 1993;97:6272-6277. DOI: 10.1021/j100125a029
- [28] Kay A, Humphry-Baker R, Gratzel M. Investigation on the mechanism of photosensitization of nanocrystalline TiO<sub>2</sub> solar cells by chlorophyll derivatives. *Journal of Physical Chemistry*. 1994;98:952-959. DOI: 10.1021/j100054a035
- [29] Harborne JB. *Phytochemical Methods*. 1st ed. London; Chapman and Hall; 1973. 277 p. DOI: 10.1007/978-94-009-5921-7
- [30] Ehret A, Stuhl L, Spitler MT. Spectral Sensitization of TiO<sub>2</sub> Nanocrystalline Electrodes with Aggregated Cyanine Dyes. *Journal of Physical Chemistry B*. 2001;105: 9960-9965. DOI: 10.1021/jp011952+
- [31] Sayama K, Tsukagoshi S, Mori T, Hara K, Ohga Y, Shinpou A, Abe Y, Suga S, Arakawa H. Efficient sensitization of nanocrystalline TiO<sub>2</sub> films with cyanine and merocyanine organic dyes. *Solar Energy Materials and Solar Cells*. 2003;80:47-71. DOI: 10.1016/S0927-0248(03)00113-2
- [32] Vladkova R. Chlorophyll a Self-assembly in Polar Solvent–Water Mixtures. *Photochemistry and Photobiology*. 2000;71(1):71-83. DOI: 10.1562/0031-8655(2000)071<0071: casaip>2.0.co;2
- [33] Krautler B. Breakdown of Chlorophyll in Higher Plants—Phyllobilins as Abundant, Yet Hardly Visible Signs of Ripening, Senescence, and Cell Death. *Angewandte Chemie International Editions*. 2016;55:4882–4901. DOI: 10.1002/anie.201508928
- [34] Kamat PV. Photochemistry on nonreactive and reactive (semiconductor) surfaces. *Chemical Reviews*. 1993;93(1):267-300. DOI: 10.1021/cr00017a013
- [35] García-Salinas MJ, Ariza MJ. Optimizing a Simple Natural Dye Production Method for Dye-Sensitized Solar Cells: Examples for Betalain (Bougainvillea and Beetroot Extracts) and Anthocyanin Dyes. *Applied Sciences*. 2019;9:2515. DOI: 10.3390/app9122515
- [36] Saelim N, Magaraphan R, Sreethawong T. TiO<sub>2</sub>/modified natural clay semiconductor as a potential electrode for natural dye-sensitized solar cell. *Ceramics International*. 2011; 37:659-663. DOI: 10.1016/j.ceramint.2010.09.001
- [37] Hemmatzadeh R, Mohammadi A. Improving optical absorptivity of natural dyes for fabrication of efficient dye-sensitized solar cells. *Journal of Theoretical and Applied Physics*. 2013;7: 1-7. DOI: 10.1186/2251-7235-7-57
- [38] Gomez-Ortiz NM, Vazquez-Maldonado IA, Perez-Espadas AR, Mena-Rejon GJ, Azamar-Barrios JA, Oskam G. Dye-sensitized solar cells with natural dyes extracted from achiote seeds. *Solar Energy Materials and Solar Cells*. 2010;94:40–44. DOI: 10.1016/j.solmat.2009.05.013
- [39] Kamat PV, Tvrdy K, Baker DR, Radich JG. Beyond Photovoltaics: Semiconductor Nanoarchitectures for Liquid-Junction Solar Cells. *Chemical Reviews*. 2010;110:6664–6688. DOI: 10.1021/cr100243p
- [40] Kartini I. Progress on Nanomaterials for Photoelectrochemical Solar Cell. In: *E3S Web of Conferences*. The 4th International Conference on Energy, Environment, Epidemiology and Information System (ICENIS 2019); 7-8 August 2019; Semarang; Indonesia: 2019;125, 14015. DOI: 10.1051/e3sconf/201912501001



- [41] Wang J, Jin EM, Park JY, Wang WL, Zhao XG, Gu HB. Increases in solar conversion efficiencies of the ZrO<sub>2</sub> nanofiber-doped TiO<sub>2</sub> photoelectrode for dye-sensitized solar cells. *Nanoscale Research Letters*. 2012;7:98. DOI: 10.1186/1556-276X-7-98
- [42] Wei Z, Yao Y, Huang T, Yu A. Solvothermal growth of well-aligned TiO<sub>2</sub> nanowire arrays for dye-sensitized solar cell: Dependence of morphology and vertical orientation upon substrate pretreatment. *International Journal of Electrochemical Science*. 2011;6: 1871-1879. DOI: 10.1016/j.jphotochem.2007.01.023
- [43] Flores IC, Freitas JN, Longo C, Paoli MAD, Winnischofer H, Nogueira AF. Dye-sensitized solar cells based on TiO<sub>2</sub> nanotubes and a solid-state electrolyte. *Journal of Photochemistry and Photobiology A: Chemistry*. 2007;189:153-160. DOI: 10.1016/j.jphotochem.2007.01.023
- [44] Bijarbooneh FH, Zhou Y, Sun Z, Heo YU, Malgras V, Kim JH, Dou SX. Structurally stabilized mesoporous TiO<sub>2</sub> nanofibres for efficient dye-sensitized solar cells. *APL Materials*. 2013;1:1-7. DOI: 10.1063/1.4820425
- [45] Kartini I, Evana, Sutarno, Chotimah. Sol-Gel Derived ZnO Nanorod Templated TiO<sub>2</sub> Nanotube Synthesis for Natural Dye Sensitized Solar Cell. *Advanced Materials Research*. 2014;896: 485-488. DOI: 10.4028/www.scientific.net/AMR.896.485
- [46] NREL efficiency chart [internet]. 2019. Available from: <https://www.nrel.gov/pv/assets/pdfs/best-research-cell-efficiencies.20190802.pdf> [Accessed: 2019-09-25]
- [47] Dey A., Dhar A, Roy S, Das BC. Combined Organic-Perovskite Solar Cell Fabrication as conventional Energy substitute. *Materials Today: Proceedings*. 2017;4:12651-12656. DOI: 10.1016/j.matpr.2017.10.077
- [48] Mandal B, Sarkar S, Sarkar P. Theoretical Studies on Understanding the Feasibility of Porphyrin-Sensitized Graphene Quantum Dot Solar Cell. *Journal of Physical Chemistry C*. 2015; 119:6,3400–3407. DOI: 10.1021/jp511375a
- [49] Mohan K, Bora A, Dolui SK. Efficient way of enhancing the efficiency of a quasi-solid-state dye-sensitized solar cell by harvesting the unused higher energy visible light using carbon dots. *ACS Sustainable Chemistry and Engineering*. 2018;6:10914-10922. DOI: 10.1021/acssuschemeng.8b02244
- [50] Ivashchenko O, Przysiecka L, Peplińska B, Flak D, Coy E, Jarek M, Zalewski T, Musiał A, Jurga S. Organic-Inorganic Hybrid Nanoparticles Synthesized with *Hypericum perforatum* Extract: Potential Agents for Photodynamic Therapy at Ultra-low Power Light. *ACS Sustainable Chemistry and Engineering*. 2021;9(4): 1625-1645. DOI: 10.1021/acssuschemeng.0c07036
- [51] Ormond AB, Freeman HS. Dye Sensitizers for Photodynamic Therapy. *Materials*. 2013;6(30):817-840. DOI: 10.3390/ma6030817
- [52] Kim D-H, Cha J-H, Lim JY, Bae J, Lee W, Yoon KR, Kim C, Jang J-S, Hwang W, Kim I-D. Colorimetric Dye-Loaded Nanofiber Yarn: Eye-Readable and Weavable Gas Sensing Platform. *ACS Nano*. 2020;14(12):16907-16918. DOI: 10.1021/acsnano.0c05916
- [53] Riaz RS, Elsherif M, Moreddu R, Rashid I, Hassan MU, Yetisen AK, Butt, H. Anthocyanin-Functionalized Contact Lens Sensors for Ocular pH Monitoring. *ACS Omega*. 2019;4(26):21792-21798. DOI: 10.1021/acsomega.9b02638



# Photochromic Dyes for Smart Textiles

*Virendra Kumar Gupta*

## Abstract

Photochromism is a light induced reversible color change phenomenon in photochromic molecule due to light and heat effect and molecular species exist in two forms which have different absorption spectra. The fascinating color change by photochromic molecules in response to specific wavelength of light produces number of applications such as U.V. protective fabrics, ophthalmic photochromic lenses, optical data storing, optical switch, sensors and display. This chapter provides a brief and conclusive review of photochromism their mechanism and application in Textiles. Although photochromic materials are in use since 1960 in lenses and sunglasses, but the development is slow due to technical difficulties and poor commercial application. Now there is renewed interest in photochromic materials which are used in nanofibers in smart textiles and in allied items.

**Keywords:** photochromic colorants, thermochromic colorants, U.V. radiation

## 1. Introduction

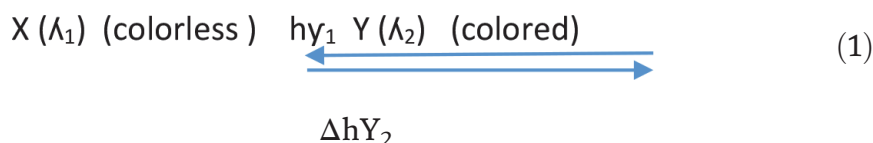
The wide and increasing application of photochromic and thermochromic colorants in different fields initiates new interest in dyes and pigments. The photochromic compounds got excited when irradiated at particular wavelength in range of 200–400 nm and few compounds in 430–455 nm range. But researchers are more interested to develop organic rather than inorganic photochromic materials because their response in 400–700 nm visible region. The use of photochromic and thermochromic colorants in making smart materials such as medical thermography, photochromic lenses [1], food packaging materials, liquid crystal alignment [2, 3], optical data storage [4, 5], non linear optics [6, 7], photo switching, molecular photonic devices and in photochromic polymers [8] are well known. There is demand for application of photochromic and thermochromic colorants in making smart textiles, which are designed to sense and respond to external environmental conditions and stimuli. Photochromic and thermochromic colorants are prone to change their colors temporarily and reversibly in presence of UV light, visible light, acids [9], alkalis, water, mechanical strain, temperature and in electric field. These dyes became colored when exposed to these environmental conditions temporarily and revert back upon disappearance of external environment. The photochromic dyes [10] are categorized as inorganic and organic molecules. In inorganic types the important are metal oxide, alkaline earth metals, sulphides, copper compounds and mercury compounds. The organic types are effective and environment friendly and they belong to the families of spiropyrans, spirooxazines, chromomenes, fulgides,

fulgimides and diarylethenes. Spiropyrans, spirooxazines and chromomenes are sensitive to thermal effect and reverse to colorless state under heat or visible light however fulgides, fulgimides and diarylethenes are thermally stable. Out of these spiropyrans are having more scientific interest than any other class.

Spiro compounds have pyran ring and linked to another heterocyclic ring through spiro group. Spirooxazines molecules contain nitrogen atom at the place of carbon in spiro group. These molecules (colorless) have non planer structure and that inhibit delocalization of  $\pi$  electrons in the molecules. In presence of UV light, molecules absorb photon energy and breaking of  $-C-O-$  bond in pyran ring takes place and there is formation of colored planar structure molecule. The planarity of molecule allow delocalization of  $\pi$  electrons and molecule become colored. This is short term phenomenon and after absorption of heat or visible light molecules convert into original structure (colorless) as shown in **Figure 1**.

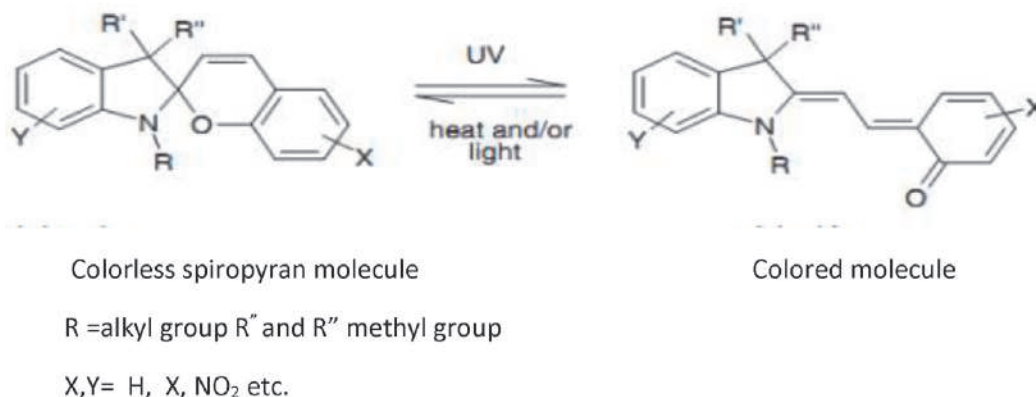
The photochromism [11, 12] may be defined as a reversible light –induced color change or reversible transformation between two different molecular structures with different absorption spectrum in reversible manner due to electromagnetic radiations. Photochromic materials are kind of chromic materials in which photochromic and thermochromic materials are of paramount importance. In photochromism the colorless molecule became colored in presence of UV Portion of light however in the thermochromic molecules heat is responsible for change of color [4].

The general physicochemical reaction of photochromic molecules are as given in equation no. 1 [13, 14].



$\lambda_1$  and  $\lambda_2$  are the wavelength of maximum absorption by corresponding molecules and  $h\nu_1$  and  $h\nu_2$  are the energy absorbed by the molecules during transformation.  $\nu_1$  is the frequency of wave in U.V. region and  $\nu_2$  is the frequency of wave in either U.V. or visible region and  $\Delta$  is heat requirement. The factors which influence reaction 1 are [15].

- Wavelength of incident light
- Speed of recovery or fatigue resistance
- Long term stability of molecule to produce high number of cycles



**Figure 1.**  
Conversion of colorless spiropyran molecule into colored molecule.

## 2. Types of photochromism

### 2.1 Positive photochromism

In this photochromism photochromic molecule absorb UV light whose  $\lambda_{\max}$  falls in UV region and colorless molecule became colored and on reversal during bleaching process in visible wavelength it become colorless.

### 2.2 Negative photochromism

It is opposite to the positive photochromism instead of coloration discoloration observed on exposure to UV light i.e. the original molecule is colored and after exposure to UV light it loss their color.

### 2.3 (c) Photo responsible materials

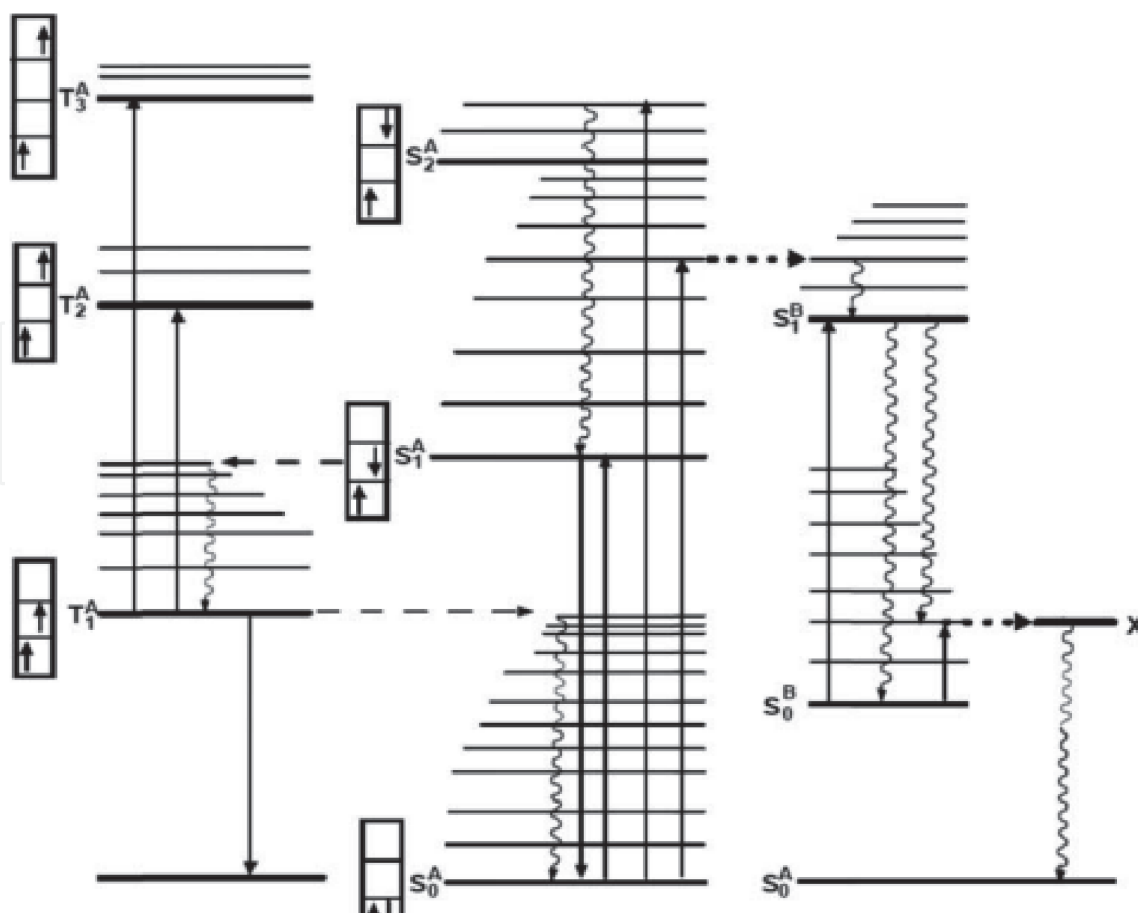
In photochromic reactions, there is conformational modifications in the structure of photochromic molecules and due to that there are change in physico-chemical properties of two form of the photochromic molecules and the change observed in physico- chemical properties of both molecules (colored and colorless) are called photo responsible materials [16].

## 3. Mechanism of Photochromism

Photochromic reaction leads to change in electronic absorption spectra of molecules. The formation of new absorption band due to transition of electrons from various vibrational levels in the excitation of colorless molecules from  $S_1A$  level to excited state  $S_1B$  after absorption of energy photon in UV region [17] and then after the colored molecules deactivated to ground state  $S_0B$ . Subsequently there is spontaneous energy release process and molecules come to original  $S_0A$  ground state. Thermodynamically the molecules in B state due to higher energy are less stable and after releasing energy became colorless and more stable. The transition from state B to A takes place via a transition state X, whose energy is higher than the triplet state of colored form  $S_0B$  and it is thermally activated. There are six mechanism which responsible for the photochromic effect and they are,

- Triplet triplet photochromism.
- Hetrolytic cleavage
- Hemolytic cleavage
- Trans-cis isomerisation
- Tautomerism
- Photodimerisation

The transition of molecules after absorption of light in different energy levels is shown in **Figure 2**.



**Figure 2.**  
Representations of electronic, radiative and non radiative transitions in photochromic materials.

#### 4. Classification of photochromic materials

Classification of photochromic materials are based on back reaction i.e., if it from colored state to colorless state is brought in the presence of light then it is called P type photochromic materials (**Figure 1**), where as if back reaction occurred due to heat energy, it is called T type of photochromic materials.

The p type photochromic materials exist in two reversible forms upon irradiation and have good thermal stability with better fatigue resistance. In p type photochromic materials [18, 19] during exposure to UV light ring opening takes place. After ring opening, molecules absorb visible wavelength light and became colored. This state of molecule is temporary and again it became closed ring system (colorless). Most of the p type photochromic materials do not follow trans- cis isomerism and which follow they have they have open ring structure in colorless form after exposure to UV light they became closed ring structure (colored). The reverse reaction i.e. ring opening is promoted by visible wavelength [20, 21].

In T type photochromic materials photochromic reactions takes place due to thermal irradiation or by photo irradiation with visible light [ 22, 23]. It shows reversible equilibrium between trans and cis isomerism of different stability. In T type photochromism there is no breaking of bonds occur however there is rearrangement of electrons between energy levels and alteration in geometric arrangement of the molecules. The thermal reversal of molecule takes place in dark. The important T type photochromic materials are perimidinespirocyclohexadienes, spirodihydroindolizines and anils. There are some requirement in T type photochromic materials which are,



- Smaller concentration should produce intense color with effective color change.
- The conversion from colorless to colored form upon exposure to U.V. light must be very quick.
- The photochromic molecules should have minimum time to loss their absorbance half i.e., photo chromic effect should be lost as soon as removal of activating light takes place.
- The photochromic molecules should have quick response in presence of U.V. radiation.
- The life time of photochromic molecules should be longer (Approx. 2 years) in both colored and colorless form. It should also have good resistance to fatigue.
- The photochromic molecules should be less vulnerable to variation in temperature.

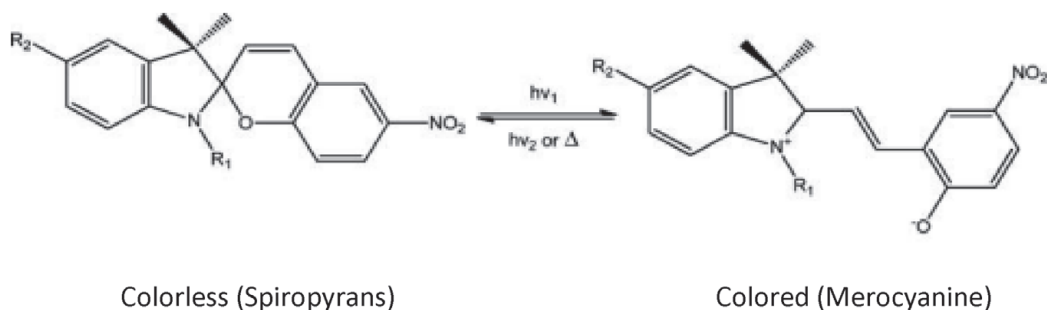
## 5. Types of photochromic materials (T types)

## 5.1 Spiropyrans

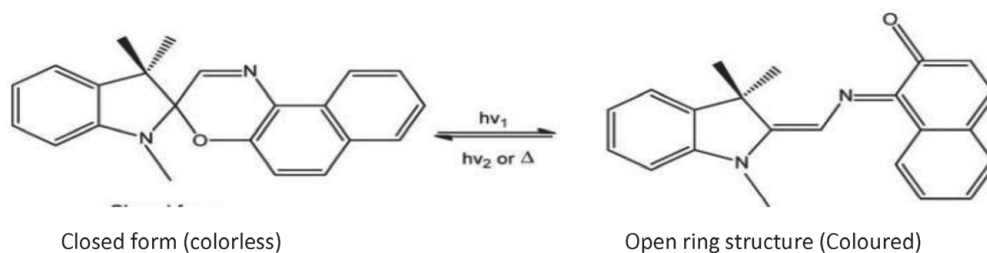
It is first T type photochromic molecules and widely used in the industry. It have application in memory disks, optical switches, sensors and as a photochromic dyes in textiles and plastics. The general structure contain a second ring structure, which attach to pyron core at position two [24–29]. The coloring of the molecules take place under exposure to U.V. light. The ring opening in molecular structure occur under U.V.light and merocyanine form is created and that exist as cic-cis/trans-trans mixture. The absorption of either U.V. or visible wavelength takes place after ring opening and after absorption, new wavelength in visible region is produced. It has low thermal bleaching rate and at high temperature the color became weaker. In **Figure 3** the ring opening of spiropyrans and formation of conjugated structure is shown.

## 5.2 Spirooxazines

The chemical structure is similar to spiropyrans, the difference exit that instead of pyron core, it has oxazine group [ 30, 31] (**Figure 4**). The spirooxazines has very good resistance to photo degradation. The spirooxazines produces fast fading blue

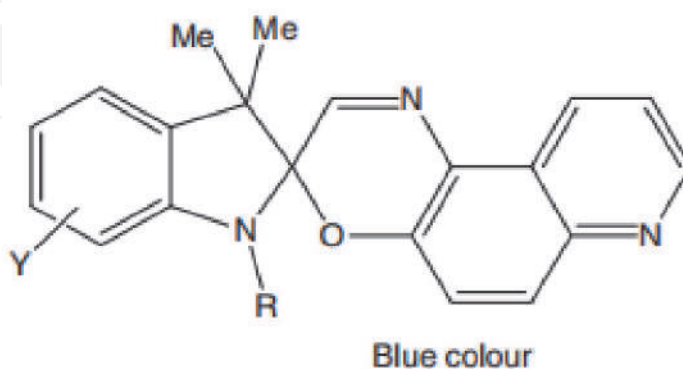
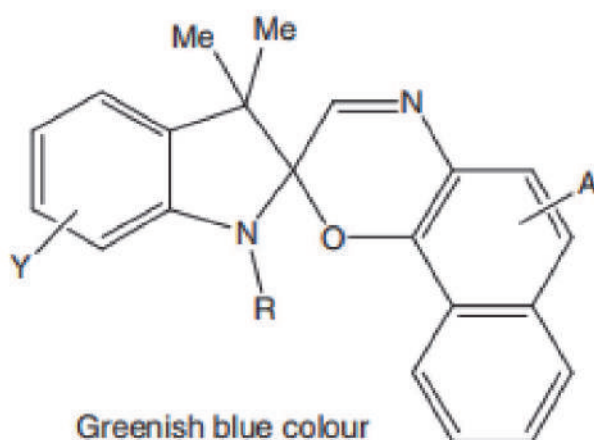
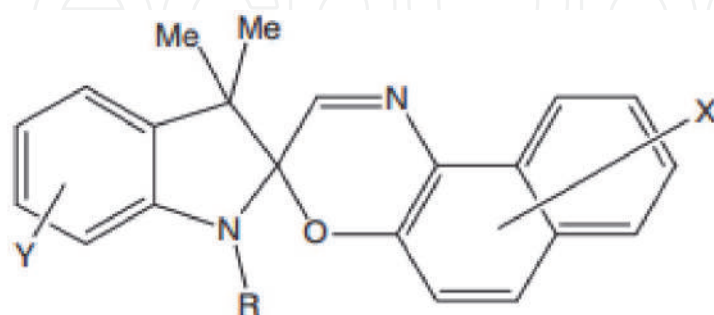


**Figure 3.**  
*Photochromic reaction of spiopyrans (from closed ring structure to open ring structure).*



**Figure 4.**

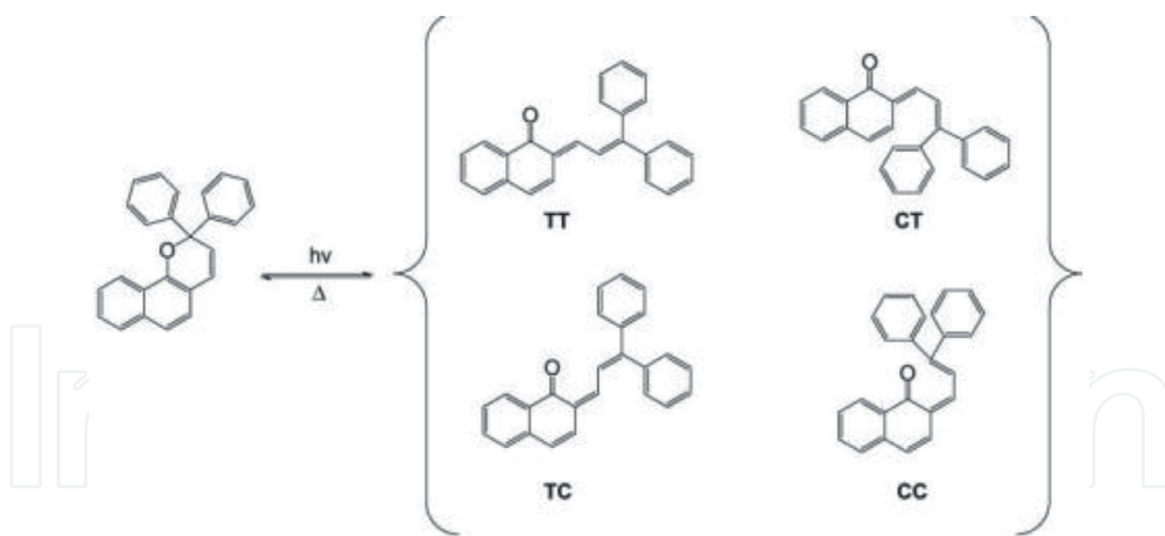
*Photochromic reaction of spirooxazines (from closed ring structure to open ring structure).*



**Figure 5.**

*Different structures of photochromic oxazine ( $R$  = alkyl group,  $X$  = H, amino, hetaryl  $Y$  = H, halogen,  $a$  = electron acceptor).*

photo coloration. The different chemical structure of spirooxazines are shown in **Figure 5**. The presence of different alkyl groups  $R$  at nitrogen atom decide the fading and color strength of molecules [32]. In 1990s, plastic photochromic



**Figure 6.**  
 Photochromic reactions of naphthopyrans (TT trans-trans, CT cis-trans, TC trans-cis, CC cis-cis).

ophthalmic lenses were manufactured using spiropyrans. Other applications are photochromic inks, dyes and various cosmetics items.

### 5.3 Naphthopyrans/benzochromenes

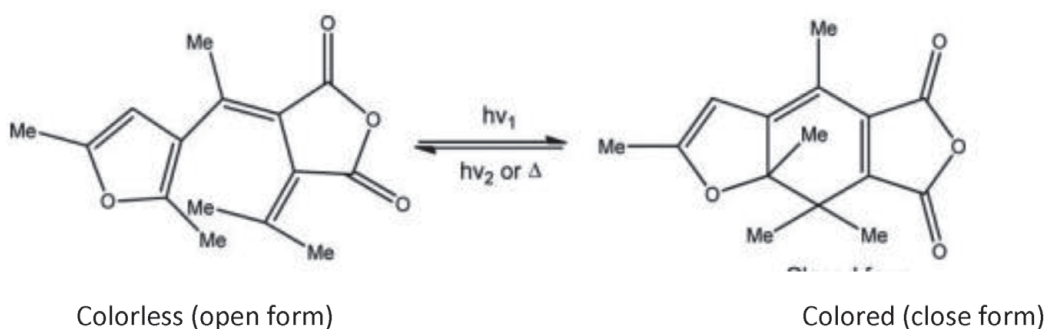
It has wide commercial applications such as in plastic photochromic lenses. The photochromism mechanism of benzo and naphthopyron are similar to spiropyrans [33]. They all have breaking of C—O bond in the pyron core. The photochromic reactions of naphthopyrans/benzochromenes by the light induced ring opening is shown in **Figure 6**. The ring opening of molecular structure produces more planer structure with greater conjugation of bonds. The planer conjugated structure are capable to absorb visible region wavelength and produces color. The naphthopyrans are less sensitive to temperature.

## 6. P type photochromic materials

The p type photochromic materials have applications in computing, optical circuitry, memory technology and in ultra high density storage devices. The p type photochromic materials are of two types such as fulgides and diarylethenes. In p type photochromic molecules, the open ring structures are colorless and closed ring structures are colored [34–36].

### 6.1 Fulgides

The fulgides and fulgimide family belong to P type photochromic materials (**Figure 7**). In 1905 Stobbe synthesized some photochromic fulgides named as phenyl substituted bismethylene succinic anhdides. Heller et al. [37] developed a compound succinimide called fulgimide. It exhibit good photochromic properties. It has shows absorption spectrum of both forms with efficient photoreaction, thermal and photochemical stability. The application of fulgides are In optical switches, sensors, dye inks and memory disks.



**Figure 7.**  
Photochromic reaction of fulgides.

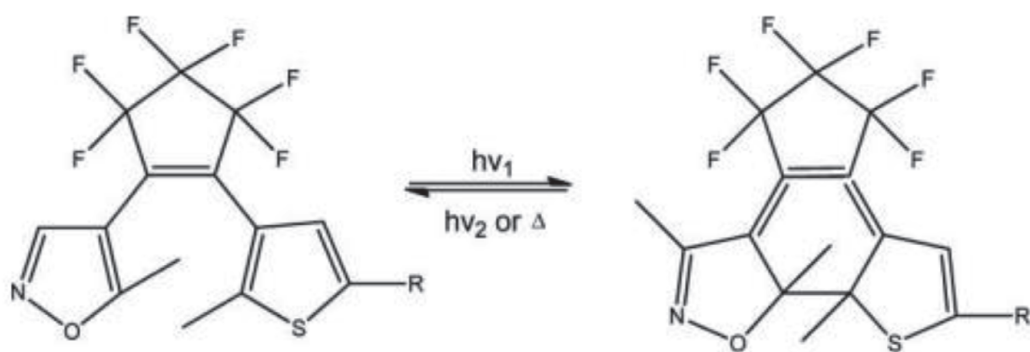
## 6.2 Diarylethenes

It has hetrocyclic five membered rings such as thiophene or benzothiophene rings and undergo thermally irreversible and fatigue resistant photochromic reactions as shown in **Figure 8**. The thermal stability of both isomers of diarylethenes are due to presence of aryl groups and when aryl groups are furan or thiophene, the closed form is thermally stable. However diarylethenes exhibit thermally reversible reactions when the aryl group is phenyl or indole.

## 7. Effect of temperature

Surrounding temperature influence the performance of photochromic dyes. The bleaching effect of photochromic dyes are accelerated by the temperature of sample [38–40]. Dulic et al. find that ring opening process of diarylethene is temperature dependent whereas ring closing process shows only slight dependence. Ortica [41] reviewed the effect of temperature on the characteristics of various photochromic materials such as spirooxazines, chromenes and arylethenes, which are as follows,

- In thermo reversible photochromic materials, thermal bleaching increase with increasing temperature.
- Specific temperature can induce spontaneous coloration in thermochromic materials however decreasing temperature will not help in reducing the complexity of photochemical reactions.



**Figure 8.**  
Photochromic reactions of diarylethenes.



- In nitro substituted chromenes, it was observed that temperature variations influenced the coloration which developed due to substitution in the molecular structure.
- A combination of photochromic and thermochromic materials possess synergistic effect and give superior performance at high temperature.

## 8. Applications in textiles

### 8.1 By exhaust dyeing

#### 8.1.1 Method 1

In this method the photochromic dyes are dispersed with dispersing agent [42] and dissolved in water keeping the M:L ratio of dyeing 1:50. The dyebath pH is maintained between 4.5–5.5. The dyebath temperature raised from 40 °C to 60 °C with 2 °C/min gradient and then after it is reduced 1 °C/min and final dyeing temperature is maintained at 90 °C and dyeing is continued at this temperature for 60 min. After completion of dyeing, soaping, rinsing and washing are done to improve fastness properties.

#### 8.1.2 Method 2

In this method the photochromic dyes can be applied as a disperse dye on polyester fabrics by exhaust method of dyeing [43]. The dye is pasted with acetone and then stirred in water with dispersing agent (1%) keeping the M:L ratio of dyeing 1:50. The pH of the dyebath is maintained between 4.5–5.5. The aqueous dyebath is boiled to evaporate acetone, subsequently temperature is raised to 120 °C and dyeing is done at this temperature for 45 minute. After dyeing reduction clearing treatment is given at 70 °C for 20 min. and finally sample is soaped, rinsed and washed.

### 8.2 By continuous dyeing

In this method photochromic dyes are dissolved in acetone and then mixed with binder solution and padded with padding mangle at appropriate pressure. After padding fabric is dried at 80 °C and cured at 140 °C for 3.0 minute in hot air oven or stenter machine [44].

#### 8.2.1 As a disperse dyes in printing

Photochromic dyes can be used as a disperse dyes which are insoluble in water. The photochromic dyes are disperse with dispersing agent and wetting agent of anionic nature. The dye dispersion is milled on a roller mill by using ceramic balls in glass jar. The dye dispersion is mixed with sodium alginate thickener solution to get printing paste. The polyester or nylon fabric can be printed with printing paste. The fabric is dried at 100 °C and cured at 140 °C for 5 minute. After reduction clearing treatment, printed samples were soaped with nonionic detergent and finally neutralization is done.

### 8.3 Application of thermochromic materials

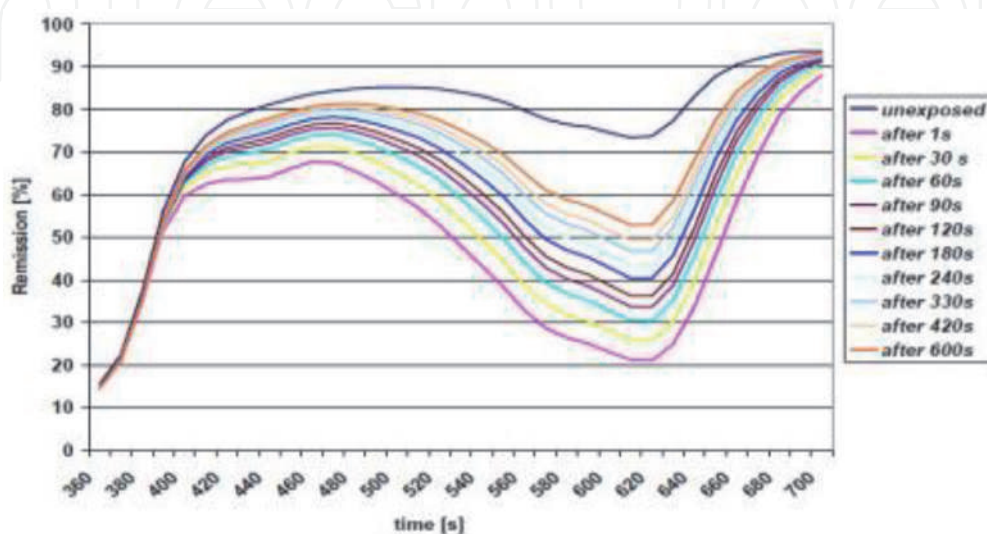
Photochromic materials have applications in both textiles and non textiles. In the textile field new fashionable colors in T-shirts, hand bags and caps are produced by dyeing with photochromic dyes. There is application of photo colorable textured yarn in knitting, weaving and embroidery. Polypropylene threads are produced by mass coloration by adding photochromic dyes in melt polymer solution, which on exposure to U.V. light produces different colors. Photochromic colorants are also used in developing camouflage patterns for military protective clothing. The patterns change their colors on exposure to sunlight and match with surrounding environment. Photochromic microencapsulated fabrics are produced which change their color on exposure to sun light. In non textile field photochromic materials are used in ophthalmics, surface coating applications and dye lasers.

### 8.4 Color measurement

Due to reversible color changing properties of photochromic dyes, it is very difficult to measure color value of the shade produced due to photochromic effect. For measuring the color value, it is essential to control several parameters such as temperature and time interval between U.V. irradiation of sample and measurement. A.F. Little et al. [45] developed a technology to measure the color value of photochromic textiles using independent U.V. irradiation with traditional spectrophotometer. The temperature of sample measuring cabinet was controlled by localized air heating system. The temperature of sample cabinet is maintained at 24 °C and time interval of 30 sec. is kept between irradiation and measurement of sample which can be seen in **Figure 9**.

### 8.5 Washing fastness test

Due to dynamic color change properties of photochromic dyes, it is difficult to measure the fastness properties. The traditional assessment method of color fastness using gray scale standards [46] are not appropriate, therefore it is measured by comparative test method. In this method we measure the color difference of sample before and after wash and compare with color difference before U.V. irradiation and after 1 min. Exposure to U.V. irradiation. The level of photo coloration



**Figure 9.**  
Color measurement (color bleaching) of photochromic dye fabric samples in 30 sec. Time interval.

developed by U.V. irradiation varies with photochromic colorant classes. It was revealed that in selected spirooxazine colorants the degree of photo coloration increases with initial washing and subsequently decreases. In case of naphthopyrans, the degree of photo coloration decreases continuously with successive number of washings. In case of printing the washing fastness more depends on binder quality.

## 8.6 Light fastness/photostability

The conventional method of exposing the sample to accelerated fading instruments (Xenotest or MBTF) is not applicable to photochromic colorants. In photochromic colorants due to dynamic color change properties, for light fastness measurement a normalized value of color value to be calculated. The normalized value is defined as the degree of photo coloration after a particular time of exposure on the xenotest instrument to the fraction of initial degree of photo coloration i.e.,  $\Delta E/\Delta E_0$ .

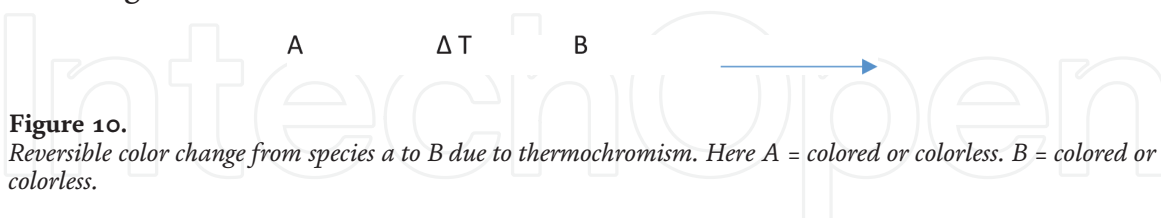
$\Delta E_0$  = color difference before and after U.V. Irradiation without exposing to xenotest instrument.

## 9. Thermochromism

Thermochromism may be defined as the reversible change in the color of compound due to temperature change [47]. The phenomenon of thermochromism may occur even in small temperature interval. The thermochromism can be depicted as shown in **Figure 10**.

The following type of materials can exhibit thermochromism properties [48].

- Organic compounds
- Inorganic compounds
- Polymers
- Sol gels

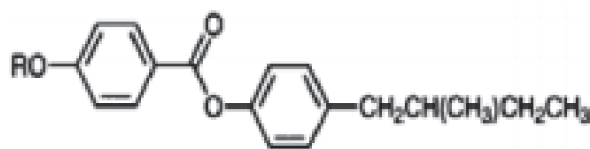


## 10. Organic compounds

It may occur as a result of equilibrium between molecular species such as acid – base, keto-enol and different crystal structure. The organic thermochromic materials have application in fibers, optics and optical sensors. The organic thermochromic compounds show sharp color change due to temperature variation. The different organic thermochromic compounds may be classified as follows.

### 10.1 Liquid crystals

Some organic materials when pass from crystalline solid to isotropic liquid state, they form stable intermediate phases (mesophase). Transitions between phases are



**Figure 11.**  
*Chiral molecules in cholesteric mesophases form.*

brought either by influence of temperature or solvent respectively [49]. The cholesteric (chiral nematic) are the most important type of liquid crystals for thermochromic systems. Here molecules are arranged in helical form. The reflection of light by liquid crystals are influenced by temperature. The pitch of the helical arrangement of the molecules decides the wavelength of reflected light [50]. The liquid crystals are microencapsulated to get the thermochromic effect. They are applied to the fabric with the help of binder (**Figure 11**).

## 10.2 Stereoisomerism

Organic molecules which possess stereoisomerism, show thermochromism especially ethylenes. When change in temperature takes place, molecules of these compounds switch between different stereoisomers. Generally the required temperature for thermochromism to take place is more than 150 °C. So they can not be used for textiles application [51].

In another case, the crystal violet lactone is pH dependent rather than temperature dependent. At pH above 4.0 crystal violet lactone is colorless and below 4.0 pH, it is violet.

### 10.2.1 Rearrangement

Due to molecular rearrangement of organic compounds more conjugated structure resulted and formation of new chromophores take place. Such type of molecular arrangement occurs due to temperature variation, change in polarity of the solvent or pH of the solution.

## 11. Inorganic thermochromic system

Thermochromic behavior is exhibited by solid or liquid inorganic molecules. In such type of molecules thermochromic properties are due to following mechanism [52],

- Phase transition
- Change in ligand geometry
- Equilibrium between different molecular structures
- Change in the number of solvent molecules in the co-ordination sphere.

These compounds show thermochromic properties at high temperature (150 °C), therefore they are not suitable for textile application.



## 12. Microencapsulation

In reversible thermochromic compounds a colorless dye precursor and color developer both are dissolved in hydrophobic non volatile organic solvent and resulted solution is encapsulated [53]. On heating, melting of organic solvent occurs and there is appearance of color in thermochromic compound. On cooling solvent solidify and system comes to original color. Microencapsulation has some advantages that it protect sensitive coloring agents from external environment and allows several thermochromic colorants to be combined together and produces several narrow color ranges.

The organic solvents used in microencapsulation are alcohols, hydrocarbons, ester, ketones, thiols and alcohol –acrylonitrile mixture. The important thermochromic colorants are N-acyl leuco-methylene blue derivatives, fluoran dyes and diphenylmethane compounds. There are large number of compounds work as color developers such as phenol derivatives specifically bisphenol A and bisphenol B. In some recent work there are use of 1,2,3 triazoles such as 1,2,3 benzotriazole, dibenzotriazole, thioureas and 4 hydroxy coumarin derivatives.

## 13. Application of thermochromic pigments on textiles

### 13.1 By exhaust method

- Cationic agent 5–8% (owf)
- Thermochromic Pigments 10–15% (owf)
- Non ionic leveling and dispersing agent 10–15% (owf)
- Acrylic Binder 10–15%

Thoroughly pretreated fabric taken in water keeping M; L ratio 1:20 and we add cationic agent at temperature of 60 °C and run in the aqueous media for 15 min to get positive charge on fabric. After treatment fresh water is taken in the bath and thermochromic pigments are added, temperature is maintained at 70 °C run fabric for 10–15 min. During dyeing non ionic dispersing agent and leveling agent are added. Finally acrylic binder is added and we run the fabric at 70 C for 15 min. The fabric sample is soaped and washed. In microencapsulated fabric the melting temperature of solvent control the temperature at which decolonization/colorization of thermochromic colorant occur.

### 13.2 Continuous method (In solution)

- Cationic agent 10–15%
- Thermochromic pigment 50%
- Nonionic dispersing and leveling agent 10–15%
- Acrylic binder 20%

### 13.3 Application technique

Pad  $\longrightarrow$  Dry  $\longrightarrow$  Cure  
At room temperature (expression 70%) 80 C (3 min.) 140 C (2–3 min.)

### 13.4 Printing recipe

- a. Thermochromic Colorant 20 part
- b. Emulsion thickner 76 part
- c. Acrylic binder 4 part

## 14. Thermochromic cellulose fiber

Marcin Rubacha et al. [54] developed a method to get thermochromic pigment added cellulosic fiber called Lyocell. 1–10% chromicolor AQ-INK magenta type 27 pigmentation was used as a thermochromic modifier.

## 15. Photochromic polymers

A photo chromic polymer has photo chromic, chromophoric groups inside the polymer backbone chain. The chromophoric group respond to external radiative stimuli during the photo-irradiation of the polymers, there are change in physical chemical and optical properties of polymer in reversible manner. In 1967 Lovrien attempted to produce a polymer chain with photo irradiation sensitive properties by incorporating azo chrysophenine into polymethacrylaic acid. In 1970 Agolini and Gay [55] investigated photo chromic polyamides incorporating azo benzene. The potential application of photo chromic polymers are in photo chromic glasses, UV sensors, halographic recording media, non linear optics and memory devices.

## 16. Textile printing

Feczko et al. [56] printed cotton fabric by using photo chromic dyes based on Ethyl cellulose –spirooxazine nano particles with light absorbers. They use micro-encapsulation technique to incorporate photochromic colorants. Vikova [57] applied photo chromic pigments on different fabrics such as cotton, polyester and poly acrylonitrile by screen printing using pigment printing method.

## 17. Sol –gel coating methods

A sol is dispersion of solid particles in liquid where particles are sufficiently small (0.1–1.0  $\mu\text{m}$ ). Due to inorganic nature [58] of layers formed by the sol gel process it possess strong wear resistance and very thin nanometric sized layers. The preparatory materials in preparing sols are inorganic metal salts or organometallic compounds. The preparatory materials are submitted to series of hydrolysis and polymerization reactions to produce colloidal suspension or sol, once the polymerization is completed the colloidal form of the sol developed. Cheng et al. [59–61]

prepared silica as a matrix material for fixing the photo chromic dye 5 Chloro 1,3 dihydro-1,3,3 trimethyl spiro on the surface of wool fabric through sol–gel process.

## 18. Mass coloration

Mass coloration or dope dyeing is method in which colorants are added in the spinning composition before extrusion of filaments. Photo chromic polypropylene [62] thread was prepared by this method. Vikova et al. [63, 64] prepared polypropylene multi filaments by adding photo chromic pigments during dope preparation. Concentration of photo chromic pigments was 0.25,0.5,1.5 and 2.5% by weight.

## 19. Conclusion


Photochromic and thermochromic materials presenting a new field of research which are yet not fully explored in field of textiles and other allied fields in context of application and durability. The photochromic and thermochromic colorant occupied a niche position in colorant industry. Their application mainly concerned with fashion, leisure and sports garments. Incorporation of photochromic colorants in nanofiber based photochromic textiles can be made use of in smart textiles because of their ability to react with external stimuli, which may work as chromic sensor. Efforts can be done to improve properties such as light fastness and simplistic application procedure. Presently two types of thermochromic system liquid crystals and molecular rearrangement types have successful commercial applications. Japan and U.S, A had developed wide range of thermochromic and photochromic materials, but innovations are required for commercial applications. The factors influencing the equilibrium between colored and colorless form of colorant has to be further explored. Presently only small number of commercial organizations are engaged in research and development work of improved compositions. There is need of study with respect to formulations, encapsulations and application of photochromic and thermochromic materials in textiles.

## Author details

Virendra Kumar Gupta  
Department of Textile Chemistry, M.L.V. Textile and Engineering College,  
Bhilwara, Rajasthan, India

\*Address all correspondence to: [virendra1970@rediffmail.com](mailto:virendra1970@rediffmail.com)

## IntechOpen

© 2021 The Author(s). Licensee IntechOpen. This chapter is distributed under the terms of the Creative Commons Attribution License (<http://creativecommons.org/licenses/by/3.0>), which permits unrestricted use, distribution, and reproduction in any medium, provided the original work is properly cited. 

## References

- [1] Eds H.R. Mattila, Intelligent Textiles and Clothing, Woodhead Publication Limited, Cambridge, England. 2006, 296.
- [2] Pardo R., Zayat M. and Levy D., Chem. Soc. Rev. 40(2011)672.
- [3] Lee E.M., Gwon S.Y., Ji B.C., Wany S. and Kim S.H., Dyes Pigments 92(2012) 542.
- [4] Janus K., Sworakowski J. and Luboch E., Chem. Phys., 285 (2002)47.
- [5] Dong H., Zhu H., Mang Q., Gong X and Hu W., Chem. Soc. Rev., 41 (2012) 1754.
- [6] Sun Z., Li H., Liu G., Fan C. and Pu S., Dyes Pigments 106 (2014)94.
- [7] Nigel Corns S., Partington S.M. and Towns A.D., Coloration Technology 125 (2009)249.
- [8] Cheng T., Lin T., Brady R. and Wang X., Fibers Polymers 9 (2008)301.
- [9] Eds J.C. Crano and R.J. Guglielmetti, Organic Photochromic and thermochromic compounds, Volume 1, Main photochromic families, Kluwer academic press. New York, N.Y.1999.
- [10] Periyasamy A.P., Vikova M. and Vik M., Textile Progress, 49 (2017)54.
- [11] Corns S.N., Partington S.M., Towns A. D., Color Technol, 2009, 125, 249.
- [12] Rawat M.S.M., Mal S. and P. ,Open Chem.J.2 (2015) 7.
- [13] Corns S. Nigel, Partington S.M. and Towns A.D., Coloration Technology,125 (2009)249.
- [14] Hadjoudis E. and Mavridis I.M., Chem. Soc. Rev., 33(2004)579.
- [15] Christie R.M., Color Chemistry, The Royal Society of Chemistry, London, 2001.
- [16] Durr H., General Introduction in Photochromism: Molecules and System, B.L. Henri and H. Durr, Eds., Elsevier, B.V. Amsterdam, 2003,1.
- [17] Vikova M., Photochromic Textiles, Heriat Watt University, Scottish Burdens, Edinburgh, 2011.
- [18] Evans R.C., Douglas P. and Burrows H.D. (eds), Applied Photochemistry, Springer International Publishing Work, New York, NY, 2013.
- [19] Zhang J.Z., Schwartz B.J., King J.C and Harris C.B., J. American Chemical Society.114 (1992)10921.
- [20] Tamai N. and Miyasaka H., Chemical Rev., 100(2000)1875.
- [21] Preigh M.J., Stauffer M.T., Lin F.T. and Weber S.G., J. Chem. Soc., Faraday Trrans, 92(1996)3991.
- [22] Adamo C. and Jacuemin D., Chem. Soc.Rev., 42(2013)845.
- [23] Zhang C., Zhang Z., Fanand M., Yan W., Dyes Pigments, 76(2008)832.
- [24] Christie R.M., Advances in dyes and colorants, In advances in the dyeing and finishing of technical textiles, M.L. Gulrajani, ed, Woodhead Publishing Limited, Cambridge, U.K., (2013) 1.
- [25] Dawson T.L., Coloration Technology, 126 (2010)177.
- [26] Oda H., J. Soc. Dye. Color, 114 (1998) 363.
- [27] Ohnishi Y., Yoshimoto S. and Kmura K., J. Photochem. Photobiol. A. Chem., 141(2001)57.



- [28] X. Li, Ji. Li, Wang Y., Matsuura T. and Meng J., *J. Photochem. Photobiol. A. Chem.*, 161(2004)201.
- [29] Chowdhury M.A., Joshi M. and Butola B.S., *J. Eng. Fibres Fabrics*, 9 (2014)107.
- [30] Corns S. Nigel, Partigton S.M. and Jowns A.D., *Coloration Technology*, 125 (2009) 249.
- [31] Billah S.M.R., Christie R.M. and Shamey R., *Coloration Technology*, 124 (2008)223.
- [32] Becker R.S. and Michl J., *J. Am. Chem. Soc.*, 88 (1966) 5931.
- [33] Oliveira M.M., Salvador M.M., Vermeersch G., Micheau J.C., Coelho P. J. and Carvalho M., *J. Photochem. Photobiol. A. Chem.*, 198(2008)242.
- [34] Ortica F., *Dyes and Pigments*, 92 (2012)807.
- [35] Little A.F. and Christie R.H., *Coloration Technology*, 126 (2010)164.
- [36] Eds Crano J.C. and Guglielmetti R.J., *Organic Photochromic and thermochromic compounds, Volume 2, Physico chemical studies, biological applications and thermochromism*, first Roc 2 Kluwer academic press. New Yark, N.Y. 1999.
- [37] Hart R.J., Heller H.G. and Salisbury K., *Chem. Commune.* (London) (1968)1627.
- [38] Irie M. and Mohri M, *J. Org. Chem.* 53(1988)803.
- [39] Padwa A., A.Au, Lee G.A and Owens W. J. *Org. Chem.* 40(1975)1142.
- [40] Tian H. and Yang S., *Chem. Soc. Rev.* 33(2004)85.
- [41] Ortica F., *Dyes Pigments* 92(2012) 807.
- [42] Little A.F. and Christie R.M., *Coloration Technology*, 126(2010)164.
- [43] Aldib M. and Christie R.M., *Coloration Technology*, 127(2011)282.
- [44] Little A.F. and Christie R.M., *Coloration Technology*, 126(2010)157.
- [45] Little A.F. and Christie R.M., *Coloration Technology*, 127(2011)275.
- [46] Standard methods for determination of color fastness of textiles and leather 5<sup>th</sup> edition, Bradford, SDC, 1990.
- [47] Day J.H., *Chem. Rev.* 63(1963)65.
- [48] Aitken D., Burkinshaw S.M., Griffiths J. and Towns A.D., *Rev. Prog. Coloration*, 26(1996)1.
- [49] Seeboth A., Luckowska A.K., Ruhmann R., Lotzch Chin D., *J. Polymer Science*, 25 (2007)123.
- [50] Mather R.R., *Rev. Prog. Coloration*, 31 (2001) 36.
- [51] Chowdhary M.A., Joshi M. and Butola B.S., *Journal of Engineered Fibres and Fabrics* 9(2014)120.
- [52] Day J.H., *Chem. Rev.*, 68(1968) 649.
- [53] Vesel A. and Gunde M.K., *Dyes and Pigments*, 86(2010) 271.
- [54] Rubacha M., *Polymer for advance technology*, 18 (2007)323.
- [55] Agolini F. and Gay F.P., *Macromolecules* 3(1970)349.
- [56] Feczko T., Samu K., Wenzel K., Neral B. and Vocin B., *Coloration Technology* 129(2013)18.
- [57] Vikova M., *Photochromic Textiles*, Heriot Watt University, Scottish Borders Campus ,Edinburgh 2011.

[58] Attia S., Wang J., Wu G., Shen J. and Ma.J., J. Matter. Sc. Technol. 18(2002) 211.

[59] Cheng T., Lin T., Brady R. and Wang X., Fibers Polym. 9(2008)301.

[60] Cheng T., Lin T., Fang J. and Brady R., Text. Res. J. 77(2007)923.

[61] Cheng T., Lin T., Brady R. and Wang X., Fibers Polym. 9(2008)521.

[62] A Glossary of AATCC Standard Terminology, Resaerch Triangle Park, NC,2007.

[63] Periyasamy A.P., Vikova M. and Vik. M., 24 th International Fedration of Association of Textile Chemist and Colourist Congress, Radim Hardina, ed, University of Pardubice, Czech Republic (2016)1.

[64] Vikova M., Periyasamy A.P., Vik M. and Ujhelyiova A., J. Text. Inst. (2016)1.